Signal Quality Assessment in Wearable ECG Devices

by

Bahareh Taji

Thesis submitted

in partial fulfillment of the requirements

for the Ph.D. degree in

Biomedical Engineering

School of Electrical Engineering and Computer Science

Faculty of Engineering

University of Ottawa

Abstract

There is a current trend towards the use of wearable biomedical devices for the purpose of recording various biosignals, such as electrocardiograms (ECG). Wearable devices have different issues and challenges compared to nonwearable ones, including motion artifacts and contact characteristics related to body-conforming materials. Due to this susceptibility to noise and artifacts, signals acquired from wearable devices may lead to incorrect interpretations, including false alarms and misdiagnoses.

This research addresses two challenges of wearable devices. First, it investigates the effect of applied pressure on biopotential electrodes that are in contact with the skin. The pressure affects skin–electrode impedance, which impacts the quality of the acquired signal. We propose a setup for measuring skin–electrode impedance during a sequence of applied calibrated pressures. The Cole–Cole impedance model is utilized to model the skin–electrode interface. Model parameters are extracted and compared in each state of measurement with respect to the amount of pressure applied. The results indicate that there is a large change in the magnitude of skin–electrode impedance when the pressure is applied for the first time, and slight changes in impedance are observed with successive application and release of pressure.

Second, this research assesses the quality of ECG signals to reduce issues related to poor-quality signals, such as false alarms. We design an algorithm based on Deep Belief Networks (DBN) to distinguish clean from contaminated ECGs and validate it by applying real clean ECG signals taken from the MIT-BIH arrhythmia database of Physionet and contaminated signals with motion artifacts at varying signal-to-noise ratios (SNR). The results demonstrate that the algorithm can recognize clean from contaminated signals with an accuracy of 99.5% for signals with an SNR of -10 dB. Once low- and high-quality signals are separated, low-quality signals can undergo additional pre-processing to mitigate the contaminants, or they can simply be discarded. This approach is applied to reduce the false alarms caused by poor-quality ECG signals in atrial fibrillation (AFib) detection algorithms. We propose a signal quality gating system based on DBN and validate it with AFib signals taken from the MIT-BIH Atrial Fibrillation database of Physionet. Without gating, the AFib detection accuracy was 87% for clean ECGs, but it markedly decreased as the SNR decreased, with an accuracy of 58.7% at an SNR of -20 dB. With signal quality gating, the accuracy remained high for clean ECGs (87%) and increased for low SNR signals (81% for an SNR of -20 dB). Furthermore, since the desired level of quality is application dependent, we design a DBN-based algorithm to quantify the quality of ECG signals. Real ECG signals with

various types of arrhythmias, contaminated with motion artifacts at several SNR levels, are thereby classified based on their SNRs. The results show that our algorithm can perform a multi-class classification with an accuracy of 99.4% for signals with an SNR of -20 dB and an accuracy of 91.2% for signals with an SNR of 10 dB.

Table of Contents

List of Figures

List of Tables

List of Abbreviation

afdb ……. Atrial Fibrillation Database

AFib……..…..…… Atrial Fibrillation

ANN…….Artificial Neural Network

AR…….…… Autoregressive

BP…….… Back-Propagation

bpm ……..……...……beat per minute

CD……..…….. Contrastive Divergence

CPE……..... Constant Phase Element

dB…….…….……Decibel

DBN…….….... Deep Belief Network

ECG……..……Electrocardiogram

EEG…….....…..…Electroencephalogram

EMG…….……...……Electromyogram

FA……..……...…. False Alarm

FN……..… False Negative

FP.....…...False Positive

HMM…….……... Hidden Markov Model

IDC.…….…….…International Data Corporation

kPa…….…….……...…Kilo Pascal

MLP…….…….……..Muli Layer Perceptron

N…….…….…….. Newton

PI….…….……patient-empowering, information-leveraging

PPG ……...…….…….……...……. Photoplethysmogram

RBM…….……..... Restricted Boltzmann Machine

RMSSD……..… Root Mean Square of Successive R-R Differences

SE…….…….……. Shannon Entropy

SNR……..…….……... Signal to Noise Ratio

SQI…….…….……...……Signal Quality Index

SVM……..…….……..Support Vector Machine

TN…….…….…. True Negative

TP…….…….……True Positive

TPR…….…….....Turning Points Ratio

Acknowledgements

I would like to express my gratitude to my supervisors Prof. Shervin Shirmohammadi and Prof. Adrian D.C. Chan for their continuous support of my PhD research, for their flexibility and trust, and immense knowledge. Their supervision helped me throughout my PhD research and writing of this thesis. Besides my supervisors, I would like to thank the rest of my thesis committee: Dr. Ali Etemad, Prof. James Green, Prof. Voicu Groza and Prof. Hilmi Dajani for their insightful comments and feedback. Additionally, I would like to thank the Canadian federal and provincial governments for funding my research over the past couple of years, through QEII-GSST. Last but not least, I am profoundly grateful to all my family members: my amazing husband Mehdi, my dedicated parents and my siblings, for their strong and continuous support which propelled me to complete this work.

Chapter 1 **Introduction**

1.1 Background and Motivation

There is a growing global trend towards the use of wearable biomedical measurement devices. The market is expected to increase from $6.22 billion USD in 2017 to $14.41 billion USD by 2022 [1]. The International Data Corporation (IDC) reports that 125.5 million wearable devices were shipped in 2016, and that number is expected to approximately double to 240.1 million wearable devices by 2021 [2]. Wearable devices can be used in various applications, such as healthcare, fitness, rehabilitation, safety monitoring, and early diagnosis. In healthcare, wearable devices can help in conditions that only present intermittently (e.g., atrial fibrillation) or those that require immediate attention (e.g., myocardial ischemia).

Continuous monitoring is necessary in these cases, and such monitoring is possible with wearable devices since they not only allow individuals to carry on with their normal daily activities but also make the monitoring more effective (versus requiring an individual to remain in a hospital or clinic for an extended period of time). There is particular interest in wearable devices in healthcare due to the aging population because they support independent living, allowing people to continue to live at home while being appropriately monitored.

Figure 1.1 illustrates how a wearable device gathers health-related data and wirelessly sends it to a smart device. Data are stored and processed locally (through a smart device) or in the cloud, and health-related information as well as the information extracted from the acquired signals can be sent to various end users. In a healthcare application, such users include the person using the device, caregivers, clinicians, and family members.

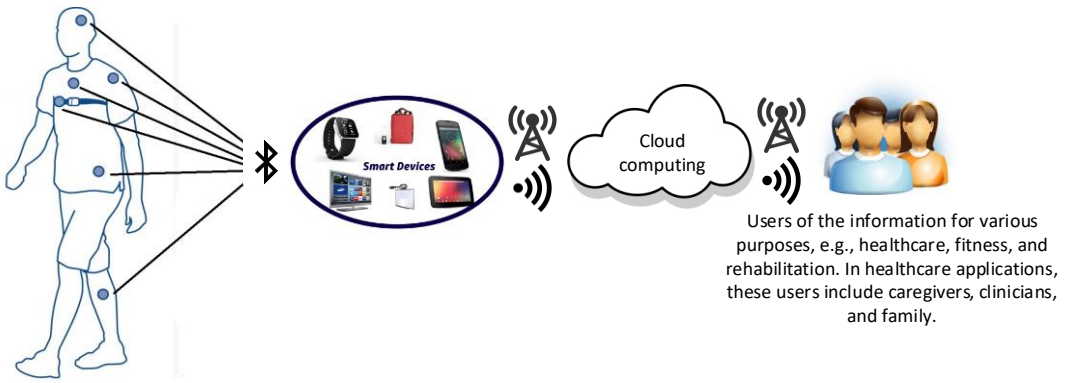

Figure 1.1 Wearable device and its data path

Wearable devices can measure various signals, including temperature, movement (e.g., accelerations), and biosignals. Biosignals (e.g., ECG (electrocardiogram), EMG (electromyogram), and EEG (electroencephalogram)) are bioelectric signals associated with different functions of the body. To acquire biosignals non-invasively, wearable devices can use biopotential electrodes, which make contact with the surface of the skin. Non-invasive,

wearable devices for acquiring biosignals are the focus of this thesis, with a particular emphasis on ECGs.

Figure 1.2 shows a general biosignal acquisition system. As shown in the figure, data are collected from the body, amplified, converted to a digital form, and then denoising techniques are applied. Data processing and analysis is the last step, where the events can be detected. Contaminants integrate themselves into the recorded signal in all the steps prior to data processing, even during the analog-to-digital conversion, when some denoising techniques (e.g., filtering) could also be applied.

In a conventional biosignal recording system, there is always the risk of contaminants (e.g., noise and artifacts) affecting the quality of the recorded signals. Sources of contaminants in ECGs include power line interference, contact noise, motion artifacts, electromyographic (EMG) noise, baseline drift, data-collecting device noise, electrosurgical noise, quantization, and signal processing artifacts [3]. In a clinical biosignal acquisition system, contaminants are often controlled to some extent during data collection, using strategies such as electromagnetic shielding and limiting the patient's movements during signal recording. Furthermore, experts are available in clinical settings to set up the system and ensure high-quality data acquisition. They can manually evaluate the signal quality and recollect the biosignal if required.

It is not always possible to completely remove the contaminants. However, in a clinical data-acquisition system, interfering contaminants mainly include power line and motion artifacts, which are easier to control with filtering and by asking the subject not to move during the data-collection process. In such systems, there is always an opportunity to discard low-quality signals and repeat the data collection if the acquired signal quality is not satisfactory or information is missing. Despite these efforts, however, contaminants may often be present

in the data. Interfering contaminants affecting the quality of acquired signals can result in some undesired issues, such as false alarms and misinterpretations (e.g., misdiagnosis) and inaccurate physical activity measurements. To avoid such difficulties, signal processing techniques can be applied to mitigate the contaminants and ensure a reliable and consistent signal. For example, previous research has proposed various filters, such as adaptive filters, to mitigate the effects of contaminants [4], [5].

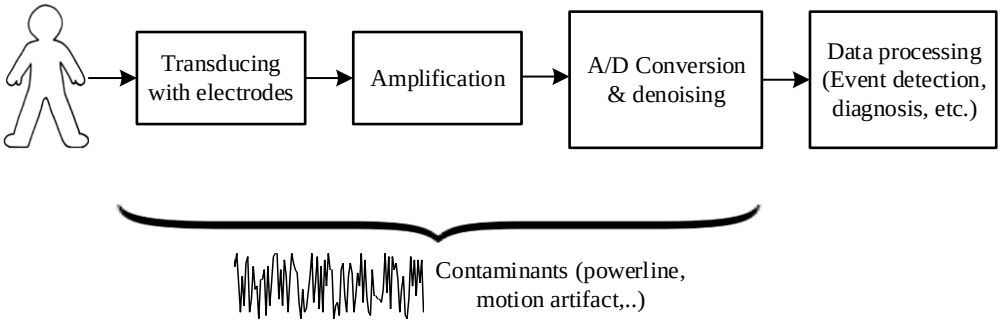

Figure 1.2 A general biosignal monitoring system block diagram

Wearable biosignal devices are more susceptible to contaminants for multiple reasons, such as non-expert users, uncontrolled environments, continuous monitoring, wireless transforming (e.g., the distance between sender and receiver can affect the data transmission), and the inexpensive parts that are used to make the devices affordable. Thus, the signals that are recorded by wearables are highly susceptible to quality issues, leading to more undesirable problems in all applications. For instance, in a study examining ambulatory ECG monitoring for telehealth, only 28% of the records were free of artifacts, and 18% were completely unusable [6]. In wearable devices, undesirable issues may occur due to contaminated signals, including misinterpretation (e.g., misdiagnoses) and false alarms in healthcare. Moreover, in rehabilitation applications of wearable devices, imprecise movement data capture due to

contaminated signals, can negatively affect rehabilitation process. Manually examining the quality of the signals, which is an option in clinical systems, is not possible for wearable devices due to the huge volume of data and potential real-time constraints. Hence, to achieve reliable and accurate analyses, interpretations, and results, signal quality investigation is required.

Biomedical signal quality analysis can be categorized into detection, identification, quantification, and mitigation [7]. In the context of signal quality analysis, signal detection refers to determining whether or not the signal is contaminated (beyond a certain threshold). Signal identification refers to identifying the type(s) of contaminants within the data. Signal quantification refers to determining the extent of contamination (this could be numerical, such as SNR, or categorical, such as low, medium, high). Signal mitigation is the procedure for reducing or eliminating the contaminants within a recorded signal (e.g., noise cancellation). There has been extensive research on signal mitigation techniques (e.g., in relations to wearables [8]). Mitigation is not always possible, especially in wearable devices where some recorded data are deemed to be "unusable" [6].

There are some specific issues associated with wearables compared to conventional biomedical monitoring devices. These issues include 1) varying pressure on the contact area and 2) a high degree of contaminants that cannot be addressed by manual evaluation and recollection of data. The materials used in such devices must be flexible enough (e.g., spandex) to conform to the user's body. This allows the device to maintain contact when the user's body volume changes with breathing and flexing. However, the connection between the skin and the electrode transducers changes as the applied pressure on the electrode varies with body volume changes. Varying pressure applied to the contact area results in changes in

skin–electrode impedance, which may affect the quality of the signals collected by wearable devices [9]. This is often not an issue in clinical biosignal acquisition systems, which typically use disposable adhesive electrodes. High levels of contaminants are also not as serious of an issue for conventional clinical biosignal devices compared to wearables because of the controlled environment and the presence of an expert to verify the setup and data quality.

There is high growth and potential in wearable biomedical technology. While there is a good foundation of knowledge in biomedical monitoring—with much that is transferable to wearables—there are some gaps, which are examined in this research. The specific issues examined in this thesis can be enumerated as follows:

1- **Effect of external pressure on contact-based biopotential electrodes:** Wearable devices for biosignal recording typically have electrodes that make direct contact with the skin. The electrodes are often embedded in a flexible material that ensures that electrode contact with the body is maintained. The applied pressure on the electrode will vary due to changes in body volume (e.g., due to breathing and muscle flexing). The varying applied pressure, in turn, will cause skin–electrode impedance to vary. The impacts of varying pressure on skin–electrode impedance are investigated in this research.

2- **Signal quality assessment of ambulatory ECG:**

   Another common issue of wearable devices is the quality of the biosignals recorded by these devices. Wearable devices are ambulatory recording devices, and the signals they record are widely exposed to noise, such as motion artifacts. Low-quality signals can result in misleading information and potentially lead to incorrect interpretations, including misdiagnoses or false alarms. Due to the

volume of data and potential real-time constraints, an automated method is required to discriminate signals based on their quality. This would enable the identification of signals that are of acceptable quality to undergo further processing as well as low-quality signals, which should be mitigated or discarded. In wearables, signals are susceptible to various types of contaminants, which can appear in various combinations; this can make it challenging to design a method for effectively assessing signal quality. Advanced machine learning methods, such as deep learning techniques, which are able to learn complex functions, could be effective in addressing this problem.

3- AFib false alarm rate reduction by signal quality gating:

AFib is a common type of heart arrhythmia, and there are many algorithms to automatically detect it. Wearables are appropriate devices for AFib detection because the condition can present intermittently. Because they provide ambulatory monitoring, wearables do not interrupt the user's normal daily activities. However, as already noted, wearables are more susceptible to contaminants, which can lead to false alarms. A possible solution for this would be to apply signal quality assessment methods and define a quality threshold indicating which segments have sufficient quality to go through the AFib detection algorithm and which should be restricted. Signal quality assessment can identify low-quality segments that can be gated or discarded. By implementing this gating system, we can reduce the number of false alarms in the AFib detection algorithm in a wearable device designed to detect this arrhythmia.

4- ECG signal classification based on SNR:

ECG acquisition usually has a specific purpose for a certain application. That application determines to what degree of quality is required to avoid misdiagnosis and/or misinterpretations. By applying a multi-class classification based on the level of quality of ECG signals (SNR), an application can select ECG signals that are of acceptable quality, suitable for that application, while rejecting lower quality signals.

1.2 Thesis Objectives

Despite the many advantages of wearable devices, there are still significant challenges that need to be examined. The overall objective of this research is to conduct a thorough investigation of skin–electrode impedance variation under changing pressure, which is a specific concern in wearable devices, and also to analyze the quality of the biosignals collected with a wearable device. The specific objectives of this research are as follows:

Objective 1. **Examine the characteristics of biopotential electrodes when they are in contact with the body and under varying pressure.** This research investigates the effects of cycles of varying external pressure on biopotential electrodes, specifically, the effects on skin–electrode impedance, using a Cole–Cole electrical circuit model. Levels of pressure expected with wearables and electrode types that may be used in wearables are employed.

Objective 2. **Develop an accurate and robust method for identifying the quality of ECG signals**. In this research, we implement and evaluate a deep learning-based method to separate clean and noisy signals. The method is applicable to the signals recorded by wearables, as such signals are highly susceptible to various types of noise, such as motion artifacts.

Objective 3. **Develop a method for reducing the rate of false alarms due to low-quality signals in AFib detection algorithms**. We propose, implement, and evaluate a novel machine learning-based method to reduce the false alarm rate resulting from poor-quality ECG signal measurement during AFib detection. We determine an "acceptability" threshold for ECG signal quality for the signal to be applicable in an AFib detection algorithm. We further develop a gating technique based on machine learning methods to determine the "acceptability" of signals and identify those that are eligible for AFib detection.

Objective 4. **Develop a method to classify ECG signals based on their level of quality**. Four different quality levels of ECG signals are considered, and machine learning techniques are applied to classify them based on their level of quality in terms of SNR.

1.3 Contributions

The contributions of this thesis are as follows:

1. **Examine the effects of varying externally applied pressure on skin–electrode impedance**. Utilizing an equivalent circuit model (Cole–Cole), we investigate the variation in skin–electrode impedance due to varying externally applied pressure. Three types of electrodes are examined, including Ag/AgCl, conductive textile, and orbital electrodes. Our findings show that pressure decreases skin–electrode impedance, and the magnitude of this change decreases with successive cycles of applying pressure and releasing it. In addition, we find that changes in skin–electrode impedance are partially sustained during the application and removal of pressure.

2. **Propose, develop, and evaluate a method based on DBN to classify ECG signal segments in terms of their signal quality**. We employ ECG signals from the

MIT-BIH arrhythmia database and contaminate them with motion artifacts at varying SNR levels. We use a DBN to discern clean versus noisy ECG segments. The results demonstrate that our algorithm can successfully differentiate clean and noisy signals with a higher accuracy when discriminating low-quality signals from clean ones, while the classification accuracy drops when the quality of the signal increases.

3. **Propose, develop, and evaluate an algorithm for reducing the rate of false alarms in AFib detection**. We utilize ECG signals with AFib from the MIT-BIH atrial fibrillation database and contaminate them with motion artifacts at various SNR levels. We develop a gating technique based on DBN to evaluate ECG signal quality and to determine if the signal qualifies for use in the AFib detection algorithm to lower the number of false alarms resulting from low-quality ECG signals. AFib detection algorithm accuracy is highly dependent on signal quality. It decreases from 87% with high-quality signals (no added noise) to 58.7% with poor-quality signals (SNR -20 dB). Applying the gating technique based on DBN, the accuracy of the AFib detection algorithm for low-quality signals (SNR -20 dB) improves to 81%.

4. **Propose, develop, and evaluate a multi-classification method based on DBN to classify ECG signal segments in terms of SNR**. Using ECG signals from the MIT-BIH Normal Sinus Rhythm and MIT-BIH Atrial Fibrillation databases and contaminating them with motion artifacts at several SNR levels, we develop a multi-class classification algorithm based on DBN that can distinguish the level of quality of four classes of ECG signals. The results show that DBN can be applied in multi-

classification applications, and accuracies of 99.4% for signals with an SNR of 20 dB and 91.2% for signals with an SNR of 10 dB are achieved.

The contributions of this thesis have been disseminated in the following publications:

1. B. Taji, A.D.C Chan, and S. Shirmohammadi, "Effect of Pressure on Skin–Electrode Impedance in Wearable Biomedical Measurement Devices," Accepted in *IEEE Transactions on Instrumentation and Measurement,* 2018.

2. B. Taji, A.D.C. Chan, and S. Shirmohammadi, 2018. "False Alarm Reduction in Atrial Fibrillation Detection Using Deep Belief Networks," *IEEE Transactions on Instrumentation and Measurement,* 67(5), pp. 1124–1131.

3. B. Taji, A.D.C. Chan, and S. Shirmohammadi, "Classifying measured electrocardiogram Signal Quality using Deep Belief Networks," in Instrumentation and Measurement Technology Conference (I2MTC), 2017 IEEE International. IEEE, 2017, pp. 1–6.

4. B. Taji, A.D.C Chan, and S. Shirmohammadi, "Externally applied pressure on the skin electrode impedance," In *World Congress on Medical Physics and Biomedical Engineering, June 7-12, 2015, Toronto, Canada, 2015* (pp. 923–923). Springer International Publishing.

1.4 Organization of the Thesis

This thesis is organized as follows:

In Chapter 2, we present a literature review of skin–electrode impedance models, including the one applied in this thesis, as well as skin–electrode measurement methods and works related to the effects of applying pressure on skin–electrode impedance.

Moreover, this chapter covers the background of DBN, provides the definition of AFib, and describes its characteristics and symptoms as well as related works in ECG signal quality assessment and classification.

Chapter 3 presents our proposed method for investigating the effects of applying pressure on the skin–electrode interface. The measurement setup and experimental results are depicted, tabulated, and presented in this chapter.

Chapter 4 presents our proposed method for applying DBN as a classifier to differentiate clean and noisy ECG signals and shows the results.

Chapter 5 lays out our method for reducing the false alarm rate in the automatic AFib detection algorithm. We propose and implement a technique for gating ECG data before processing to detect AFib events. The implementation of the method is described, and the results are presented.

Chapter 6 presents our method for applying DBN as a classifier of ECG signals based on their SNRs. The results show that DBN can accurately recognize the SNRs of ECG signals.

Chapter 7 presents a summary of the results and offers some directions and plans for future work.

Chapter 2 **Background and Literature Review**

A new generation of devices potentially transforming the biomedical monitoring industry, are patient-empowering, information-leveraging technologies [10]. These devices help people by providing them with technology accommodation that can increase self-awareness and self-management in their health concerns. This allows them to be involved in such concerns and therefore being able to play an effective role in managing them. This is called "patient empowering" which is a critical element in prevention, wellness and safety. Furthermore, such devices leverage the rapidly growing technology in information and communication and their public adoption to collect ones' medical condition, improve patient and clinical staff (doctors, nurses, physical therapists, caretakers, etc.) interact and deliver strong coordination of care and therefore, contribute in significant improvement in the healthcare industry. Patient-empowering, information-leveraging devices can provide relevant information and analyses

directly to users, enabling real-time feedback. Although, this will be possible only if the data collected by them is reliable in terms of quality.

Health IT leaders need to embrace innovations such as patient-empowering, information-leveraging (PI) technologies, because they can help solve some critical and prevalent challenges, such as increasing cost of healthcare, supporting the aging population, and shortage of healthcare professionals. One major class of such products are wearable devices which have a wide range of applications including healthcare, fitness, well-being, and performance monitoring to provide information for healthy people via devices such as smartphones [11]. Their main applications are categorized into five groups: health and wellness monitoring, safety monitoring, home rehabilitation, assessment of treatment efficacy, and early detection of disorders [12]. Hence, wearable devices not only help people with health concerns, but also support healthy users and their active lifestyles. In their healthcare applications, wearable devices enable continuous measurement of biosignals (e.g., electrocardiogram (ECG) and electromyogram (EMG)) and can provide useful information regarding the function and status of the body. Cloud-based services further increase the value of such wearable monitoring devices (e.g., [13], [14]).

Wearable devices have similarities to conventional non-wearable devices. For example, both wearable and conventional devices include transducers (e.g. electrodes) and bioinstrumentations (e.g. bioamplifiers, filters). Furthermore, in both types of devices, signals are preprocessed to remove or reduce the noise and eventually used to detect, estimate or diagnose relevant events. These similarities allow for knowledge transfer from conventional non-wearables to wearables. Research on biosignal monitoring devices to improve signal quality (e.g., [4], [5], [15]) are applicable to wearable and non-wearable devices. Nonetheless,

there are some challenges unique to wearables that have not been well researched; this includes varying pressure applied to electrodes and high levels of contaminants.

Since wearable devices, as their name suggests, are being worn to monitor the biosignals, a new factor will appear due to the changes in body volume underlying the electrodes, due to breathing or muscle contraction. The electrodes, typically integrated in body conforming material, will be pushed towards the body with varying levels of pressure, which impacts the skin–electrode impedance, which in turn can impact the quality of the acquired signal. There is not a thorough and detailed research investigating effects of pressure in wearable devices, which is addressed in this research.

Moreover, with a wearable device (e.g. an ambulatory ECG device), the signal will be recorded or monitored while the user is performing normal daily activities. The motion of the user and the varying, uncontrolled environments that the user will encounter, will expose the device to a variety of contaminants. Such contaminants can lead to misinterpretation or misdiagnoses, including false alarms. The volume of data and real-time constraints make an automatic assessment of the quality of recorded signals necessary, which is investigated in this research.

In this chapter, we present the background information and literature related to the challenges and issues which are unique to wearable devices.

2.1 Literature Review for Effects of Externally Applied Pressure on Electrodes

Wearable devices typically integrate electrodes in a material that conforms to the body, which applies pressure to electrode to ensure good contact between the skin and electrode. Associated with the contact area between the skin and the electrode is the skin–electrode impedance. In this thesis, we investigate the effect of a varying applied pressure on the skin–

electrode impedance. To investigate the impacts of pressure we first need to model the skin–electrode impedance. Therefore, we discuss various models of skin–electrode impedance and then discuss previous research that has examined the effects of applied pressure on electrodes.

2.1.1 Skin–Electrode Impedance Modeling

Skin–electrode impedance is the impedance between the body and the electrode which plays a major role in the quality of the signal sensed by the electrode [16], [17], [9]. A low skin–electrode impedance is desired because higher skin–electrode impedances are associated with a lower signal-to-noise ratio and increased susceptibility to artifacts and interference [18], [19].

An electrical circuit model can be helpful in order to better understand and analyze skin–electrode impedance behavior. Warburg [20] was the first to propose such circuit model for the electrode-electrolyte interface (shown in Figure 2.1); however, Helmholtz was the one who proposed that a double layer of charge occurred in this interface [21]. Assambo et al. [22] identified the components of the electrode circuit model, analyzing its electrical properties in AC and DC measurements. Their study helped in estimating the values of capacitors and resistors in the skin–electrode electrical model. Three popular electrical models suggested for skin–electrode interface are: 1) the single-time constant model, 2) the double-time constant model, and 3) the Cole–Cole model.

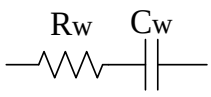

Figure 2.1 Warburg model

2.1.1.1 Single-Time Constant Model

Recognizing limitations with the Warburg model which includes one resistor and one capacitor, Geddes and Baker [23] suggested a model for skin–electrode impedance, which is a combination of a resistor in series with a paralleled resistor and capacitor as shown in Figure 2.2, where E_{hc} is the half-cell potential, C_d is the capacitance between the electrode and the skin [18], [24], R_d is the resistance between the skin and electrode during charge transfer [18], [25], and R_s represents the total resistance of electrolyte gel (if any) or sweat [19], [26]. This model is known as the single-time constant model [27] and implies that the total impedance is frequency dependent. At low frequencies, the capacitor (C_d) acts like an open circuit, thus impedance approaches $R_s + R_d$. At high frequencies, C_d acts like a short circuit resulting in an impedance that approaches R_s.

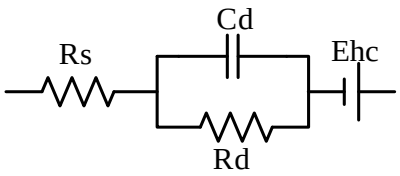

Figure 2.2 Single-time constant skin–electrode interface model

2.1.1.2 Double-Time Constant Model

Kaczmarek and Webster [28] suggest a more complicated model for the skin–electrode impedance. As depicted in Figure 2.3, it is actually composed of two stages of the single-time constant model and is known as the double-time constant model. The first stage represents the electrode–electrolyte interface and the second stage represents the electrolyte–skin interface. Parameters in the first stage include C_d and R_d representing the impedance associated with the

electrode–electrolyte interface and R_s which is the effective resistance between the electrode and the skin [18]. Parameters in the second stage show the electric impedance of the epidermal layer of the skin that behaves as a parallel RC circuit (R_e and C_e) and R_u represents the resistance of subcutaneous tissue [18].

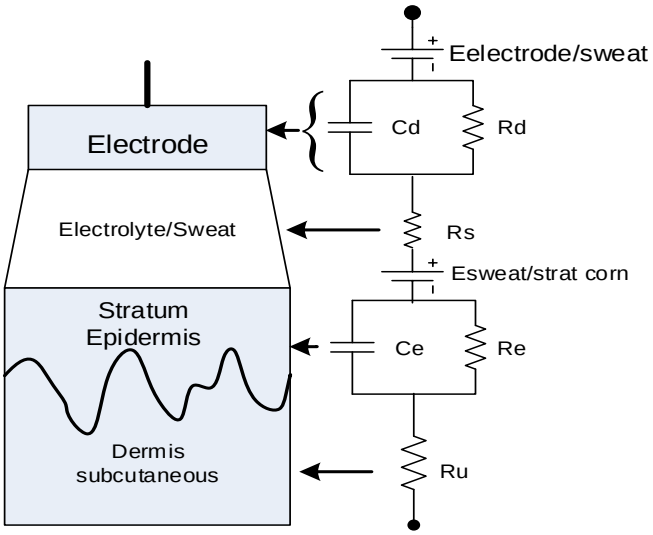

Figure 2.3 Double-time constant model, based on [18]

2.1.1.3 Cole–Cole Model

The Cole–Cole impedance model is a popular impedance model, especially for biological tissues [29], [30]. Since in a double layer (double-time constant) model, impedance of the skin (as a tissue) dominates the total impedance [24], this model is also applicable to skin–electrode impedance. Therefore, Cole–Cole is a popular model for skin–electrode impedance analysis [31] and has previously been used for that [32]. Figure 2.4 presents the Cole–Cole model equivalent circuit diagram which is composed of a low-frequency resistor (R_0), a high-frequency resistor (R_∞), and a constant phase element (CPE) which is also known as the fractional capacitor [33]. A fractional capacitor is a passive element which gives a phase angle

(between 0 and 90 degrees) and remains constant with frequency. The impedance of this component is equal to:

$$Z_{CPE} = 1/(j\omega C)^{\alpha} \quad (2.1)$$

where C is the capacitance and α is its order ($0 < \alpha <= 1$) [33] and can interpret the voltage–current relationship of CPE [34].

In this thesis, we use the four components of this model (C, R_0, R_∞ and α) to explore each electrode's behavior under pressure.

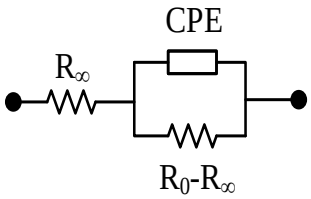

Figure 2.4 Cole–Cole model schematic view [33]

2.1.2 Skin–Electrode Impedance Measurement

Skin–electrode impedance has always been of interest because it is an important factor in biosignal quality. Thus, many papers in the literature have discussed measurement methods for skin–electrode impedance and methods to improve the measurement accuracy. A method with the measurement setup shown in Figure 2.5 is proposed in [35]. In this method, three electrodes are applied on the arm, and the skin–electrode impedance of the electrode in the middle is calculated. The current flowing between A and B can be calculated by measuring the voltage drop in E_r . A buffer unit is utilized to prevent any significant current flow between electrodes B and C (i.e., $I_c \approx 0$). Furthermore, a known sine wave is applied to electrode B and the voltage between B and C is measured. Thus, impedance of B can be obtained using the following equation:

$$Z_B = \frac{E_{B-C}}{I_{A-B}} \tag{2.2}$$

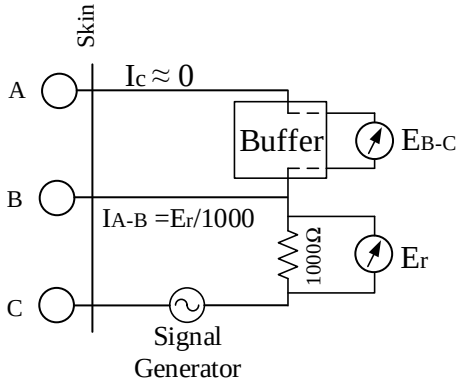

Figure 2.5 Skin–electrode impedance measurement setup [35]

Another method is presented in [36], which employs a two-electrode configuration, as shown in Figure 2.6 Two electrodes are applied on the forearm and a known sine current is injected and the voltage drop between the electrodes is measured. In this setup, the skin–electrode impedance of both electrodes plus body impedance (between the two electrodes) is measured. It has previously been shown in [37] that the body impedance at relatively low frequencies (<50 kHz), can be considered a resistor (< 500 **Ω**). In a Cole–Cole model, body impedance is comparable to R_∞ which plays an important role only in high frequencies; at low frequencies the impedance is dominated by CPE and R_0. Since many biosignals are low bandwidth signals (e.g., ECG frequency components are primarily between 0.05-100Hz [38]), the impact of body impedance is negligible. Therefore, assuming the skin–electrode impedances are equal, and the body impedance is negligible, the resultant measurement can be simply divided by two to obtain the impedance for one skin–electrode.

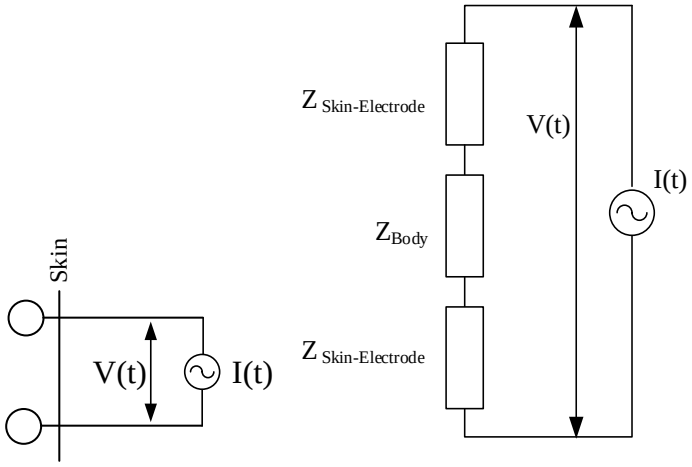

Figure 2.6 Two-electrode configuration for skin–electrode impedance measurement [36]

2.1.3 Effects of Applying Pressure on the Skin–Electrode Impedance

Skin–electrode impedance is affected by a variety of factors, including electrode material [39], [40], electrode size [39], [41], skin preparation [42], [43], [44], skin type [45], [46], sweat secretion [45], [47], heat [48], [49], and atmospheric humidity [49]. An external pressure or force, applied to the electrode, has also been shown to influence the skin–electrode impedance [50], [51].

It has been generally observed that increasing the applied pressure is associated with a decrease in skin–electrode impedance [50], [52], [53]. In [54] and [55] skin–electrode interface impedance is modeled by a double-time constant equivalent circuit as shown in Figure 2.3 and two levels of external pressure (0.67 kPa and 2.7 kPa) are applied on three types of carbon-inlayed silicone rubber. Electrodes are placed on the lower abdomen (almost hair free area) of subjects in [54] and on the same area as well as chest of the subjects in [55]. The effect of externally applied pressure is shown to not only being dependent on the electrode type [54] [55], but also varying from person to person [53], [54]. A single-time constant

model is used for skin–electrode interface impedance in [50] and [53] where a hysteresis effect was observed in them, since applying pressure to the electrodes caused irreversible decreases in the skin–electrode impedance. In [53], skin–electrode measurements were performed on only two subjects, using large applied forces (including 0 Newton (N), 8.8 N and 22.3 N) that are not representative for wearable devices.

In [51], it is noted that skin–electrode impedance is influenced by the applied force, and that the larger force or pressure we apply, the more skin–electrode impedance decreases. However, the objective of the paper was to introduce a new type of dry and capacitive electrode appropriate for long term ECG monitoring. Since the effects of applied pressure on skin–electrode impedance were not a main concern, unfortunately, limited details are provided with regards to the methodology of applying pressure, skin–electrode impedance measurement method, and its variation under pressure, making it difficult to evaluate their findings.

In [50], the application area of interest was impedance plethysmography rather than biosignals; the results only included skin–electrode impedance values at 5 kHz, well above the bandwidth for non-invasive biosignals. While [56] was also directed towards impedance plethysmography, skin–electrode impedances for Ag/AgCl, Aluminum (Al), and Silver (Ag) electrodes were measured between 1 Hz and 1 MHz. Measurements were performed for one subject, so the repeatability and generalizability of the findings is unknown. In both [50] and [56], a decrease in skin–electrode impedance was associated with increased applying pressure. In addition, larger decreases in skin–electrode impedance were noted for dry electrodes than for wet electrodes, where an electrolytic gel is employed. Smaller changes in skin–electrode impedance were noted in [56] compared to [50]; these differences were attributed to

differences in how the electrodes were initially applied [56]. Such inconsistencies motivate us to perform a comprehensive systematic research which addresses all the aspects of impacts of pressure on skin–electrode impedance.

2.2 Literature Review for ECG Quality

With advances in technology, including increased computing power, improved batteries and power saving methods, enhanced wireless connectivity, and miniaturization, there has been an associated advancement in medical devices, including portable and wearable devices that allow medical measurements to be recorded anytime and anywhere. Such devices, however, also come with their own unique challenges and issues. Signals recorded by such devices are generally more susceptible to noise and artifacts. Measurements can be made in a wide variety of environments (e.g., patient's home), which are not well-controlled. The patients may also be ambulating resulting in motion artifact. Noise and artifacts reduce the quality of the recorded signal and can result in misinterpretation during signal analysis, such as false alarms. The increase in medical monitoring, including pervasive and continuous monitoring, results in a volume of data that makes human inspection impractical and automated signal quality analysis a necessity [7], [57], [58]. Thus, quality assessment of such signals is important. In this subsection we investigate some quality assessment techniques available in the literature with a focus on ECG signals, since it is the biosignal of the main interest of this thesis.

2.2.1 ECG Quality Assessment

There have been a number of works that have analyzed the signal quality for ECG [57], [59], [60], [61], [62], [63]. Some of these works perform signal quality analysis by defining a

signal quality index (e.g., [59], [61], [62], [64]), which may be based on some features of the ECG and data fusion.

In [59] ECG quality assessment is performed by implementing and evaluating four ECG quality measures, including (A) empty lead detection, (B) spike detection and (C) number of lead crossing points (calculated from basic signal properties) and (D) QRS-based detection parameter.

Li et al. in [60] perform an ECG signal quality assessment by combining four different SQIs including (1) comparison of multiple beat detection algorithms on a single lead, (2) comparison of the same beat detection algorithm on different ECG leads, (3) evaluation of the randomness of a segment of the ECG and (4) calculating the proportion of the spectral distribution of an ECG segment. Then they fuse the result of ECG quality assessment and Kalman filtering for robust heart rate estimation even for noisy ECG signals.

In [61], an alarm gating system for myocardial ischemia is designed which quantifies the quality of ambulatory ECG signals by defining and computing a signal quality index and rejects alarms with low SQIs.

A signal quality index based on ECG signal SNR is introduced in [62]. This SQI is used to reduce the false identification rate in an ECG based biometric system.

Another approach using data fusion is presented in [64] where reliability of heart rate is estimated by assessing the quality of the ECG and photoplethysmogram (PPG) and separately computing heart rates from each of them, and then fusing the obtained information to compute a heart rate quality index. In this work, a machine learning waveform classifier (SVM) is used to separate bad and good quality waveforms.

Some other works also employ machine learning for ECG signal quality assessment and classifying signals based on their quality (e.g., [57], [65], [66]). However, applying machine learning methods for signal quality analysis is not limited to ECG and has been also utilized for this purpose in other signals such as audio signals [67] and EMG [68], [69]. We will further explore signal quality assessment approaches which are based on machine learning methods in the following subsection.

2.2.2 Machine Learning in ECG Quality Assessment

Machine learning algorithms are recently embedding themselves into a wide variety of purposes from image processing to financial applications. In the context of biosignals, machine learning algorithms are used for applications such as medical diagnoses [70], [71], [72], prosthetic control [68], [73], and human identification [74], [75]. They have also been employed in biomedical signal quality analysis [7], [57], [65], [66], [69]. Support vector machines (SVM) and artificial neural networks (ANNs) are machine learning algorithms that have been used for classifying biosignals (e.g., ECG and EMG) based on their signal quality [7], [57], [65], [66], [69], [76].

In [57], ECG segments including normal sinus ECG rhythm and wide variety of arrhythmic ECG segments, each one 10 seconds, are manually evaluated by experts in terms of their signal quality and classified into to good and bad quality classes. Signal quality indices (SQIs) are derived from ECG segments and are applied as inputs to the SVM classifier which is trained to estimate the quality of ECG segments. Results show that accuracy of the classifier depends on the rhythm of the segments and suggest that the SQIs should be rhythm dependent and the classifier should be separately trained for each specific rhythm.

Another utilization of SVM for ECG quality assessment is presented in [66]. In this paper, a method based on the combination of simple rules is used to detect most common errors encountered during ECG measurement (e.g., fell off electrodes) and SVM classifier is implemented and tested. A threshold (based on results of simple rule tests and SVM classification) is defined to determine if an ECG recording is acceptable or not. This combination differentiates acceptable and non-acceptable ECG recordings and the best obtained result is 83.6%, however it is not clarified what metric it is.

In [65], an automated machine learning-based algorithm to detect poor-quality ECG signals is described. The objective of that research is to find a novel and general approach to automatically identify the trustworthy signals for clinical applications. Data were drawn from Physionet Challenge 2011, in which 12 lead ECG recordings are labeled by experts based on their acceptability for clinical interpretation. Seven signal quality indices (SQIs) are defined and calculated for each lead. SQIs are as follows:

1- iSQI: the percentage of beats detected on each lead which were detected on all leads.

2- bSQI: the percentage of beats detected by *wqrs* that were also detected by *eplimited*. (*wqrs* and *eplimited* are two different QRS detection algorithms)

3- pSQI: the relative power in the QRS complex: $\int_{5Hz}^{15Hz} \frac{P(f)df}{\int_{5Hz}^{40Hz} P(f)df}$

4- sSQI: the third moment (skewness) of the distribution.

5- kSQI: the fourth moment (kurtosis) of the distribution.

6- fSQI: the percentage of the signal x_m which appeared to be a flat line.

7- basSQI: the relative power in the baseline: $1 - \frac{\int_{0Hz}^{1Hz} P(f)df}{\int_{0Hz}^{40Hz} P(f)df}$

Then two different classifiers, a multi-layer perceptron (MLP) artificial neural network and a support vector machine (SVM) are applied to classify ECG signals in terms of their clinical acceptability and results are compared. It is shown that SVM obtains slightly better results than MLP, however MLP is faster than SVM in execution time.

In [76], a five-level ECG quality classification is proposed, tested and validated by using Physionet MIT-BIH arrhythmia database [77]. ECG signals are contaminated with signals available in NSTDB MIT-BIH Noise Stress Test Database (NSTDB) [77] in several SNR levels. A support vector machine (SVM) is trained to classify ECG signals into five classes of quality. Feature extraction is performed and thirteen features (including all features introduced in [65]) are extracted. Different combinations of features are trained and tested and the optimum combination is selected and applied to SVM classifier. SVM is validated using MIT-BIH arrhythmia database [77] where an accuracy of $88.07 \pm 0.32\%$ is obtained.

Deep learning algorithms have also gained a lot of attention because of their ability to precisely execute complicated computational tasks, especially when it comes to big and complex data [78]. A Deep Belief Network (DBN) is a deep learning algorithm that is able to perform the feature extraction part of the learning process by itself [78]. This is an attractive property because feature extraction can be a time consuming and costly process. In the context of biomedical signals, DBNs have been applied to extract features from six ECG signal types for arrhythmia classification [79]. Benefiting from this feature of DBN, we will investigate its applicability for ECG signal quality analysis and assessment. DBNs are further explored in the next subsection.

2.2.3 Deep Belief Networks Architecture

In general, multiple processing layers composed of several linear and non-linear transformations can create deep architectures [80]. Such architectures have been assessed to be more effective than the other classifiers in image and audio data processing [81], [67], [82].

Hinton first introduced DBN [83]. The main idea of creating DBN is designing a stack of Restricted Boltzmann Machines (RBM), which uses training data to create an influential generative model. Each RBM is a neural network with one visible and one hidden layer. RBMs are principally a specific type of Boltzmann Machine with no connection between hidden units and no connection between visible units. Figure 2.7 shows how a general Boltzmann Machine differs from an RBM as it is used in DBNs.

In DBN, the hidden layer of each RBM plays the role of the visible layer of the next RBM. Obviously, this does not apply for the RBM on the top of the stack. Figure 2.8 demonstrates a regular stack of RBMs and also a stack of RBMs when they are attached in a way to create a DBN [84] and as it shows, DBN is a multi-layer neural network made of several layers of RBMs [79].

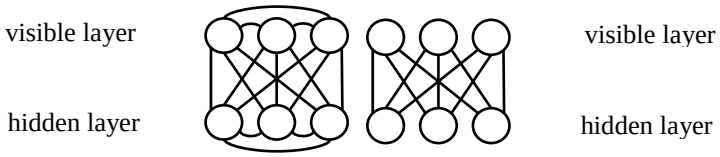

Figure 2.7 (a) General Boltzmann Machine, in which hidden and visible layers have internal connections as well as external connections (b) Restricted Boltzmann Machine, applied in DBNs, in which there is no internal connection in the visible or hidden layers

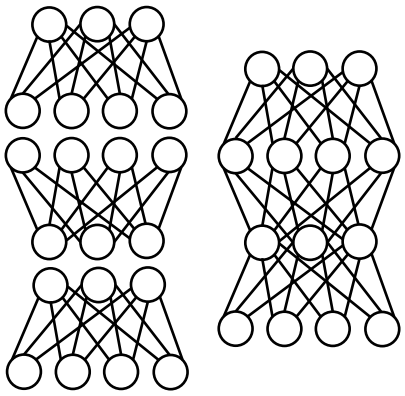

(a) (b)

Figure 2.8 (a) General Stack of RBMs, each RBM is independent from the others (b) Stack of RBMs when they are forming a DBN, hidden layer of each RBM is acting as the visible layer of the next RBM [84].

In a regular neural network having several hidden layers, there is always the risk of being trapped in a local minima. In addition, in such neural networks with many layers, a huge number of parameters are needed which make the training a time-consuming process. DBN is an alternative option to defeat such non-efficiencies and difficulties in neural network performance [85]. Training DBNs can be achieved by using a layer-wise greedy algorithm. RBMs are trained layer by layer, and then a fine-tuning process is performed to adjust all parameters of DBN and the combination of these two steps makes training of DBN a fast process [83].

2.3 Atrial Fibrillation

AFib occurs when the sinoatrial (SA) node (Figure 2.9), which is the heart's natural pacemaker, sends too many impulses, resulting in an irregular atrial activation at the rate of

350-600 beats per minute (bpm). Although not all of them can cause a heartbeat, it still results in a quick and irregular heart rate [86] between 100 to 175 bpm whereas a normal heart rate is 60 to 100 bpm.

1: Sinoatrial (SA) Node
2: Atrioventricular (AV) Node

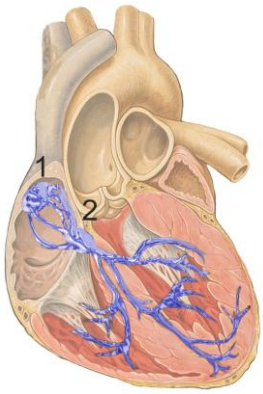

Figure 2.9 Heart diagram, SA and AV nodes (Wikipedia)

AFib is associated with a wide variety of symptoms such as dizziness, fatigue, weakness, chest pain and reduced ability to exercise. Clinical events associated with AFib include death, stroke and hospitalization. Rate of death is doubled in patients with AFib and risk of stroke is dramatically increased and results in more severe consequences such as long-term disability [87]. The reason why the risk of stroke is high in people having AFib is that blood may not be pumped sufficiently out of the heart, resulting in conditions that can promote blood clots to form inside the heart. Clots formed inside the heart during atrial fibrillation episodes begin to move once the patient's heart rhythm gets back to normal [88]. Such clots can block blood circulation and increase the risk of stroke.

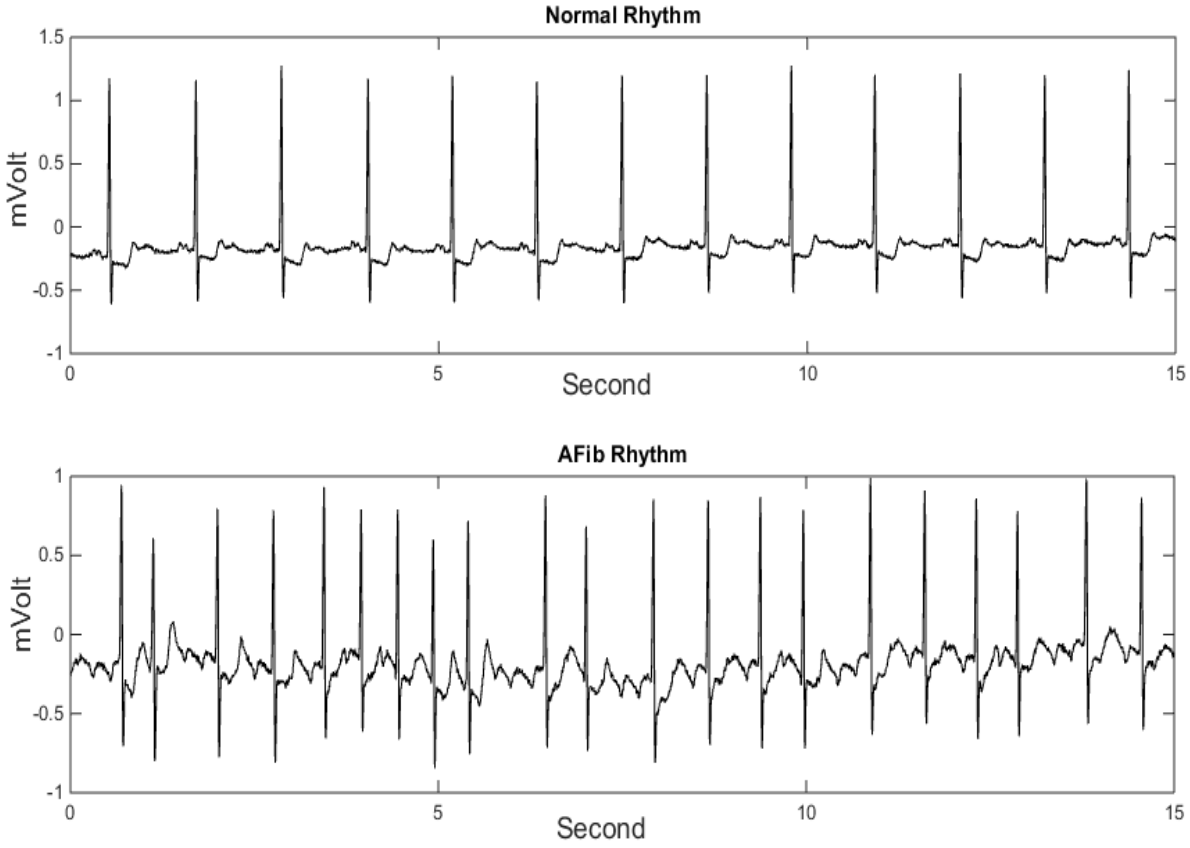

Figure 2.10 Normal and atrial fibrillation ECG

Additionally; hospitalization in patients with AFib is frequent and contributes to low quality of life and exercise [86].

Figure 2.10 compares a regular sinus ECG and an atrial fibrillation ECG from recording "07910" of the MIT-BIH Atrial Fibrillation Database [77].

Chapter 3 **Effect of Pressure**

3.1 Introduction

Wearable devices have garnered a great deal of attention as they offer the potential to become an effective state-of-the-art tool enabling people to take care of their health, for medical or non-medical purposes.

A common functionality of these devices is to acquire biosignals. Biosignals can be acquired noninvasively using biopotential electrodes placed on the surface of the skin. These biopotential electrodes then serve as the transducers between the body and the measurement device. Selection of an appropriate electrode is important for ensuring a good quality signal; however, potentially competing considerations are usability factors. Disposable non-polarizable biopotential electrodes (e.g., Ag/AgCl) may be preferable in a clinical environment for individual, short-term monitoring tests; whereas, reusable, washable dry

electrodes are preferred in wearable devices. While dry, polarizable electrodes have traditionally been thought to have poor performance compared to wet, non-polarizable electrodes, research has demonstrated that the recorded signal quality can be comparable [39], [89].

The skin–electrode impedance plays a major role in the quality of biosignal recordings [16], [17]. Many wearable devices use some sort of elastic material to conform to the body shape and to provide pressure in order to ensure good contact between the skin and the electrode. Electrodes can be integrated in this manner into a variety of wearable form factors, including belts, bands, shirts, and pants. Tighter fitting clothing may increase the applied pressure, decreasing the skin–electrode impedance, which in turn improves the quality of biosignal recordings, but they may also reduce comfort, especially during extended recording periods. In addition, muscle contractions and respiration can alter the body volume under the electrodes; this would affect the tightness of clothing, modulating the applied pressure on the electrode, which in turn would modulate the skin–electrode impedance. Changes in skin–electrode impedance can affect the quality of biosignal recordings and can result in measurement contaminants, such as motion artifact [17], [90]. In [9], it was shown that QRS detection is influenced by the skin–electrode impedance and its effects cause a risk of misinterpretation of the ECG. Similar issues were noted for ECG acquisition in ambulatory assistive devices, where electrodes were integrated in the handles of a rollator, and the grip and loading forces varied during recordings [91]. Skin–electrode impedance information could be applied as an indication of motion artifact [92] and can be used in adaptive methods to mitigate motion artifact [93].

In this thesis, we extend our previous study in [52], where we measured the skin–electrode variation, as pressure was applied, for one electrode type (conductive textile) and for three subjects. In that research, impedance was measured as pressure was step-wise increased to a high pressure (16 kPa); the context of this previous work was blood pressure monitoring with ECG. In this thesis, we examine applied pressure and its impacts on the skin–electrode impedance in the context of wearable devices. Three electrode types are examined as pressure is repeatedly applied and removed over several trials and for six subjects. We also verify the reversibility of the skin–electrode impedance variations before applying pressure and after removing it. An electric circuit is used to model the electrode impedances to better understand the resultant changes in skin–electrode impedance. The main contributions of this chapter of the thesis can be summarized as:

1) Studying the variation of skin–electrode impedance associated with three electrode types: Ag/AgCl electrodes, conductive textile and Orbital electrodes under pressure. We propose a data acquisition procedure and pressure applying method in order to measure skin–electrode impedance variation with and without applying pressure. All measurements are performed for six subjects. We will demonstrate how the impedance changes when pressure is applied and removed. Results obtained from all electrode types are compared.

2) We parameterize the skin–electrode impedance with Cole–Cole impedance model [29], [30]. We extract these components of the skin–electrode impedance and measure their variation rate in response to applying pressure. We investigate how each component varies in each electrode type and compare them.

3) Irreversible changes in skin–electrode impedance and its corresponding components that occur due to applying pressure is also verified in three electrode types and they are compared in terms of the extent they sustain the changes after we remove the pressure.

3.2 Methods

3.2.1 Electrodes

Three types of electrodes are utilized in this research: 1) Ag/AgCl surface electrodes (Model T-00-S/25, Ambu Blue Sensors T), 2) conductive textile electrodes (medical grade silver plated 92% nylon and 8% dorlastan stretchable conductive fabric with the thickness of 0.50 mm) and 3) Orbital electrodes (Orbital Research Inc., Cleveland OH, USA). All three are shown in Figure 3.1 and are referred to in this research as Ag/AgCl, conductive textile, and Orbital electrodes, respectively. The Ag/AgCl electrodes are wet electrodes, pre-gelled with an electrolytic gel, whereas conductive textile and Orbital electrodes are dry electrodes. These Ag/AgCl electrodes have a diameter of 10 mm and are used extensively in research and in clinical practice, including EMG and ECG recordings. Conductive textile electrodes are basically made of silver coated nylon filaments (AgNy). Each textile electrode is a 3cm x 30cm strip and is wrapped around the subjects' biceps during the measurement procedure. The results will be applicable to ECG wearable devices, however; ECG electrodes might be on the chest, still the trend of variations of the impedance and components of representing equivalent model will be the same. These electrodes have been used in wearable devices and also for collecting ECG, EEG and EMG signals for research purposes. The Orbital electrodes have a diameter of 25.0 mm and have an array of micro-features that embed themselves in the stratum corneum layer of the skin. The objective of these micro-features is to circumvent the

need for an electrolytic gel or skin preparation [94]. These electrodes are targeted for ECG acquisition. A larger sized electrode results in a larger contact area, which leads to smaller absolute impedance. We mainly investigate relative impedance changes to account for size differences between electrode types.

(a) (b) (c)

Figure 3.1 Electrodes used in this research: (a) Ag/AgCl, (b) Conductive textile, and (c) Orbital electrodes

3.2.2 Measurement Set up

Skin–electrode impedance was measured with a pair of electrodes that were placed above the right biceps. Electrodes were spaced 7 cm apart, as shown in Figure 3.2. A snap electrode lead was used to interface the electrodes to the impedance measurement system. Since our objective is to simulate the use case of a home health care device, we avoided the use of skin preparation. While skin preparation would improve the skin–electrode impedance, it can be a barrier to use by non-expert users due to issues such as comfort, convenience, and time. The Omron Heart scan and the FavoritePlus Easy ECG are examples of popular portable ECG recording devices that do not instruct users to perform any skin preparation. Various electrode types, including conductive textiles, have shown good promise in delivering adequate signal quality without skin preparation [89], [95], [96]. From a usability standpoint, wearable devices that do not require skin preparation are ideal and more easily accepted by users. The literature

also suggests that adequate signal quality can be obtained without any skin preparation [39], [89], [95], [97]. Orbital electrodes, used in this study, were in fact designed to avoid the need for skin preparation [98]. It is also noted that no significant amount of hair was observed at the electrode sites (anterior part of arm, above the biceps) for any of the subjects who participated in this study. We also measured the skin–electrode impedance of one subject, with and without skin preparation (cleaning the area with alcohol wipe); results are presented in Figure 3.3. As expected, the measured impedance for each electrode with skin preparation is lower than the impedance without skin preparation; however, differences were not large. Cleaning with an alcohol wipe is limited skin preparation but would be as much as would be expected by wearable device users. Large difference in impedance measurements as result of this skin preparation are not anticipated. Invasive skin preparation methods that could yield large decreases in impedance measurements, such as skin abrasion using sand paper, are not performed in this study.

Results of this research can help us understand how each type of electrode in an actual wearable device will react under the pressure which will be applied on it during users' breathing, moving and bending.

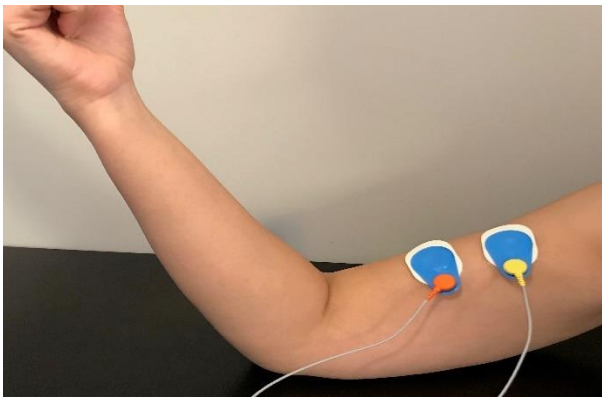

Figure 3.2 Electrode placement on the bicep

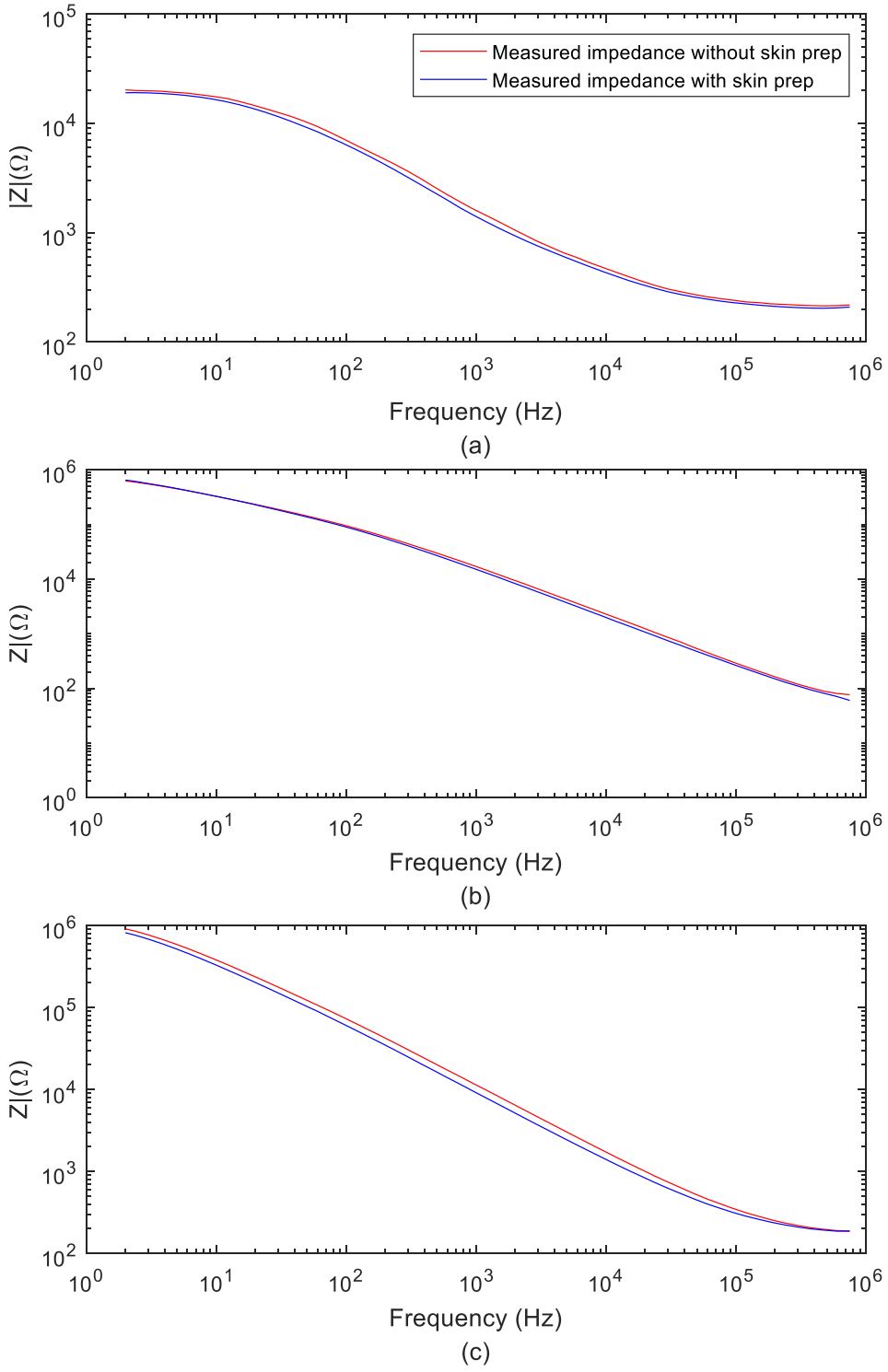

Figure 3.3 Measured impedance with and without skin preparation a) Ag/AgCl, b) Conductive textile and c) Orbital electrodes

We utilized commercially available state-of-the-art devices that are designed specifically for this purpose in order to measure skin electrode impedance variation over a particular frequency range. A block diagram of the experimental setup is shown in Figure 3.4. This represents a two-electrode configuration that includes a frequency response analyzer (FRA) (Model 1255B, Solartron Analytical, UK) and an impedance interface device (Model 1294A, Solartron Analytical, UK), as well as a personal computer. Skin–electrode impedance was measured, using a 100 μA AC current. We measure 10 points per decade, averaging 30 cycles per frequency, sweeping the frequency from 750 KHz down to 2 Hz. Each impedance measurement took approximately two minutes to complete. The impedance measurement includes impedance of the two electrodes plus the underlying tissue impedance, which is modeled in Figure 3.5.

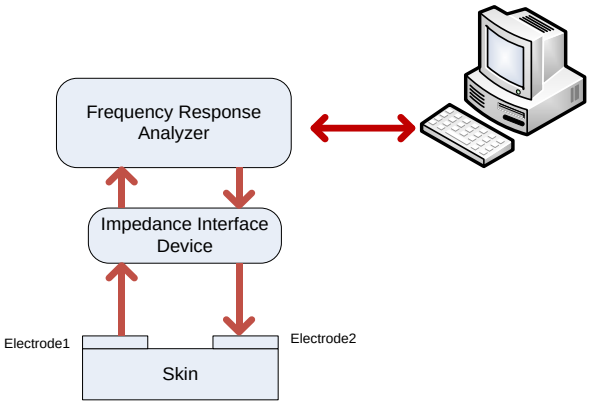

Figure 3.4 Experimental setup for skin–electrode interface measurement

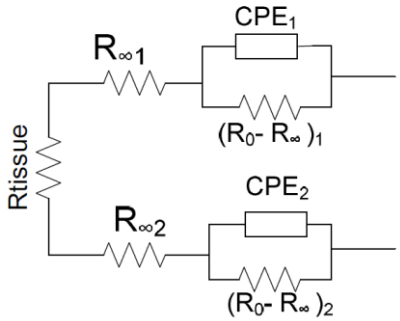

Figure 3.5 Schematic view of skin–electrode impedance measurement

Measurements were carried out on six healthy subjects (4 females, 2 males). None of the volunteers were taking any medication or had a known history of cardiovascular disease. Table 3.1 shows subjects' characteristics in terms of sex, height, weight, body mass index (BMI) and age. The research was reviewed and approved by the Carleton University Research Ethics Board.

Table 3.1 Subjects' characteristics

	Sex	Height (cm)	Weight (Kg)	BMI	Age
Subject1	Female	172	68.0	23.25	36
Subject2	Female	163	70.3	26.45	26
Subject3	Male	177	95.0	30.32	66
Subject4	Female	163	47.0	17.69	28
Subject5	Male	177	71.0	22.66	35
Subject6	Female	164	72.8	27.06	31

3.2.2.1 Applying Pressure to the Electrodes

In order to investigate the effects of applying pressure to the electrodes, we designed our own system for applying pressure using a blood pressure cuff. This system consists of a microprocessor (CC2531F256, Texas Instruments), a motor, a pump, a bleed valve, a pressure sensor (26PC series, Honeywell) and an Omron blood pressure cuff. We apply pressure by inflating the cuff while the electrodes are located underneath the cuff. The pressure sensor is sensing the pressure inside the cuff, which the microprocessor uses to turn on the motor to drive the pump and inflate the cuff to the desired pressure and maintain the pressure due to any pressure leakage in the system. Therefore, we have a constant level of pressure during each measurement.

3.2.2.2 Experimental Procedures

Each electrode type is tested separately for six subjects. Measurements are done first for Ag/AgCl electrodes. On a separate day, we repeated the procedure for conductive textile and Orbital electrodes. There was a five-minute waiting period between conductive textile and Orbital electrodes measurements. A new Ag/AgCl electrode was used each time; whereas the other electrodes were reused. The electrodes and the blood pressure cuff were placed on the subject's bicep, as shown in Figure 3.6. The impedance was measured in eleven trials with the cuff pressure in each trial shown in Table 3.2. The first eight trials the cuff was alternating between 0 Pa and 4 kPa (30mm Hg). 4 kPa is almost 1/3 of the lowest pressure which is applied by a blood pressure cuff during a blood pressure measurement, since normal diastolic pressure is around 90mm Hg. We also check with the subjects if they feel comfortable with this level of applied pressure on their biceps. 4 KPa is just enough to stay in contact with the body but not annoying and this is what we expect in wearable devices. In the last three trials,

the pressure was kept at 0 Pa to observe the reversibility of pressure loading effects on skin–electrode impedance. There was a one-minute waiting period between each two consecutive measurement trials. The entire measurement procedure is summarized as follows:

a. Both electrodes are placed on the subject's right bicep at a 7 cm distance from each other and connected to the Solartron devices.

b. The Omron cuff is wrapped around subject's bicep on top of the electrodes.

c. The pressure is set to 0 Pa or 4 kPa appropriate for the trial (Table 3.2).

d. Wait for 1 minute.

e. The impedance is measured by the Solartron device (~ 2 minutes).

f. Repeat, starting from step c, until all trials are completed.

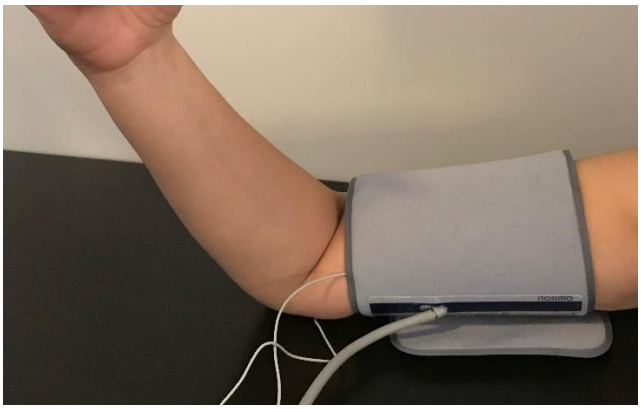

Figure 3.6 Cuff placement on the bicep

Table 3.2 Cuff pressure per trials

Trial	**T1**	**T2**	**T3**	**T4**	**T5**	**T6**	**T7**	**T8**	**T9**	**T10**	**T11**
Cuff pressure (Pa)	0	4k	0	4k	0	4k	0	4k	0	0	0

3.2.3 Skin–Electrode Impedance Modeling

The parameters of Cole–Cole model are estimated for each impedance measurement. As noted in Section II-B, the impedance measurements include the skin–electrode impedance of two electrodes and the impedance associated with the body tissue between the electrodes. Since the electrodes we apply are identical in terms of type, material and size, we assume that they have equal skin–electrode interface impedance (i.e., $C=C_1=C_2$, $\alpha=\alpha_1=\alpha_2$, $R_\infty= R_{\infty 1}= R_{\infty 2}$, $R_0\text{-}R_\infty= (R_0\text{-}R_\infty)_1 = (R_0\text{-}R_\infty)_2$). The resistance of tissues between two electrodes, R_{tissue}, is expected to be small; a value of approximately 150 Ω was measured at the middle of the upper arm [40]. Here we assume R_{tissue} = 0, so any tissue impedance will be integrated into the estimate of R_∞. Therefore, the skin–electrode impedance for a single electrode is considered as the measured impedance value divided by two.

A least squares nonlinear curve fitting method is used to estimate the model parameters (C, α, R_∞ and R_0) from the skin–electrode impedance measurements. The curve fitting algorithm required the initialization of each parameter. According to the electrical model, at high frequencies the impedance approaches R_∞, and as the frequency approaches zero, the impedance approaches R_0. Applying this fact, the initial value for R_∞ is set as the impedance measured at the highest frequency ($R_{\infty INIT} = Z(750\ kHz)$). The initial value for $R_0\text{-}R_\infty$ is set as the impedance measured at the lowest frequency, less R_∞, ($R_{0\ INIT} = Z(2\ Hz)$). It should be mentioned that τ is known as the characteristic time constant of the impedance and is equal to $[(R_0\text{-}R_\infty)C]^{1/\alpha}$ [33]. In order to calculate α, first we need to find φ_{CPE} as shown in Figure 3.7.

$$Z(\omega) = R_\infty + \frac{R_0 - R_\infty}{1+(j\omega\tau)^\alpha} = Z' + jZ'' \quad \text{and} \quad (j\omega)^\alpha = \omega^\alpha \left[cos\left(\frac{\alpha\pi}{2}\right) + jsin\left(\frac{\alpha\pi}{2}\right)\right]. \tag{3.1}$$

Thus $\varphi_{CPE} = \alpha\pi/2$ could be calculated and therefore α is known and we take it as its initial value (α_{INIT}) and on the other hand real part of the impedance (Z') has its maximum value at

the frequency of $1/\tau$. Therefore we can compute τ which is also equal to $[(R_0-R_\infty)C]^{1/\alpha}$. C is found to be $\tau^{\alpha}/(R_0-R_\infty)$ and the calculated value of C is also taken as its initial value (C_{INIT}).

Employing this procedure enables us to find the values of R_∞, R_0-R_∞, α and C for each measurement.

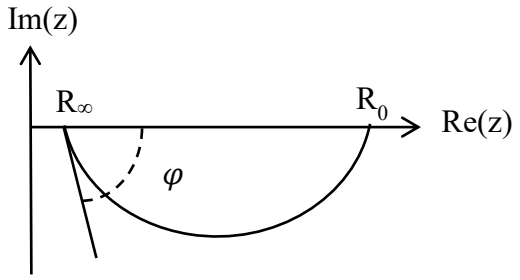

Figure 3.7 Impedance loci used to extract parameter set (R0, R∞, τ, α) (based on [33])

We picked an impedance measured in one of our trials for one of subjects (subject 1, trial 1, conductive textile electrode) randomly to illustrate the curve fitting. The least squares curve fitting on the experimental data from that trial returned the following values for the three components:

R_∞ = 207.5 Ω, R_0 = 1.08 M Ω, C = 1.92 nF, α = 0.942

In order to compare the obtained data and observed one, we substituted the values of the components in Equation (2), which shows the mathematical relation between $|Z(\omega)|$ and its four components including R_0, R_∞, α and C. Figure 3.8a illustrates the result graph of obtained $|Z(\omega)|$ and observed graph data on the same plane for comparative purposes and Figure 3.8b and c visualize our model and observed data real and imaginary parts respectively.

$$Z(\omega) = R_\infty + \frac{R_0-R_\infty}{1+(j\omega)^{\alpha}(R_0-R_\infty)C} = Z'(\omega) + jZ''(\omega) \quad (3.2)$$

Figure 3.8c shows a noticeable difference between imaginary part of the model and its corresponding measured value in low frequencies. This can be explained by the fact that we neglect the impedance of the tissue between two electrodes (2.1.2), while it has not only resistance but also some capacitance [99], especially in low frequencies. The tissue capacitance tries to keep the imaginary part of the measurement negative while imaginary part of the model tends to return to zero, because the impedance of the model when frequency is 0 approaches R_0 which is real and thus its imaginary part is equal to 0.

3.3 Results

In this thesis, we expand our preliminary measurements done for three subjects and one electrode type (conductive textile) [52]. We perform the measurements for more subjects and three different types of electrodes to compare their behavior when applying pressure and discuss their appropriateness for use in wearable devices. According to this and to achieve our objective in terms of comparing different parameters in obtained results, we present them as follows.

1- Skin–electrode impedance across five trials (trials 1,2,7,8 and 11), one subject (subject1) and three electrode types (Figure 3.9)

2- Skin–electrode impedance variation in 30 Hz frequency, for eleven trials, three electrodes types and six subjects (Figure 3.10)

3- Reversibility of skin–electrode impedance (Table 3.3)

4- Component *C* variation in eleven trials, six subjects and three electrode types. *C* is normalized to its value in the last trial (Figure 3.11).

5- Component R_0 variation in eleven trials, six subjects and three electrode types. R_0 is normalized to its value in the last trial (Figure 3.12).

6-Component R_∞ variation in eleven trials, six subjects and three electrode types. R_∞ is normalized to its value in the last trial (Figure 3.13).

7-Component α variation in eleven trials, six subjects and three electrode types. α is normalized to its value in the last trial (Figure 3.14).

8- Reversibility of the skin–electrode impedance components (Table 3.4, Table 3.5)

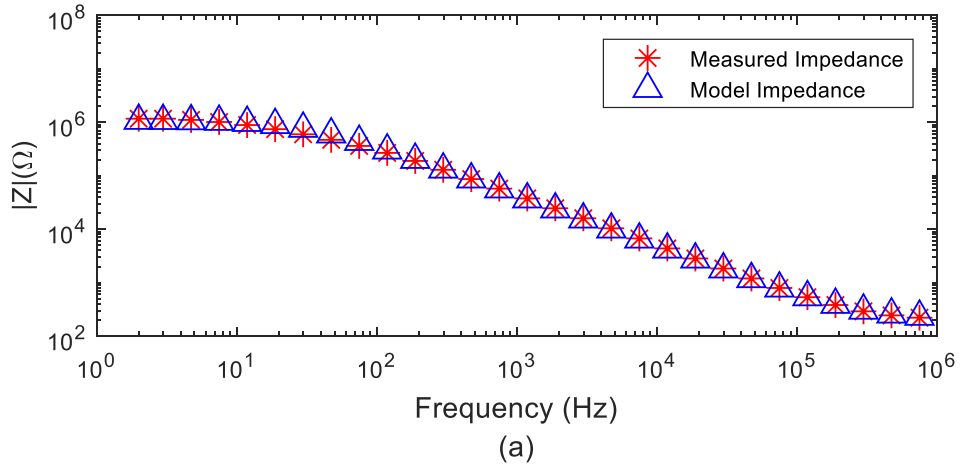

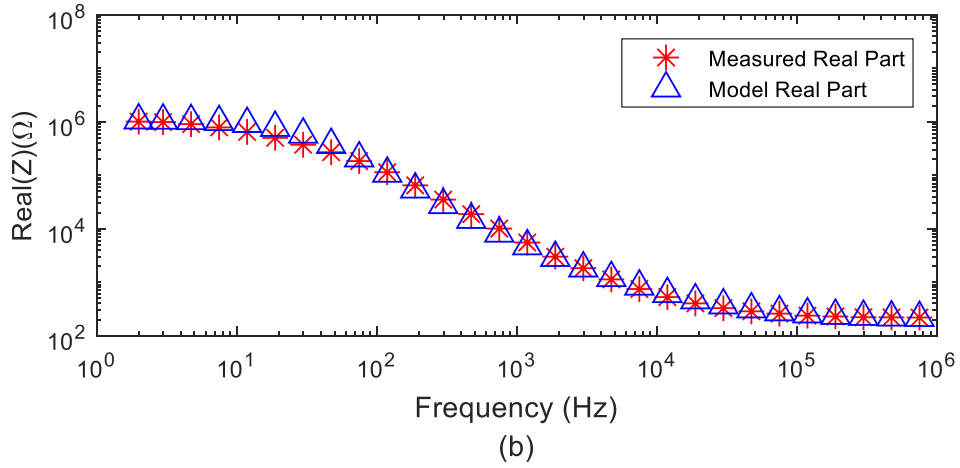

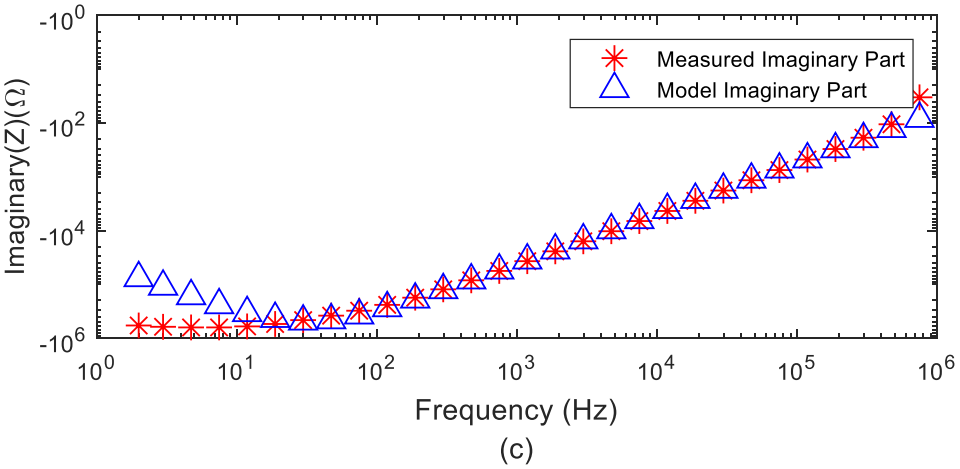

Figure 3.8 a) Measured impedance and the corresponding skin–electrode model impedance, b) Real part of measured and model impedance and c) Imaginary part of measured and model impedance

The reason why we picked trial 11 and not trial 1 for normalizing values, is that trial 11 better represents the "settled" skin–electrode impedance and it is more important to know how the impedance is relative to this value. Another reason is that impedance measured in trial 1 would be highly variable because it is the initial application of the electrode. If for example, the initial application was very poor with little skin–electrode contact, the initial impedance would be extremely high and normalizing to this would make all other values a really small percentage.

Figure 3.9 depicts the magnitude of the skin–electrode impedance for Subject 1 for three electrodes, showing the skin–electrode impedance of the first and last 0 Pa/4 kPa pair (trials 1,2, 7 and 8), and the last trial (trial 11). All electrodes have lower impedance when pressure is applied for the first time (trial 2) compared to their initial state (trial 1) and this is consistent with what we observe in the last 0 Pa/4 kPa pair (trials 7 and 8). However, we observe a smaller change in the last 0 Pa/4 kPa pair compared to the first 0 Pa/4 kPa pair. Skin–electrode impedance value in the last trial (trial 11) is close to its value in the last pressure applying trial (trial 8) which shows the irreversible changes in skin–electrode impedance after several pressure loading and unloading trials. Ag/AgCl electrode shows the smallest value of skin electrode impedance and also the smallest amount of variation due to applying pressure (Figure 3.9). The conductive textile has the largest skin–electrode impedance and shows the largest amount of variation before and after applying pressure. The low variation in skin–electrode impedance for Ag/AgCl electrodes and relatively high variation for conductive textile electrodes was consistent for all subjects.

Figure 3.10 depicts the magnitude of the skin–electrode impedance measured at 30Hz for six subjects, for all electrode types. We pick 30Hz because our interest is studying effects of

electrodes on biosignals, which are of low frequencies. In addition, many commercial electrode impedance meters test at this frequency.

For all electrodes and subjects, the impedance generally decreases with increasing trials. Ag/AgCl electrodes show the smallest variation among three electrode types and the impedance does not change dramatically with and without pressure (Figure 3.10a).

For conductive textile, an obvious pattern with increased pressure is observed, where applying pressure decreases impedance and removing pressure increases it (Figure 3.10b). This pattern is present but less obvious with Orbital electrodes (Figure 3.10c). Such a pattern is not visible with Ag/AgCl (Figure 3.10a). Larger changes in impedance are experienced in earlier trials and maximum decrease is associated with the initial pressure application (trial 2). The fluctuations of the impedance become smaller and smaller after each pressure trial compared to the last pressure trial.

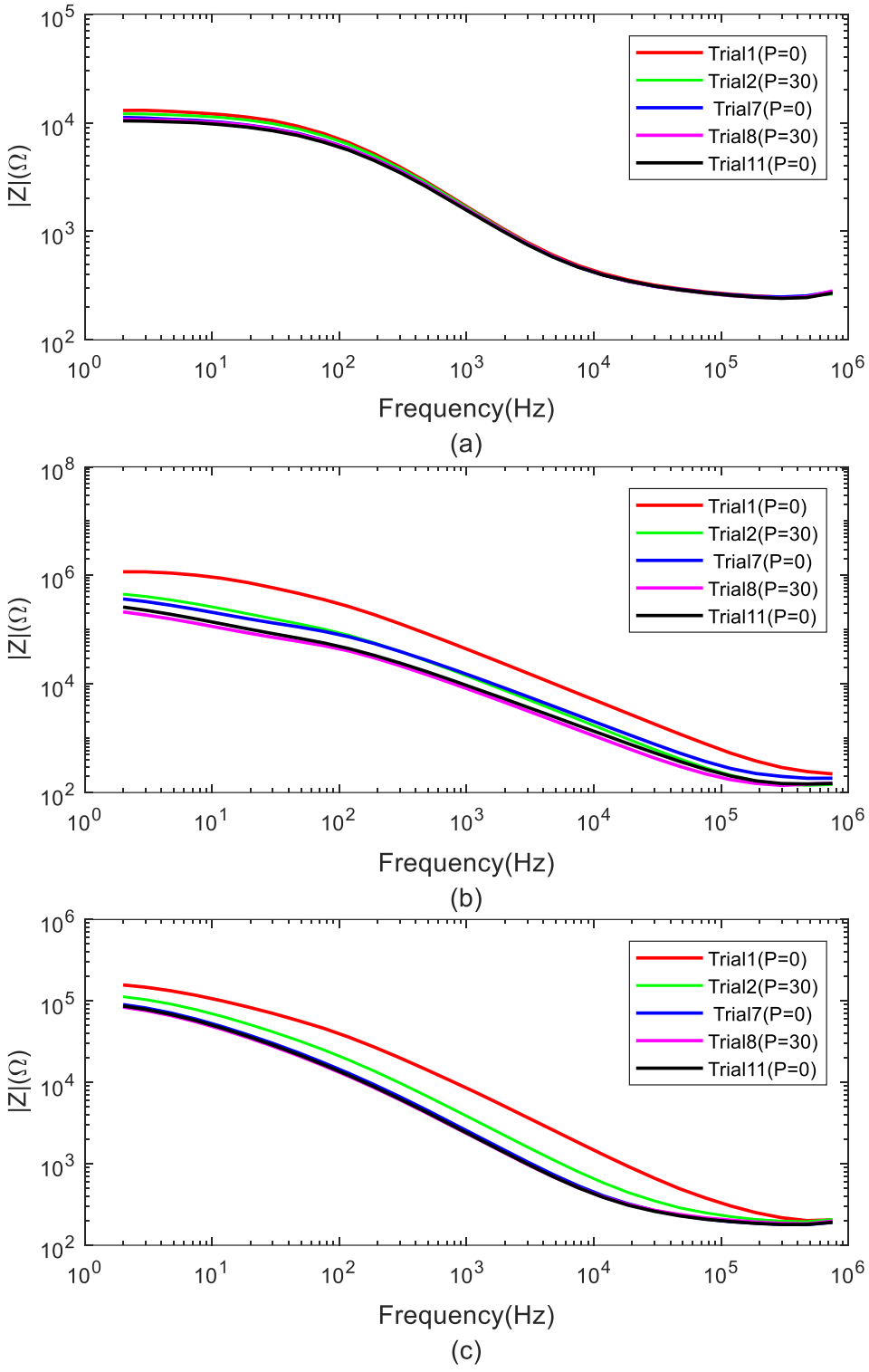

Figure 3.9 Skin–electrode impedance for three electrodes, Subject1 a) Ag/AgCl, b) Conductive textile and c) Orbital electrodes

This is to be expected as no skin preparation was done and so the skin–electrode contact is expected to be initially poor, which can be improved with applied pressure. As well, there is electrode settling, where the skin–electrode impedance decreases with time. In last three trials, which are all done without applying pressure, there is a little change compared to the last pressure trial (trial 8). This suggests that effects are irreversible from their initial state and any electrode settling is relatively stable by trial 8. Table 3.3 shows all electrodes' impedance variation normalized to the last trial, their average over 6 subjects and also measured impedance in trial 8, normalized to the measured impedance at the last trial. We observe that Ag/AgCl electrodes are fairly stable and after releasing the pressure keep the impedance almost equal to the last time pressure is induced (Average (Z8/Z11) = 1.06), whereas conductive textile shows the maximum variation in the first trial among all three electrode types. All electrodes are subject to irreversible changes and Z8/Z11 ratio is close to one. Having the minimum value of this ratio compared to the other electrode types, conductive textile is the one which keeps the changes less than others.

Table 3.3 Measured impedance at the first trial (Z1) and the last time pressure is applied (Z8) normalized to the last measurement (Z11)

	Z_1/Z_{11} Range (f=30Hz)	**Z_1/Z_{11} Average (f=30Hz)**	**Z_8/Z_{11} Range (f=30Hz)**	**Z_8/Z_{11} Average (f=30Hz)**
Ag/AgCl	1.24 to 1.90	1.49	1.06 to 1.10	1.06
Conductive Textile	1.67 to 7	4.47	0.67 to 0.93	0.79
Orbital electrodes	0.92 to 7.06	2.74	0.95 to 1.01	0.98

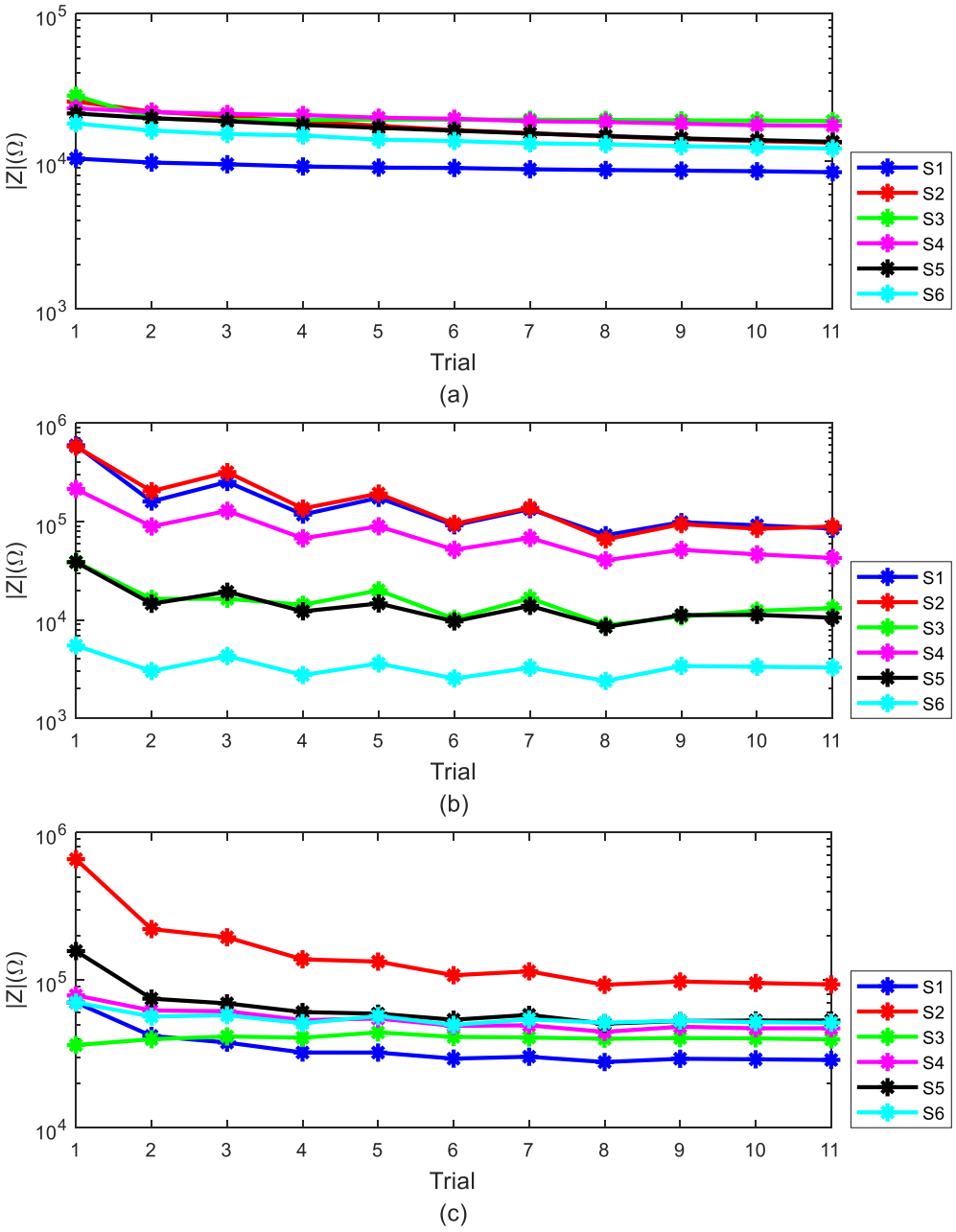

Figure 3.10 Measured Impedance at f=30 Hz, a) Ag/AgCl, b) Conductive textile and c) Orbital electrodes

To visualize how the circuit model components variations during applying pressure and releasing it, they are plotted as a function of trial. These values are normalized to the values from the last trial.

Figure 3.11 shows the variation of C per trial for six subjects and for all electrodes. For Ag/AgCl electrodes, C slightly increases and does not come back to its initial value after removing the pressure, as opposed to conductive textile and Orbital electrodes which in them, C goes up when applying pressure and goes down when releasing it; however, it still remains higher than its previous value. This leads to a generally increasing irreversible trend for C in these two electrode types. As Figure 3.11 shows, we observe the strongest fluctuations of C in conductive textile. Ratio of C in the first trial to C in the last trial in Ag/AgCl electrodes varies from 0.96 to 1.15 from subject to subject and the average is equal to 1.05 while this ratio for conductive textile varies from 0.14 to 1.00 and the mean value is 0.46. For Orbital electrodes this ratio varies from 0.05 to 0.70 with the average of 0.40 (Table 3.4).

Figure 3.12 depicts the variation of R_0 per trial for six subjects and for all electrodes. As it can be observed in these graphs, R_0 keeps decreasing in Ag/AgCl electrodes, regardless of applying pressure or releasing it. In conductive textile electrodes, this component goes down with applying pressure and again goes up when releasing it, but it still remains lower than its previous value under pressure (Figure 3.12 b). Therefore, it has a general decreasing trend. In Orbital electrodes, R_0 keeps decreasing in applying pressure measurements and stays the same in the next non-pressure trial (Figure 3.12 c). It also has a general decreasing trend in the entire process including eleven trials. In one subject (S3) we observe an increasing trend for this component. Ratio of R_0 in the first trial to R_0 in the last trial in Ag/AgCl electrodes varies from 1.28 to 2.99 with the average of 1.75 and this ratio for conductive textile fluctuates from 2.03 to 6.75 and the average is equal to 3.74, while this ratio for Orbital electrodes is in the range of 0.64 to 4.42 with the average of 2.03 (Table 3.4).

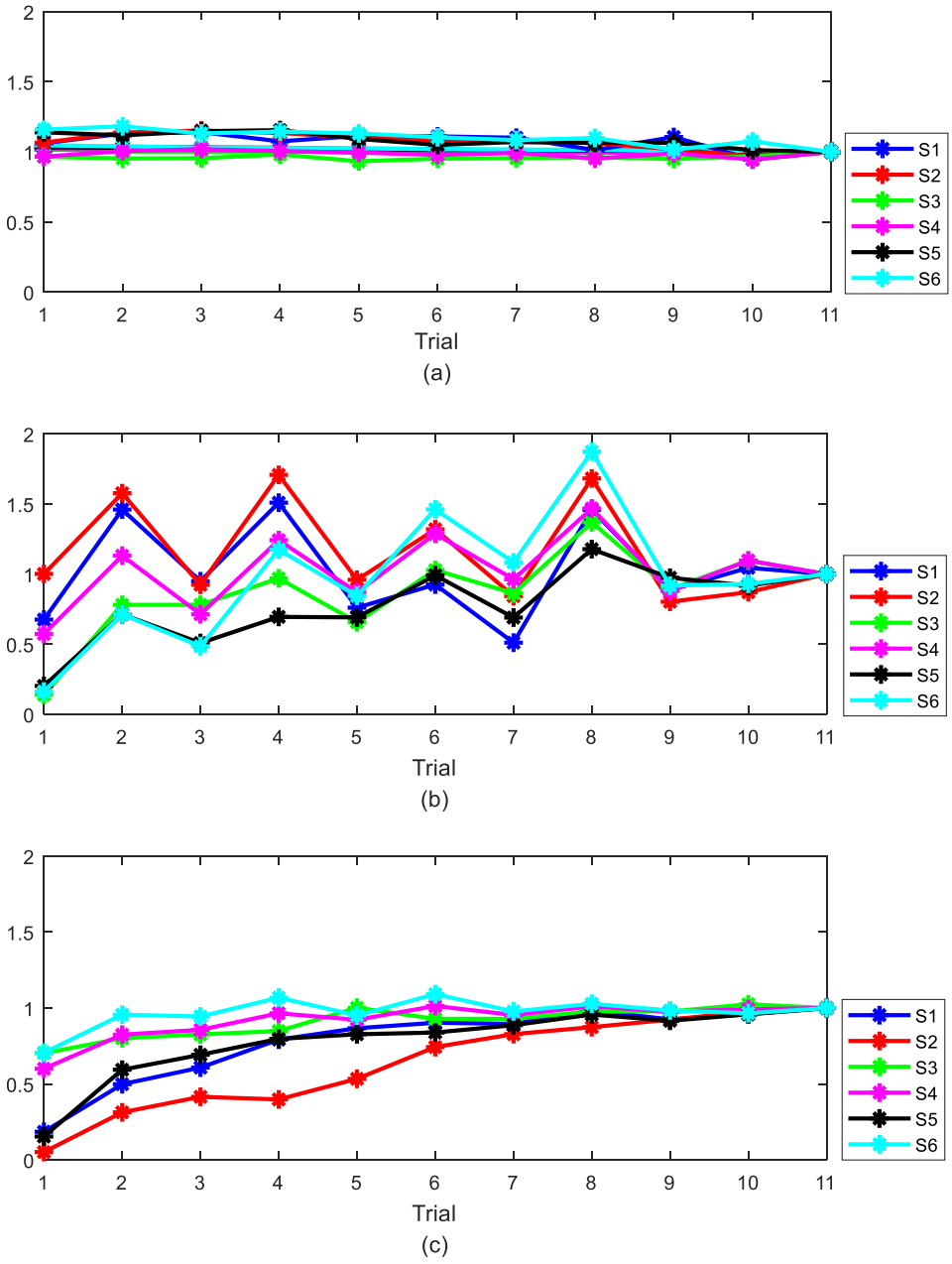

Figure 3.11 a) C Ag/C Ag (trial11), b) C Textile/C Textile (trial11), c) C Orbital/C Orbital (trial11)

As electrical equivalent circuit (Figure 2.4) shows, the skin–electrode impedance is dominated by R_0 at low frequencies. Noninvasive biosignals are comprised of primarily low

frequencies (e.g., ECG < 250 Hz, EMG < 500 Hz, and EEG < 150 Hz). Hence; R_0 is the parameter that determines the electrodes' behavior throughout these experiments. This parameter R_0 appears to have more sensitivity with dry electrodes (Conductive textile and Orbital) as compared to wet electrodes (Ag/AgCl); however, for many applications such as wearable devices, reusable dry electrodes are preferable [89], [100]. It does appear that skin–electrode impedance remains relatively stable once an initial pressure is applied, even when it is removed after a while. This suggests that dry electrodes may have a lot of noise initially in a wearable device, but this noise level quickly reduces as the skin–electrode impedance stabilizes.

Figure 3.13 depicts the variation of R_∞ per trial for six subjects and for all electrodes. R_∞ in Ag/AgCl and Orbital electrodes do not show much change in pressure and non-pressure trials (Figure 3.13a and c). In conductive textile, R_∞ is affected by pressure with a modulation pattern consistent with the loading and unloading (Figure 3.13b). Ratio of R_∞ in the first trial to R_∞ in the last trial in Ag/AgCl electrodes varies from 0.98 to 1.08 with the average of 1.03 and this ratio for conductive textile varies from 0.12 to 1.66 and its average value for all 6 subjects is 1.02. This ratio for Orbital electrodes varies from 1.06 to 2.08 with the average equal to 1.01 (Table 3.4). Estimated components in the first trial (P = 0) and the last time pressure is applied (trial 8, P = 4 kPa) normalized to the last trial (trial11, P = 0) are also calculated and shown in Table 3.4.

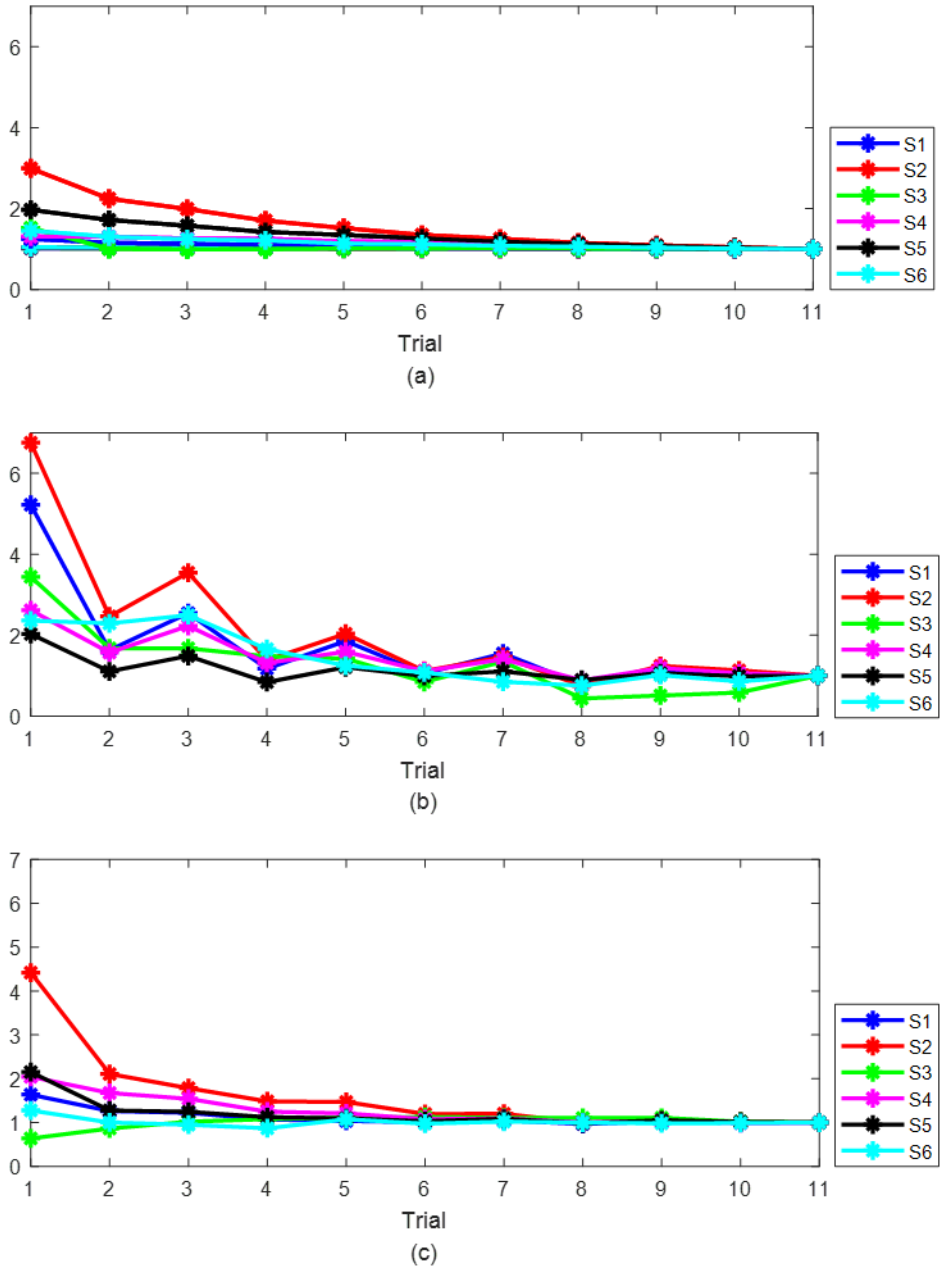

Figure 3.12 a) (R0)Ag/ (R0)Ag (trial11), b) (R0)Textile/ (R0)Textile (trial11), c) (R0)Orbital/ (R0)Orbital (trial11)

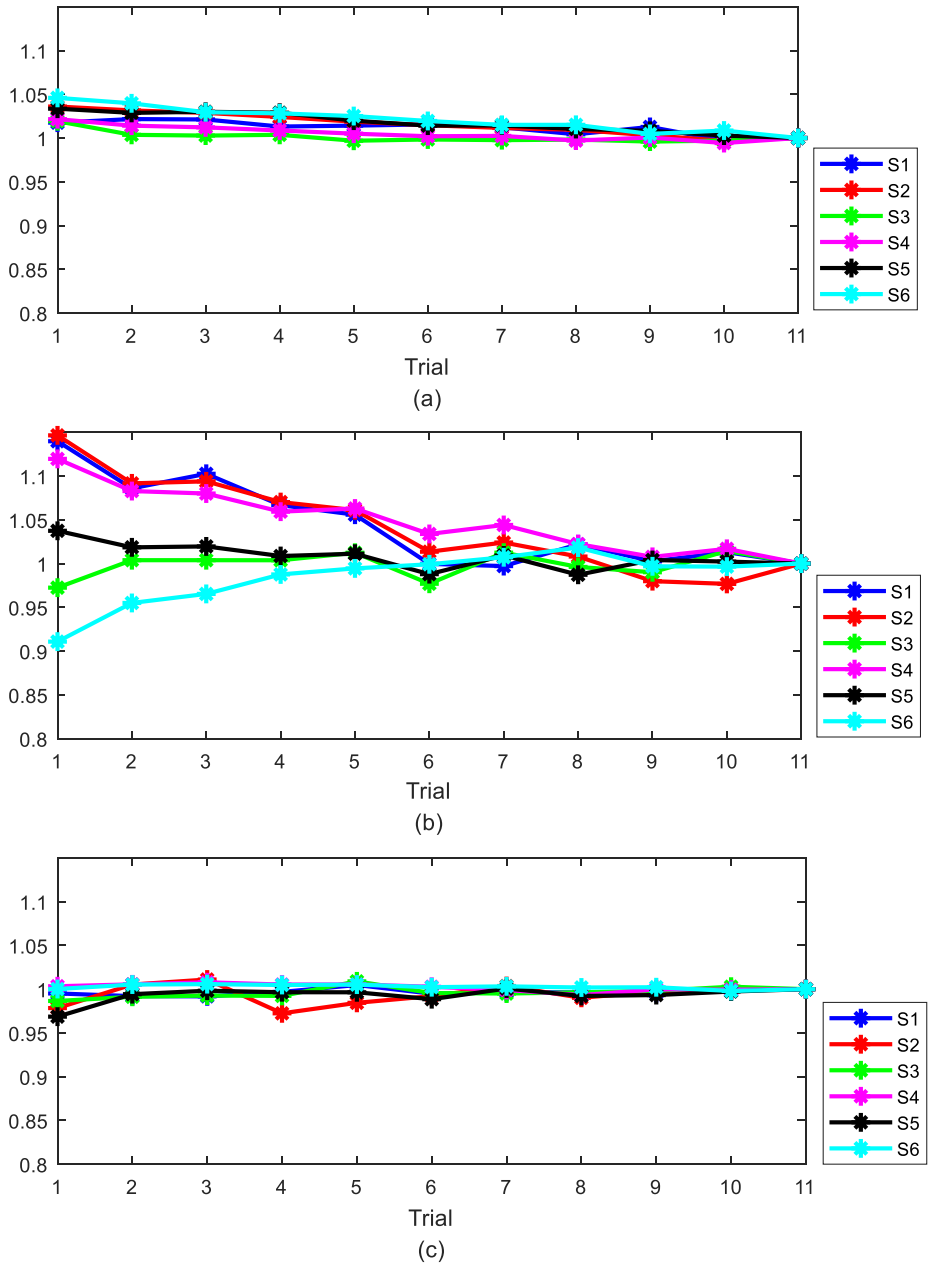

Figure 3.13 a) R∞Ag/ R∞Ag (trial11), b) R∞Textile/ R∞Textile (trial11), c) R∞Orbital/ R∞Orbital (trial11)

Figure 3.14 shows the variation of α in each trail for all subjects and three types of electrodes. In Ag/AgCl and Orbital electrodes, α does not show much change in pressure and non-pressure trials and is almost stable. However, in textile electrodes changes are more

readily observed. For four subjects out of six, α decreases under pressure and increases when unloading the pressure. Ratio of α in the first trial to α in the last trial in Ag/AgCl electrodes varies from 1.02 to 1.04 with the average of 1.02 and this ratio for conductive textile varies from 0.91 to 1.14 and its average value for all 6 subjects is 1.05. This ratio for Orbital electrodes varies from 0.97 to 1.00 with the average equal to 0.99 (Table 3.5).

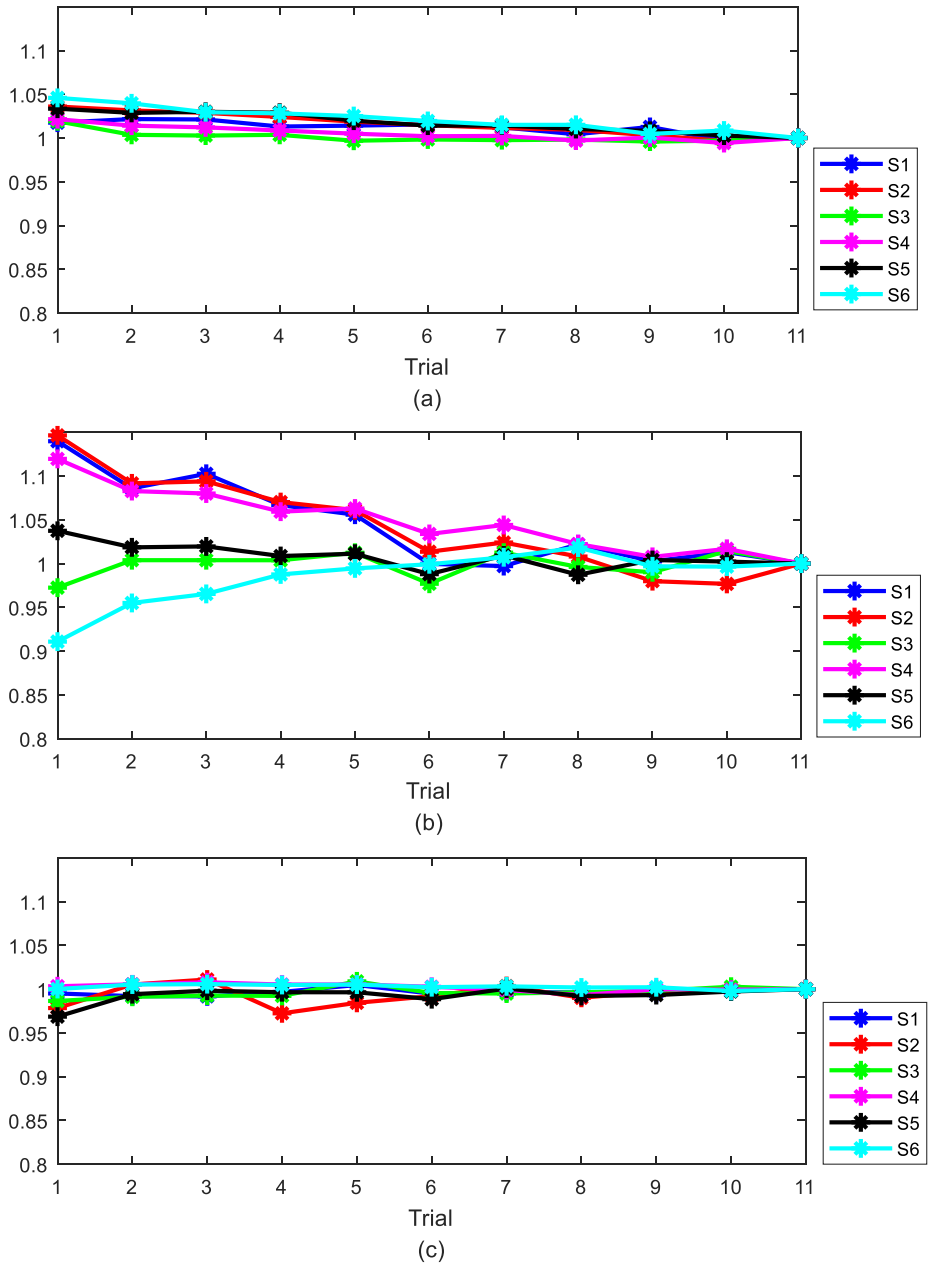

Figure 3.14 a) αAg/ αAg (trial11), b) αTextile/ αTextile (trial11), c) αOrbital/ αOrbital (trial11)

Table 3.4 is created to compare circuit model components changes due to the first pressure application and also their irreversible changes. Based on the results, R_∞ has the least variation among all components and R_0 appears to have the maximum variation. In addition,

components corresponding to Ag/AgCl electrodes are the most stable ones and those of conductive textile have the maximum variation that is consistent with the previously presented results in Table 3.3.

Table 3.4 Estimated electrical components in the first trial (P = 0) and the last time pressure is applied (trial 8, P = 4 kPa) normalized to the last trial (trial11, P = 0)

	C_1/C_{11}	C_1/C_{11} **Avg**	C_8/C_{11} **Avg**	$(R_0)_1/(R_0)_{11}$	$(R_0)_1/(R_0)_{11}$ **Avg**	$(R_0)_8/(R_0)_{11}$ **Avg**	$R_{\infty 1}/R_{\infty 11}$	$R_{\infty 1}/R_{\infty 11}$ **Avg**	$R_{\infty 8}/R_{\infty 11}$ **Avg**
Ag/AgCl	0.96 to 1.15	1.05	1.02	1.28 to 2.99	1.75	1.08	0.98 to 1.08	1.03	1.01
Conductive Textile	0.14 to 1.00	0.46	1.50	2.03 to 6.75	3.74	0.75	0.12 to 1.66	1.02	0.94
Orbital electrode	0.05 to 0.70	0.40	0.97	0.64 to 4.42	2.03	1.00	1.06 to 2.08	1.27	1.01

Table 3.5 Estimated α in the first trial (P = 0) and the last time pressure is applied (trial 8, P = 4 kPa) normalized to the last trial (trial11, P = 0)

	α_1/α_{11} **Range**	α_1/α_{11} **Average**	α_8/α_{11} **Average**
Ag/AgCl	1.02 to 1.04	1.02	1.00
Conductive Textile	0.91 to 1.14	1.05	1.01
Orbital electrodes	0.97 to 1.00	0.99	0.99

Results show that the application of an externally applied pressure tends to cause an increase in *C* values and a decrease in R_0 values. A plausible explanation for these trends is that the applied pressure results in a better contact between the electrode and the skin therefore the effective contact area is increased. The value of any capacitor can be expressed by the following formula:

$$C = \varepsilon_0 \varepsilon_r \frac{A}{d} \tag{3.3}$$

where *C* indicates the capacitance in Farad (F), ε_r is the dielectric constant of the material filling the distance between two parallel plates, ε_0 shows the electric constant (approximately $8.85 \times 10^{-12}\,\mathrm{Fm}^{-1}$), *A* is the effective common area between two parallel plates (m^2) and *d* (m) is the distance between two parallel plates. Capacitance is directly proportional to the area so if increased pressure results in effective surface contact area the capacitance will increase. It may also be the case that the pressure also decreases the distance between the two charged layers resulting in an increased capacitance.

Resistance of any material can be formulated as in

$$R = \rho \frac{l}{A} \tag{3.4}$$

where *R* is the resistance in ohm (Ω); ρ stands for the resistivity of the material with the dimension of (Ω.m); *L* represents the length of the material with the dimension of (m) and *A* shows the cross-sectional area of the conductor material with the dimension of (m^2). Based on this formula, resistance is inversely proportional to area, and if applying pressure makes the contact area larger it could explain why R_0-R_∞ tends to decrease with increased pressure. Another reason for this observation is that applying pressure was associated with increase sweat activity [51]. This increased sweat would result in a decrease in resistance.

R_∞ does not show significant or consistent changes for the Ag/AgCl and Orbital electrodes. For the conductive textile it goes down when pressure is applied and goes up when pressure removed. As we mentioned in section III.C, R_{tissue} is also incorporated in the estimation of R_∞, therefore its probable fluctuations due to the pressure could have masked any trend associated with R_∞. R_∞ is not important at low frequencies because it is relatively small ($R_\infty << R_0$-R_∞). It becomes a dominant term at high frequencies, but this is well beyond the bandwidth of biosignals. Any changes observed are probably not important in terms of biosignal quality.

Variations of α are also consistent with our findings about other components, as it has a very small range of changes in Ag/AgCl and Orbital electrodes, whereas it shows more deviations in textile electrodes. In general, α is very stable as Table 3.5 shows.

For all electrodes, the skin–electrode impedance was lower for trial 11 (P = 0 kPa) than trial 1 (P = 0 kPa). Thus, the applied pressure resulted in an irreversible change in skin–electrode impedance. This hysteresis effect is consistent with previous observations [53], [56]. A portion of the irreversible decrease in impedance can be attributed to electrode settling [39], [55], [56]; however, decreases in impedance are larger than what would be anticipated with electrode settling [53].

Ag/AgCl electrodes were observed have the lowest skin–electrode impedance and exhibited the least amount of effects to applied pressure. This result is likely due to the presence of the electrolytic gel, which is compliant and provides a good skin–electrode contact that is consistent across the applied pressures. Despite good performance, Ag/AgCl electrodes might not be appropriate for wearable home health care devices. With long term use, the gel may dry out and cause a large impedance to exist between the skin and electrode. From a usability perspective, a reusable system that does not require the need to apply gel to the

electrodes may also be preferable. On the other hand, dry electrodes such as conductive textile and Orbital electrodes are perhaps not appropriate for short term applications, because they need time and some pressure to establish a stable connection. The effects of applied pressure are relatively large initially but diminish with subsequent applications of pressure, with the Orbital electrodes performing better than the conductive textile

3.4 Discussions

The factor of pressure which is as an inevitable source of noise in wearable devices, affects the signals recorded by them [50], [51]. We propose and implement a new method to investigate these impacts in the context of wearable devices. We apply a Cole–Cole model for skin–electrode impedance and apply and measure the amount of pressure with a blood pressure cuff.

Other than pressure other factors (e.g., sweat) also influence the signals recorded by wearable devices as they have been mentioned in 2.1.3. In this work, we did not consider the impacts of sweating in combination of applying pressure. Sweat will affect the impedance and as the wearable device is pressed to the body we expect more and faster sweating and therefore, less magnitude of skin–electrode impedance is anticipated to be observed.

The area of locating the electrodes and applying pressure was on the biceps which allow us to apply the pressure and measure it with a blood pressure cuff. However, for a typical type of wearable ECG device, electrodes will most probably be placed on the chest which has some hair as opposed to biceps. But we believe that the findings in this research are applicable to ECG wearable devices, because the trend of variation of each component of the model and all the measurements throughout the applying and releasing pressure trails will stay the same however the magnitude of measurements will be higher on the chest area because of the hair.

3.5 Conclusions

In this part of the thesis, the impact of applying pressure in wearable devices was explored. Pressure affects the area of contact between transducers and the body. The contact area is associated with skin–electrode impedance meaning to investigate the effects of applying pressure, we need to explore how pressure affects this impedance.

In this part of our research, we have investigated how applied pressure influences the skin–electrode impedance and investigation is completed for three types of electrodes. Employing skin–electrode circuit model, components corresponding to each trial were extracted and their variations through all of them were discussed. Large changes were observed in magnitude of the skin–electrode impedance, associated with the initial application of pressure. These changes were observed to be irreversible and sustaining themselves even after we released the pressure. Besides, we observed a general increasing trend for C and a decreasing trend for R_0. An increase in effective contact area is a reasonable hypothesis of why we observe such variations in C and R_0. These changes also appeared to be irreversible.

Ag/AgCl electrodes showed less variation throughout the entire process of applying and releasing pressure compared to dry electrodes (conductive textile and Orbital electrodes). Therefore, from a practical point of view, Ag/AgCl electrodes seem relatively immune to changes in pressure. Dry electrodes skin–electrode impedance is modulated by pressure but there are irreversible changes, so the magnitude of the modulation decreases with successive applications and removal of pressure. As a result, biosignal recordings by dry electrodes may be initially poor, but will improve with time. This creates a problem with short recordings, unless skin preparation is performed, and less of a problem with long term continuous monitoring applications such as wearable devices, where dry electrodes are preferred.

Findings in this part of the study are applicable and useful for researches targeting to minimize or eliminate the effects of skin–electrode impedance in recorded signals, which can improve the quality of recorded signals, in turn making them more reliable especially for diagnostic purposes [9].

Chapter 4 **Classifying ECG Signals Based on Quality**

4.1 Introduction

Cardiovascular disease is the global leading cause of death and, in the United States, approximately 86 million people are living with some sort of cardiac disease [101]. The prevalence of cardiovascular disease and complications leads to a high cost burden on the public health sector, directly and indirectly; it also motivates research within this area. The electrocardiogram (ECG), which is the recording of the electrical activity of the heart, is an important biosignal for investigating the cardiovascular system. Early discharge and ambulatory monitoring for cardiac arrhythmia, particularly intermittent ones is essential and to do so, continuous monitoring is often needed. Advances in technology have enabled new monitoring systems, including wearables which enable continuous monitoring during normal activities of daily living [102]. Significant strides have also been achieved in computer-aided

diagnosis (CAD) for cardiac arrhythmias; however, there still exists some fundamental challenges. One of the most problematic issues are contaminants in the measured ECG signal. It is even more important in the context of wearable devices since as we have mentioned in Chapter 2, they are more susceptible to noise.

The utility of the ECG signal depends on signal quality of the measurement. ECG contaminated by various sources of noise and artifacts (e.g., baseline wandering, power line interference, and motion artifact) can lead to misdiagnosis of various cardiac arrhythmias in the form of false positives and false negatives [57], [61]. While mitigation strategies can be used to remove or reduce contaminants in the measured signal, applying such strategies on a clean signal can actually reduce the signal quality [18].

Heart arrhythmia diagnosis from ECG is currently being done clinically using some bedside monitoring or wearable devices, with an alarm activated in case of any arrhythmia occurrence. Wearable ECG measurement systems enable continuous monitoring, including during a subject's normal activities of daily living, including walking, driving, eating, sitting down, and standing up. The measured signal in wearable systems is especially prone to contamination by motion artifact. It is possible that an alarm is falsely activated due to noise in the measured ECG noisy signal. The Emergency Care Research Institute (ECRI) listed alarm hazards, including false alarms, as the top patient safety hazard from 2012 to 2015 [103], [104], [105], [106] . False alarm reduces the perceived validity and importance of alarms, which can lead to alarm fatigue resulting in alarm desensitization and missed alarms.

To address the above problems, signal quality verification should be performed prior to CAD. If ECG signal of poor quality is detected, the monitoring system must be able to act appropriately, which could include applying mitigation strategies or discarding the poor-

quality signal. Simultaneously, it is important that the system does not mistakenly consider arrhythmic signals as noisy signals, as it could result in a false negative (e.g., ECG signals being discarded and a missed true alarm). As ECG contaminants can present themselves in various forms and mixtures, biomedical signal quality analysis can be challenging.

Machine learning algorithms can provide one approach to confront this challenge. In this chapter, we design, implement, train and test a machine learning algorithm, specifically a deep belief networks (DBN) algorithm, which can discriminate between clean and noisy ECG measurements. We chose DBN after comparing it to other methods of classification and since the results are better than a similar works in the literature [76], this classifier is satisfactory. It should be mentioned we did not find any similar work other than [76] to compare our work and results with.

Our algorithm, the block diagram of which is demonstrated in Figure 4.1, works as follows. First, data is applied to the DBN. Then, two layers of Restricted Boltzmann Machine (RBM) are dedicated to feature extraction, the output of which is then applied to another layer of RBM which is specifically designed to classify the data.

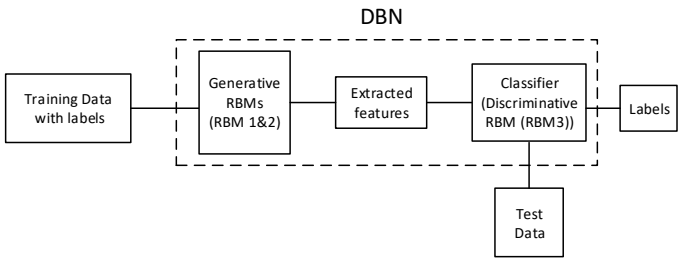

Figure 4.1 Block diagram of proposed method

4.2 Methods

4.2.1 Dataset

ECG measurements used in our study are from the MIT-BIH Arrhythmia Database [77], which includes different types of arrhythmias. Each measurement recording is approximately 30 minutes in length and has a sampling frequency of 360 Hz. There are 20 measurement recordings that are contaminant-free in their channel one.

We contaminate 8 other recordings from the same database, which are noisy in very limited periods of time (<=7 seconds) during the entire recording, with a calibrated amount of motion artifact from the MIT-BIH Noise Stress Test Database (NSTDB) [77]. Motion artifact noise is scaled appropriately to obtain five desired signal to noise ratios (SNR): -10, -5, 0, 5 and 10 dB. Noise injection is performed following the guidelines of MIT-BIH NSTDB [77].

ECG signals recorded with a wearable device has been shown in [107] to have generally 5 dB to -60 dB SNR levels. Therefore, we believe that signals with SNRs between 10 dB to -10 dB are representative of ECG signals recorded by a wearable device.

To obtain a contaminated ECG signal of a certain SNR, we should utilize (4.1) [108]:

$$SNR = 10\log(S/(N * a^2)) \quad (4.1)$$

where a is the scaling factor of noise, S is the power of signal and N is the power of noise signal. This SNR definition is different from a traditional definition of SNR and desired for ECG [108]. ECG signal power (S) is computed by measuring the peak-to-peak amplitude of 300 normal QRS complexes from channel 1 of each recording. The top and bottom 5% of the measurements are discarded and the average QRS amplitude of the recording is determined

using the remaining 90%. The signal power for the channel of the recording is estimated by dividing the average QRS peak-to-peak amplitude by 8.

The noise signal we apply to contaminate the ECG signals is the 'em' measurement, available in the MIT-BIH Noise Stress Test Database (NSTDB) [77] containing electrode motion artifacts. 'em' is approximately half an hour in duration and has a sampling frequency of 360 Hz. Noise was recorded by using standard ECG recorders, leads and electrodes on volunteers who were physically active. The electrodes were connected to their limbs in a position where their ECG was not visible. As a result, the recorded noise signal is actual noise [77]. To calculate the power of the noise (N), 300 first seconds of 'em' are broken down to one second windows and the mean amplitude and the root mean squared difference between the signal and this mean amplitude are calculated. The largest and the smallest 5% of each measurement are discarded and the RMS noise amplitude is estimated by the mean of the remaining 90% of the measurements. This estimate is squared to find the noise power.

The contaminated signal is constructed by estimating *S* and *N*, then computing the scaling factor *a* from (4.1), and finally using (4.2):

$$v_{noisy}(t) = v_{clean}(t) + a * n(t) \quad (4.2)$$

where $v_{noisy}(t)$ is the desired noisy signal, $v_{clean}(t)$ is the original clean signal and $n(t)$ is the noise signal.

Applying the above estimations and calculations, we obtain the noisy signals at five levels of SNR. A few of the original signals we picked and contaminated, may contain some limited periods (a few seconds) of being noisy, but during contaminating phase, we have treated them as if they are completely clean.

We contaminate each signal with a unique version of noise signal “em”. Each version is generated by picking a random point of the 30 minutes noise recording and set it as starting point and concatenating the rest of the original “em” signal to the end of it.

Each 30-minute recording is divided into 5 second segments. Therefore, we have 7200 clean ECG segments and 2880 segments, which are contaminated with calibrated noise. A total of five different datasets were constructed. Each dataset contains noisy signals from only one level of SNR and clean signals. We perform the classification for all the datasets separately and compare the results.

4.2.2 Training and Testing Sets

Clean data segments are labeled with a 0 and noisy data segments are labeled with a 1. One part (75%) of our datasets are labeled and used to train the RBMs. Performance of the DBN is evaluated on the remaining part (25%) of the dataset that is separate from the training data; i.e., there is no overlap between recordings (subjects) used for training and those applied for testing. A 4-fold cross validation is performed for all tests. The average across all folds is reported, accompanied with the standard deviation.

4.2.3 Applying the DBN as a Classifier

In this chapter, we designed a Deep Belief Network with three RBMs. The first two RBMs are generative RBMs which do not need labels, and the last RBM is a discriminative one which uses data with their labels and can classify data. Each RBM has 1000 hidden units and 1000 visible units. Benefiting from the Contrastive Divergence (CD) method [109], RBMs are trained through a 200 epochs attempt. For fine tuning, the Back-Propagation (BP) method [110] is employed.

Accuracy, Precision (also known as Positive Predictive Value), Recall (also known as Sensitivity) and Specificity (also known as True Negative Rate) are defined as follows:

$$Accuracy = \frac{True\ Positive + True\ Negative}{total\ number\ of\ segments} \tag{4.3}$$

$$Precision = \frac{True\ Positive}{True\ Positive + False\ Positive} \tag{4.4}$$

$$Recall = \frac{True\ Positive}{True\ Positive + False\ Negative} \tag{4.5}$$

$$Specificity = \frac{True\ Negative}{True\ Negative + False\ Positive} \tag{4.6}$$

We use these four parameters to evaluate the performance of the algorithm. For our study, a true positive (TP) is defined as a signal which is noisy, and the algorithm correctly recognizes it as a noisy one, a false positive (FP) is defined as a signal which is clean but the system takes it as a noisy signal, and a false negative (FN) is defined as a signal which is noisy but the system recognizes it as a clean signal. We also report results for noise-free segments corresponding to an arrhythmic event, separately. There are 2,220 noise-free arrhythmic segments. Ideally, these segments should be identified as clean; however, the arrhythmia could be mistakenly classified as noise.

4.3 Results

The results of all tests are presented in Table 4.1 Each column shows the performance parameters for its corresponding SNR set. As it shows, Precision and Recall rates of

classifying the ECG measurements fluctuate with the SNR. Distinguishing noisy and clean signals seems to be more difficult for high SNR; this would be expected because noisy signals have little noise and would closely resemble clean signals. However, the application of ECG signals determines what level of quality is the bottom line and any signal better than that will be good enough for that particular application. For example, in applications with low complication (e.g. heart rate measurement), signals of SNR 10dB would suffice and considered as clean. All four performance measures are in the 90s for SNR that are 0 dB or lower. With higher SNRs discerning noise is more difficult compared to lower SNRs, resulting in higher false negatives in higher SNRs (above 0dB). That is the reason why we observe lower performance metrics for high SNRs.

Table 4.1 Accuracy, Precision, Recall and Specificity (mean and standard deviation)

SNR	**-10dB**	**-5dB**	**0dB**	**5dB**	**10dB**
Accuracy (%)	99.5 ± 0.08	96.7 ± 0.43	97.8 ± 0.67	96.8 ± 0.46	75.0 ± 0.37
Precision (%)	97.7 ± 0.61	98.9 ± 0.27	92.2 ± 1.99	75.43 ± 0.99	53.4 ± 2.1
Recall (%)	100.0 ± 0	99.9 ± 0.09	99.4 ± 0. 29	96.4 ± 0.51	73.2 ± 0.62
Specificity (%)	100.0 ± 0	99.9 ± 0.14	99.4 ± 0.31	96.4 ± 0.46	73.1 ± 0.65

Results confirm that our DBN is able to identify noisy signals. For low SNRs (i.e., 0dB and lower) there is low probability that the system identifies a noisy ECG segment as a clean one. Such an error in classifying ECG measurements can potentially be hazardous because it is not a valid signal to be interpreted and can cause a critical misperception of ones' heart performance. Figure 4.2 demonstrates a five-second ECG segment with calibrated amount of motion artifact. For high signal to noise ratios (above 0dB), the level of noise is quite low and

visually these segments would be relatively difficult to identify as noisy segments. In such situations, although the DBN may falsely classify the signal as “clean”, the likelihood of a false alarm is low given that the noise is quite modest.

It is also important that the algorithm not identify arrhythmic signals as noisy signals, which could result in a false negative. Therefore, we also investigated if our algorithm can recognize the arrhythmic signals, in the clean part of our test set, as clean ones. To do so, we first, look at the number of arrhythmic segments (of each kind of arrhythmia) in our test set. Then in the fraction of our test set which is labeled “clean” by the classifier, arrhythmic segments of each kind of arrhythmia are counted and compared to their corresponding number in the test set. If arrhythmic segments of each kind in the “clean” labeled segments is equal to its corresponding number in the test set, means that our classifier has not taken arrhythmic segments as noisy signals because of their unusual (arrhythmic) shape, which is desired. Table 4.2 shows the number of arrhythmic ECG segments and the type of arrhythmia in the test set and the number of these segments in the fraction of test set which is labeled “clean” by the classifier. Results suggest that the DBN classifier does not get confused and can identify clean segments regardless of being arrhythmic or not. Results are better with lower the SNR because noisy signals are easier to discern from clean signals given the higher level of noise.

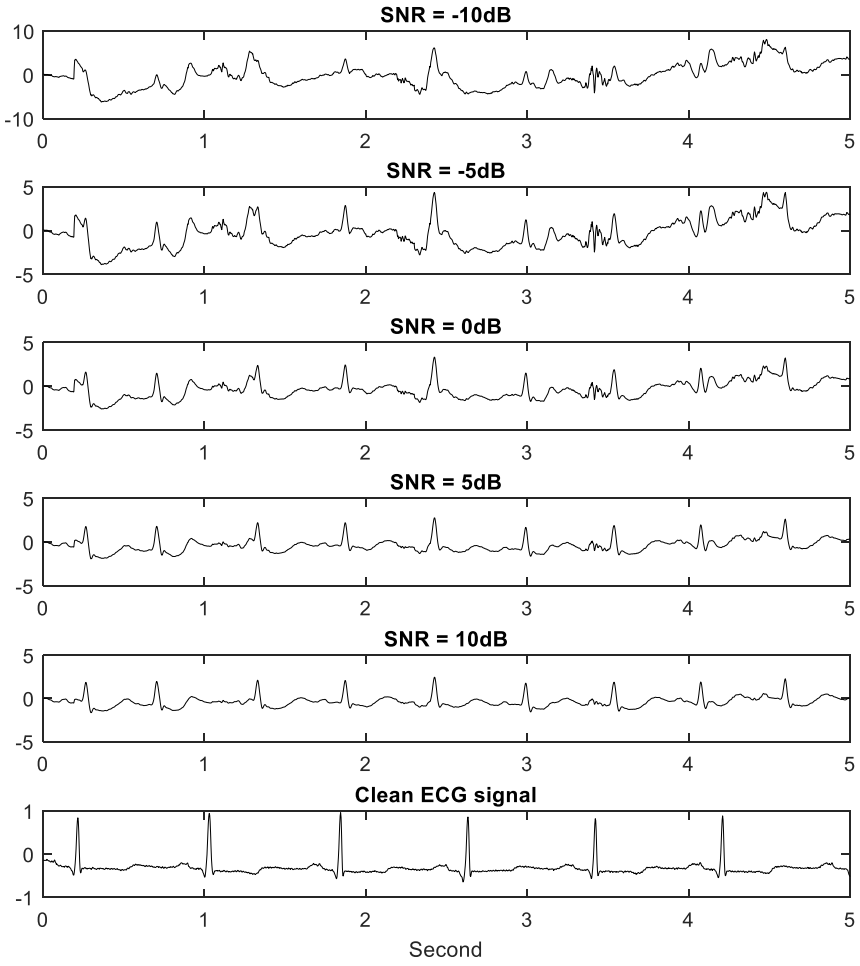

Figure 4.2 Five-second ECG segment with calibrated amounts of motion artifact

Table 4.2 Number of arrhythmias in signals that DBN takes as “clean” vs. number of them in clean test set

Arrhythmia type	Left bundle branch block	Aberrated atrial premature	Premature ventricular contraction	Fusion of ventricular and normal
Clean test signals	1254	109	845	12
signals Classified as clean (when -10dB and clean signals applied to DBN)	1253	109	843	12
signals Classified as clean (when -5dB and clean signals applied to DBN)	1254	109	843	10
signals Classified as clean (when 0dB and clean signals applied to DBN)	1097	109	834	11
signals Classified as clean (when 5 dB and clean signals applied to DBN)	1000	105	780	11
signals Classified as clean (when 10 dB and clean signals applied to DBN)	976	105	682	10

In total, results show much promise in using our DBN as an effective classifier of ECG measurements into noisy and clean signals. Such a classifier can be used in a preprocessing step that can help lower the rate of false alarms, and at the same time being intelligent enough not to gate true alarms.

So far in existing work, DBNs has mostly been used for two-dimensional data such as hand-written digits and rarely used for one-dimensional data. We have shown that our DBN has encouraging results in classifying one-dimensional signals which are fed into it as time series. Moreover, DBN extracts features automatically and therefore, feature extraction is not an issue anymore and we do not spend time and cost on it when applying DBN as the classifier. Results we obtain are consistent and good. Results are also better than the literature and thus did not explore other deep learning methods in our research. We are not also concerned about overfitting, because the dataset is large enough and the results from the cross validation suggests that overfitting did not occur.

4.4 Discussions

Signal quality assessment is a critical concern in biosignal recording devices. Specifically, in wearable devices, where signals are exposed to motion artifact and most probably contaminated with it, quality assessment becomes more important and crucial. Hence; finding a method to do so, will be a meaningful achievement. Our method, presented in this chapter, is based on a recent machine learning technique, namely DBN.

To test and validate our proposed method, we artificially contaminated ECG signals with motion artifact to create different levels of SNR. However, in this work, other types of affecting artifacts such as baseline wandering, and muscle artifact are not considered. Each of them can affect the quality of the ECG signal collected by a wearable device or a clinical one and similar investigations and analysis are required for them, too. In the best case scenario, a combination of all of them should be considered with realistic ratios of each of them. In this research, wearable devices and their issues are the main concern where motion artifact is the

dominant type of artifact. Thus, we focus on motion artifact as the main contaminating signal in wearable devices.

4.5 Conclusions

In this chapter, we contaminated signals with motion artifacts as if they are being caught by a wearable ECG signal device. Motion Artifact is the most prevalent type of noise we expect to have in signals captured by a wearable device. The goal of this part of the research is to invent a method to identify high and low-quality signals. We managed to do so using machine learning methods.

Results of this chapter suggest that DBN is an advantageous and powerful machine learning technique for separating clean and noisy ECG segments prior to any analyses for diagnoses. It can perform the task with a high precision and recall rates. The DBN can also appropriately discriminate arrhythmic ECG signals and noisy ECG signals, even if the signal is only slightly noisy (i.e., relatively high SNR).

Such algorithms can be added to an ECG monitoring device as a preprocessing step to validate adequate signal quality prior to analyses for diagnoses. This can help reduce the false alarm rate by ensuring that only clean signals are being processed.

Chapter 5 **Atrial Fibrillation False Alarm Reduction**

5.1 Introduction

As early detection is vital in many cardiac arrhythmias, many wearable devices are designed to not only monitor the patient's ECG but also detect a specific arrhythmia. Since signals acquired by wearables are widely exposed to contaminants such as motion artifacts, a high rate of false alarms is expected in such wearable devices which are equipped to detect arrhythmias. Hence; it is necessary to invent and validate a method to reduce false alarms and increase the applicability and helpfulness of such wearable devices. On the other hand, a very common type of arrhythmia is Atrial Fibrillation (AFib) and several AFib detection algorithms are designed and tested [111], [112]. So, in this part of our research we focus on AFib detection algorithms and reducing their false alarm rate due to noisy signals such as signals acquired by a wearable device.

Atrial fibrillation (AFib) is a cardiac condition that involves an irregular heart rhythm and is associated with chest pain, blood pressure, shortness of breath, and fatigue [113]. AFib is the most prevalent type of cardiac arrhythmia, with as many as 3 million Americans and 350,000 Canadians living with AFib [111], [114]. The risk of AFib increases with age, with almost 9% of people above the age of 65 suffering from AFib [115]. AFib itself is not life threatening; however, if left untreated, it can lead to life threatening incidences, such as stroke and heart failure [116]. The World Health Organization (WHO) ranked stroke as the second leading cause of death worldwide [117]. People with AFib are five times more likely to have stroke compared to people without AFib [118]. Strokes triggered by AFib are also reported to have higher severity than strokes caused by other factors [119].

Early detection of AFib is essential to prevent it from progressing to fatal outcomes. AFib detection is typically performed by examining patients' electrocardiogram (ECG). AFib is associated with an ECG that has irregular R-R intervals [88]; hence, the majority of AFib detection algorithms explore individual's ECG to detect such irregularities in the R-R intervals (e.g., [111], [112], [120], [121] and [122]).

Arrhythmias, such as AFib, can appear as transitory events and can be detected by ambulatory ECG measurement devices e.g., Holter monitors and wearables. Such measurement devices allow for ECG recordings over long time durations, enabling the capture of transitory arrhythmic events, while still permitting patient mobility. AFib detection algorithms can be performed offline to highlight segments of recordings that can be given additional scrutiny by a physician. Analyses can also be performed online, alerting a healthcare professional when certain alarm conditions are met [120]. A serious challenge such ECG devices are struggling with is false alarm (FA). Alarm hazards, including alarm fatigue

due to FAs, were identified as the top patient safety hazard for many years by the Emergency Care Research Institute [103], [104], [105], [106]; as such, the reduction of FAs is important. Simultaneously, care must be taken to avoid missing true alarms, which can also lead to disastrous results. False AFib detections can result in a large volume of irrelevant data that is incorrectly identified for subsequent analysis, leading to unnecessary workload, and alarm fatigue.

Noise and artifacts (e.g., motion artifact) are particularly prevalent in ambulatory ECG monitors. Poor signal quality, due to noise and artifacts, can result in FAs. An effective method of mitigating FAs is to assess the quality of the recorded signals and restrict signals with an unacceptable quality from being used by the detection algorithms. This approach has been used for heart rate estimation [64], myocardial ischemia [61], cardiac arrhythmias [57], and ECG biometrics [62]. To the best of our knowledge, no study for signal quality identification for AFib detection has been conducted to date and our work is the first for this purpose.

A qualified approach for detecting signals with an unacceptable quality is utilizing machine learning algorithms capable of classifying signals based on their quality. We have previously applied Deep Belief Networks (DBN) to for discerning noisy and clean ECG signals (signals with no added noise), with promising results [123]. Deep learning is a class of machine learning algorithms that have recently attracted much attention, and have been shown to outperform other classifiers in image and audio data processing [67], [81], [82] and DBN is a specific type of deep learning algorithms.

In this chapter, benefiting from our previous experiment of DBN, we enhance its application and propose and validate a method to mitigate the FA rate for AFib detection. A DBN is employed to discriminate acceptable and unacceptable ECG signals, based on signal

quality, and unacceptable signals are gated from being involved in AFib detection in order to decrease the rate of false alarms. This approach is illustrated in Figure 5.1.

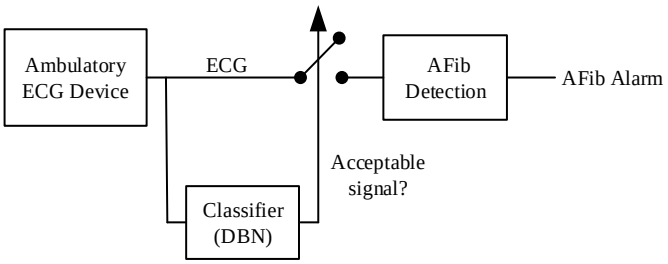

Figure 5.1 Block diagram of our proposed method.

5.2 Methods

5.2.1 Atrial Fibrillation Detection Algorithm

There have been many algorithms proposed for AFib detection, such as [111], [112] and [122]. In this work, we applied the algorithm proposed in [111]. This algorithm is a statistical AFib detection algorithm, based on the generally accepted characteristic of AFib as a random sequence of R-R intervals of ECG. Three statistical techniques are combined in this algorithm: 1) the Root Mean Square of Successive R-R Differences (RMSSD), 2) the Turning Points Ratio (TPR), and 3) Shannon entropy (SE).

5.2.1.1 Root Mean Square of Successive Differences (RMSSD)

In AFib, the ECG has higher variability in R-R intervals compared to a normal ECG. RMSSD is used to quantify beat-to-beat variability. For a given time series of R-R intervals *a(i)* of length *l*, the RMSSD is defined as:

$$RMSSD = \sqrt{\frac{1}{l-1}\sum_{i=1}^{l-1}\big(a(i+1)-a(i)\big)^2} \tag{5.1}$$

5.2.1.2 Turning Point Ratio (TPR)

In AFib rhythm, the R-R interval time series is random or as it is denoted in medical articles "irregularly irregular" [124]. TPR, a nonparametric statistical test, is used to assess the randomness of the R-R intervals. This test compares each RR interval relative to its neighbors. A series with a TPR lower and beyond the 95% confidence interval represents periodicity (e.g. sinus rhythm) whereas a TPR within the 95% confidence limit implies random characteristics [111].

5.2.1.3 Shannon Entropy (SE)

In AFib, the R-R intervals time series is considered to be a random process. SE is used to characterize its complexity. The SE during AFib is expected to be considerably higher than in sinus normal rhythm**.**

To compute the SE of R-R intervals in a given segment of an ECG signal, first eight longest and eight shortest R-R interval values are considered outliers and are removed from the time series. The remaining RRs are sorted into equally spaced bins whose limits are defined by the shortest and longest R after removing outliers. Then a histogram of the segment is constructed. In order to have a sensibly accurate measure of SE, at least 16 bins are required [111].

The probability distribution for each individual bin is calculated as follows:

$$p(i) = \frac{N_{bin}(i)}{l - N_{outliers}} \tag{5.2}$$

where $N_{bin}(i)$ is the number of heart beats in the i^{th} bin, l represents the number of beats in the ECG segment, and $N_{outliers}$ is the number of outliers (in this algorithm $N_{outliers} = 16$).

Using the probability distribution, the SE for this work is computed as follows [111]:

$$SE = -\sum_{i=1}^{B} p(i) \frac{\log(p(i))}{\log\left(\frac{1}{B}\right)} \quad (5.3)$$

where B is the number of bins ($B = 16$ in this work).

5.2.1.4 Optimization and Thresholds

An optimization process is performed by Dash et al. [111] to determine thresholds for RMSSD, TPR, and SE: RmsThresh, TprThresh, and SeThresh, respectively. By optimizing the sensitivity and specificity of the algorithm, the thresholds of each parameter were reported as [111]: RmsThresh = 0.1, 0.54< TprThresh <0.77 and SeThresh = 0.7. TprThresh range is achieved by optimizing the confidence interval threshold which is 99.9%.

A given segment of an ECG signal is classified AFib if it satisfies all following conditions [111]:

1) RMSSD/MeanRR > RmsThresh;
2) TPR within the TprThresh confidence interval; and
3) SE > SeThresh,

where MeanRR is the mean R-R interval.

In this algorithm, the length of a given segment is considered to be l=128, meaning each segment of ECG contains 128 R-R intervals and therefore has 129 beats.

5.2.2 Database

We have tested our algorithm on MIT-BIH Atrial Fibrillation Database (afdb) [77] available in Physionet. This database contains 25 holter ECG recordings of human subjects with atrial fibrillation. Each recording is approximately 10 hours in duration, with a sampling frequency of 250 Hz and 12-bit resolution over a range of ±10 millivolts. All recordings are

fully annotated and may contain normal sinus rhythm, atrial fibrillation, and atrial flutter. Recordings 04936 and 05091 are excluded form analysis because they are incorrectly annotated at some points [111]. We also exclude recordings 00735 and 03665, similar to [121] and [125], because there is no recorded data available in them.

5.2.3 Signal Preprocessing

Recordings available in afdb [77] are not noise free. Therefore, as the first step we apply a band pass filter (BPF), with a pass band of 5-15Hz, to remove baseline wandering and muscle artifact noise. Band pass filtering was achieved using low and high pass filters, designed based on the noise filtering step of the Pan-Tompkins QRS detection algorithm [126]. Using these filtered ECG recordings, which are considered as "clean", we generate ECG signals with defined levels of SNR.

To use the AFib detection algorithm, identifying R peaks is necessary. The R peaks were identified using the Complete Pan Tompkins Implementation ECG QRS detector toolbox available on MATLAB File Exchange [126], [127], which also includes the band pass filtering mentioned above.

5.2.4 Signal Contamination

"Noisy" ECG data are created by artificially contaminating the clean ECG data with electrode motion artifact. Electrode motion artifact is a real concern since it overlaps the frequency range of interest of the ECG signal (i.e., 5-15 Hz). A real sample of this signal is available in the 'em' recording of the MIT-BIH Noise Stress Test Database (NSTDB) [77]. Recording 'em' is half-hour of electrode motion artifact recording, with a sampling frequency of 360 Hz, whereas ECG recordings in afdb [77] are almost 10 hours with a sampling

frequency of 250 Hz. The sampling rate of the 'em' noise signal is initially reduced to 250 Hz.

To generate contaminated ECG signals from MIT-BIH Atrial Fibrillation Database (afdb) [77], which are approximately 10 hours long, we need a noise signal 10 hours in duration. We simulate a 10-hour long electrode motion artifact signal, using an autoregressive (AR) model of the half-hour 'em' signal. An AR model is a representation of a random process, which the output linearly depends on previous values of itself. Equation (5.4) shows the AR model of order p.

$$X(n) = c + \sum_{i=1}^{p} \varphi_i X(n-i) + \varepsilon(n) \tag{5.4}$$

where c is a constant, φ_i is a parameter of the model or AR coefficient, and ε is zero-mean white noise. In this study, we choose the order of the AR model by comparing the simulated models from orders 1 to 50 with the Akaike information criterion (AIC) [128], which evaluates the quality of a simulated model for a given data. Using AIC, an order p=20 was chosen.

In another research [129], where generating a motion artifact noise for ECG contamination was required, it was assumed that motion artifact behaves similarly to baseline drift in respiration which in turn is simulated by a low frequency sinusoid with the frequency of 0.333Hz and maximum amplitude of 1.0 mV. This approach does not resemble a real motion artifact as we can observe in 'em' recording of the MIT-BIH Noise Stress Test Database (NSTDB) [77]. The real 'em' signal visually looks like a random signal rather than a sinusoid signal.

A unique noise signal is generated for each recording of afdb [77] and is combined with it to create a contaminated signal at a particular SNR. SNR for ECG is defined in (4.1).

Eight datasets are created: one clean dataset and seven datasets contaminated with noise at levels of SNR between -20dB and 10dB, in steps of 5dB. Figure 5.2 shows a part of a clean signal and its corresponding contaminated ones at the various levels of SNR.

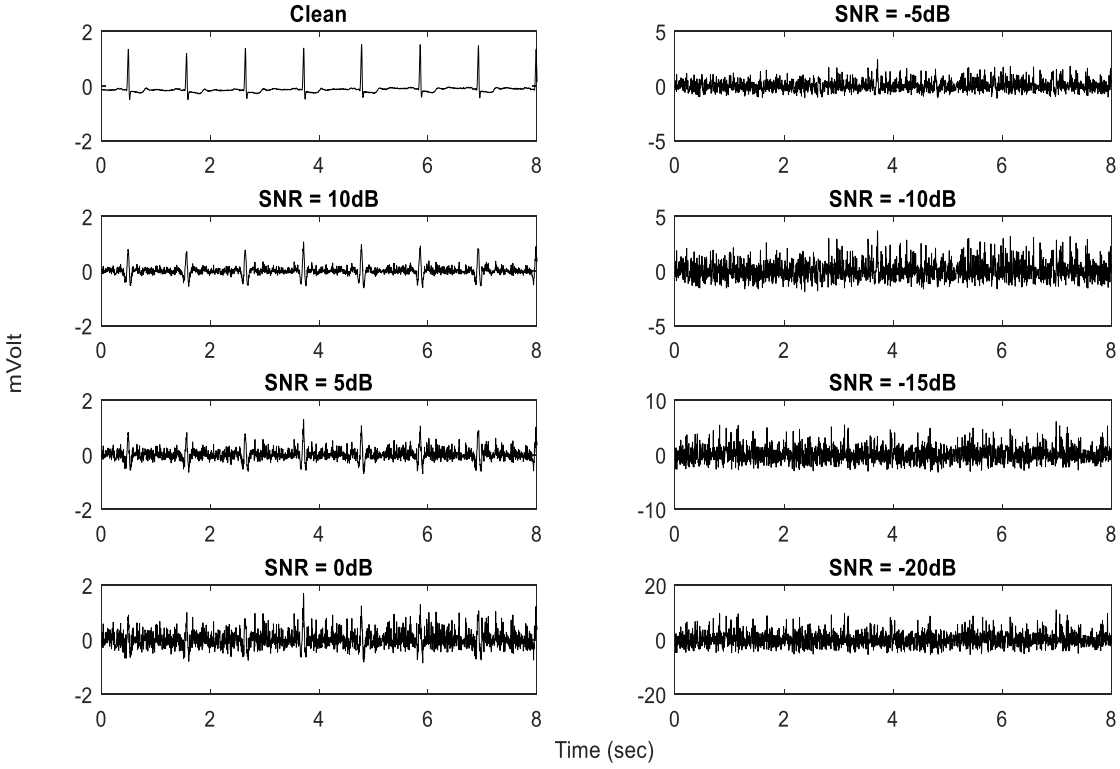

Figure 5.2 Eight-second ECG segment with calibrated amounts of motion artifact

5.2.5 False Alarm Reduction with Gating

The AFib detection algorithm (5.2.1) is applied to the eight datasets to observe the effect of signal quality on performance. Based on these observations, a threshold of acceptability for ECG signal quality can be established for AFib detection. For ECG segments with an SNR above this threshold of acceptability, which have little to no noise, the AFib detection performance would be high. For ECG segments with an SNR below this threshold of

acceptability, the AFib detection algorithm performance would be decreased, including a higher false alarm rate. Next, we train a DBN to distinguish signals that are “acceptable” and “unacceptable”, based on this acceptability threshold. Here we design the DBN to discriminate signals higher and lower than a certain threshold of SNR, whereas in Chapter 4, the DBN was designed to distinguish contaminated signal from clean signal.

Data are band pass filtered, as described in 5.2.3, prior to being applied to the DBN. The training procedure is as follows. Data are divided into segments, containing 128 R-R intervals (l=128). Each segment is given a class label, assigning 0 to segments considered unacceptable (segments from the dataset with an SNR below the acceptability threshold) and 1 to all other segments which are considered acceptable. Each segment is also labeled whether it contains AFib or not, based on the annotations available in the Physionet [77].

A training set is constructed using randomized, stratified sampling, where 75% of all ECG segments, in each of the eight datasets, makeup the training set. The remaining 25% of the ECG segments are used as the testing set. Ten-fold cross validation is performed strictly on training set while in each iteration one tenth of this set is retained as the validation set and the optimal performance is selected and applied to the test set.

In this chapter, we have designed a DBN with three layers of RBMs. The first two RBMs are generative RBMs which do not need labels, and the last layer includes discriminative RBM which uses data with their labels and classifies the input data. Each RBM has 1000 hidden units and 1000 visible units. Benefiting from the Contrastive Divergence (CD) method [109], RBMs are trained through a 200 epochs attempt. For fine tuning, the Back-Propagation (BP) method [110] is applied.

The DBN classification of the test data is used to gate AFib alarms, rejecting any alarms arising from segments that were classified as unacceptable. Figure 5.3 illustrates the block diagram of our proposed method.

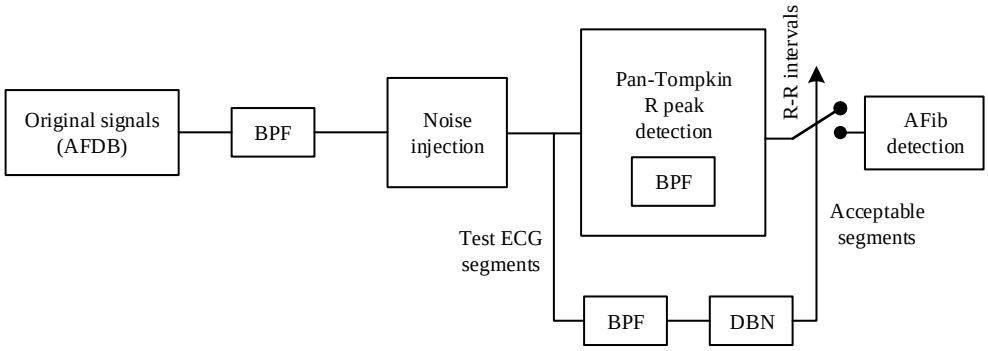

Figure 5.3 Detailed block diagram of proposed method

5.2.6 Performance Evaluation

We use the following metrics to evaluate the performance of our methods: Precision (also known as Positive Predictive Value), Recall (also known as Sensitivity), Accuracy and Specificity (also known as True Negative Rate). These metrics are defined in (4.3) to (4.6).

Generally, a true positive (TP) occurs when a segment, which has AFib is correctly classified as an AFib segment. A false positive (FP) occurs when a segment which does not have AFib, is incorrectly classified as an AFib segment. A false negative (FN) occurs when a segment which has AFib, is incorrectly classified as a segment without AFib. Finally, a true negative (TN) occurs when a segment which does not have AFib is correctly classified as a segment without AFib.

However, in DBN performance evaluation, since we utilize DBN to discern acceptable and unacceptable segments (higher and lower than the threshold SNR), TP, FP, FN and TN will

have different definitions. In this part of the study, a true positive (TP) is defined as a segment which is unacceptable and DBN correctly classifies it as an unacceptable segment. A false positive (FP) is defined as a segment which is acceptable and DBN incorrectly classifies it as an unacceptable segment. A false negative (FN) is defined as a segment which is unacceptable and DBN incorrectly classifies it as an acceptable segment. A true negative (TN) is defined as a segment which is acceptable class and DBN correctly classifies it as an acceptable segment.

To avoid confusion, we subscript parameters related to AFib detection algorithm and those corresponding to DBN classification performance with AFib, and DBN, respectively.

To measure total system performance, we need to compare the performance of the AFib detection algorithm with and without gating. In order to calculate each metric, with gating, only the segments that got through the gate are counted and signals which are not labeled "acceptable" by the DBN are not considered whether or not they include an AFib event. Applying DBN to gate AFib alarms leads to rejecting some segments, which can potentially be any of TP_{AFib}, FP_{AFib}, FN_{AFib} and TN_{AFib}. We define a new parameter "rejection ratio", to compare the rate of each type of segments (i.e., TP_{AFib}, FP_{AFib}, FN_{AFib} and TN_{AFib}) rejected by the DBN. Equation 5.5 defines this parameter. The objective of measuring such parameter is that we intend to investigate how gating influences the TP_{AFib}s and FP_{AFib}s and what portion of them in each level of SNR is being missed with gating. The "rejection ratio" is computed for TP_{AFib}s and for FP_{AFib}s. The "rejection ratio" varies between 0 and 1. If the rejection ratio for TP_{AFib} is 0, it means 0% of the TP_{AFib} segments are classified as unacceptable and none are gated; this is desirable. If the rejection ratio for TP_{AFib} is 1, it means 100% of the TP_{AFib} segments are classified as unacceptable and all are gated; this is undesirable. If the rejection

ratio for FP_{AFib} is 0, it means 0% of the FP_{AFib} segments are classified as unacceptable and none are gated; this is undesirable. If the rejection ratio for FP_{AFib} is 1, it means 100% of the FP_{AFib} segments are classified as unacceptable and all are gated; this is desirable.

$$Rejection\ ratio = \frac{number\ of\ segments\ (TP_{AFib}\ or\ FP_{AFib}) classified\ as\ unacceptable}{total\ number\ of\ segments\ (TP_{AFib}\ or\ FP_{AFib})} \quad (5.5)$$

5.3 Results

5.3.1 AFib Detection Performance as a Function of SNR

Curves depicted as "without gating" in Figure 5.4 represent the results of the AFib detection algorithm for the various SNRs, without gating. All four performance metrics (precision, recall, accuracy and specificity) decrease with SNR. With high noise, the estimation of the R-R intervals becomes unreliable.

From relevant results shown in Figure 5.4 we can conclude that 0dB is the point that metrics begin to become plateau when there is no gating. Hence, we consider segments with an SNR of 0dB and above as "acceptable" segments, and segments with an SNR below 0dB as "unacceptable" segments.

5.3.2 Classification of ECG Segment Signal Quality

To classify noisy and clean segments, we apply the ECG segments in different levels of SNR to the DBN. It classifies them and identifies if they belong to "acceptable" or "unacceptable" classes. Figure 5.5 illustrates the results.

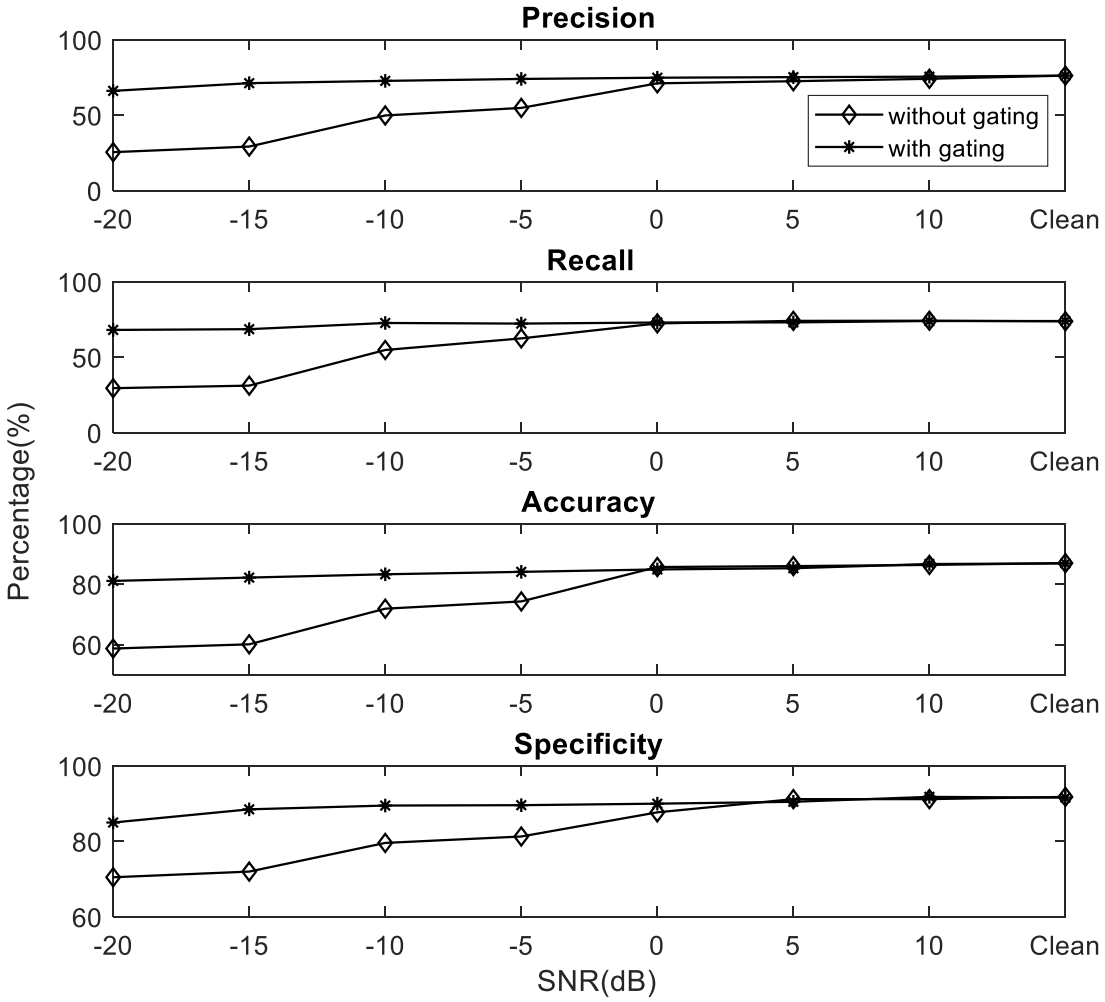

Figure 5.4 Precision, Recall, Accuracy and Specificity of AFib detection for each dataset with and without gating

When segments are slightly contaminated (high SNR) the majority of segments are classified as “acceptable”. When segments are severely contaminated (low SNR), the majority of segments are classified as “unacceptable”. A transition band is observed for moderate SNR levels. While a particular dataset is associated with a particular SNR level, the level of motion artifact varies with time, which causes some variation in SNR within each ECG segment.

5.3.3 AFib Detection Performance with Gating

The DBN has labeled segments as “acceptable” or “unacceptable”. The “unacceptable” segments are rejected and do not undergo any further processing. The segments labeled as “acceptable” are applied to the AFib detection algorithm. Curves depicted as “with gating” in Figure 5.4 represent the results of the AFib detection algorithm for the various SNRs, with gating.

Results show that for ECG with low SNR, gating significantly improves the performance of AFib detection. Without gating, the precision, recall, accuracy, and specificity at -20dB are 25.5%, 29.3%, 58.7%, and 70.5%, respectively. With gating, there is a large improvement with these metrics becoming 65%, 68.1%, 81%, and 85%. For ECG with high SNR, results are approximately identical with and without gating.

ECG segments that are classified as “unacceptable” by the DBN are rejected. Figure 5.6 depicts the rejection ratio of FP_{AFib}s and TP_{AFib}s as a function of SNR. While the rejection of “unacceptable” segments reduces FP_{AFib}s, which is desirable, there are also some TP_{AFib}s that are excluded as well. The rejection ratio is low when the SNR is high and rises as SNR decreases. While the rejection of TP_{AFib} segments is undesirable, this result can be considered acceptable because it is reasonable not to expect AFib to be reliably identified if there is low SNR. AFib is also not an immediately life-threatening condition; rejection of an unacceptable ECG is tolerable, as an acceptable ECG segment would be anticipated later.

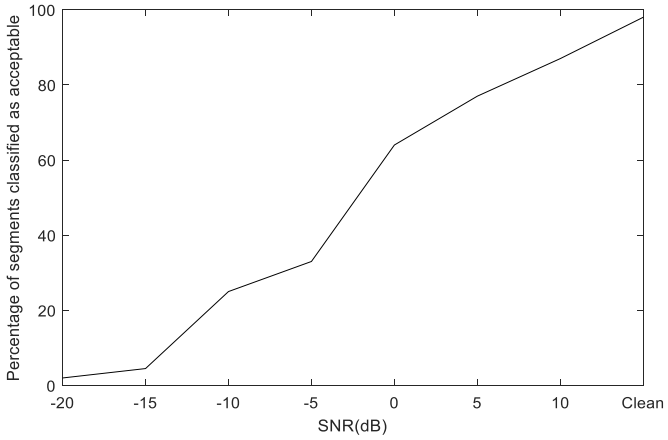

Figure 5.5 Classification of ECG segments into acceptable and unacceptable classes by DBN (acceptability threshold for AFib detection is 0dB)

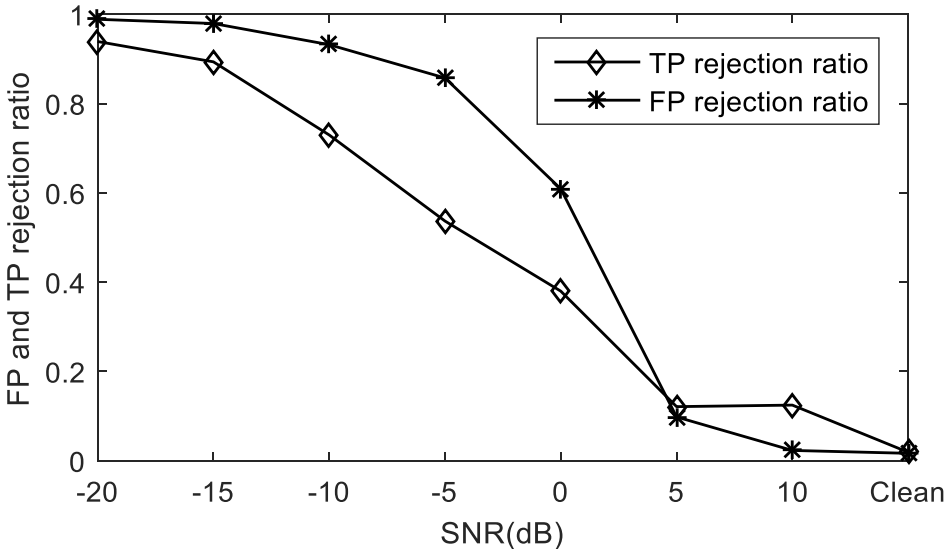

Figure 5.6 FP_{AFib} and TP_{AFib} rejection ratio

5.4 Discussions

Automatic event detection is an important application of wearable biosignal recorders and one of the reasons that explains their popularity growth in people who are struggling with chronic diseases. On the other hand, event detection is always accompanied with false event

detections and therefore false alarms. Low quality signals can mislead the event detection algorithm resulting in false alarms. Reducing the false alarms improves the reliability of the device and to achieve that, signal quality assessment can help.

In this part of our research, we developed a new technique based on machine learning algorithms to identify low quality signals and exclude them in AFib event detection to reduce the rate of false alarms leading to higher accuracy rate. To do so in the context of ECG wearable devices, which is the main interest of this thesis, we needed to create low-quality ECG signals which are contaminated with motion artifact as it is the dominant type of contaminant in wearable devices. There is only a very limited length of real motion artifact signal available in online databases whereas we need to create a huge data set of contaminated signals to test and validate our method. To overcome this issue, we have utilized auto regressive model of motion artifact signal as it has previously explained in 5.2.4. There might be other methods of generating artificial motion artifact representing its real version which we have not tested in this research. Moreover, there might be feasible ways to record motion artifact for long term periods, which we did not consider in this part of the work.

Another types of artifacts such as baseline wandering, and muscle artifact are not considered in this work, because they are not the leading type of artifact in wearable devices. Designing a method which covers all types of artifacts and a realistic combination of them to contaminate ECG signals with, is left for the future work.

Generalizing the findings to other types of heart arrhythmias other than AFib, is also left for the future research.

5.5 Conclusions

False alarms occurrence is a major drawback of all biosignal monitoring devices which are designed to detect specific events and activate alarm when it is observed. Low quality of acquired signal can trigger false alarms and their rate will be exacerbated when the monitoring device is a wearable one, due to their susceptibility to record low-quality signals. Therefore; it is important to invent a method to reduce the false alarms.

In this research we consider the above concern in atrial fibrillation (AFib) detection algorithms since AFib is a very popular heart arrhythmia as previously mentioned.

In this chapter, we proposed a novel method to reduce false alarms in atrial fibrillation detection. Our method processes the measured ECG signals and passes them through a deep belief network which can identify much of the unacceptable signals, leading to an increase in the detection accuracy, especially when signal to noise ratio is low. Results are encouraging and indicate that our proposed method can help AFIB detection wearable device designers to add a module into their device to reduce the rate of false alarms and hence improve its accuracy.

Chapter 6 **ECG Signals Classification Based on SNR**

6.1 Introduction

Quality of signals applied in medical diagnoses is a major concern for healthcare professionals. ECG is one of the most informative vital signals providing them with a reflection of patients' health condition. Contaminants can distort the ECG signal, which can result in errors in interpretation. Hence, ECG signal quality is important and depending on the application of the signal, the level of required quality varies [59]. In other words, each application has its own "acceptability" threshold. For example, a threshold of quality which is sufficient for a simple application such as heart rate measurement is not necessarily applicable to a more sophisticated application such as myocardial ischemia detection. In heart rate measurement, R-peak detection would suffice whereas myocardial ischemia detection needs looking into ST level of ECG [61] which is a small part of an ECG and therefore requires

accurate measurements and processing. Therefore, quantizing the quality of ECG can help us in finding and using signals with sufficient quality for each specific application.

On the other hand, ECG devices, designed for diagnostic purposes, might be multifunctional. That means they could be able to detect different types of arrhythmias which have different levels of acceptability threshold in terms of signal quality. Such devices will need to be equipped with an inclusive machine learning algorithm which can be adjusted to classify ECG signals (based on their quality) as required and depending on the application. One approach to implement such devices could be "signal quantification" instead of "signal detection" in the context of signal quality. Signal detection, as we have stated before in 1.1, is determining if the signal is contaminated (beyond a certain threshold) or not whereas signal quantification is determining the extent of contamination. Hence, signal quantification can be advantageous and help us in addressing this issue because a single method of quantization can be used for multiple applications with different thresholds. Moreover, the quantization allows for a gradient of quality, rather than acceptable versus unacceptable classification (a binary decision).

Signal quantification can be performed on a continuous or discrete scale. In a discrete scale, signals can be quantified in several levels of quantized quality thresholds while in a continuous scale, quality of the signals will be considered a continuous parameter with no threshold. In a discrete scale, we will expect signals closer to the threshold to be associated with decisions with less confidence, as compared to signals that are much higher or lower than the threshold.

We have already shown the powerfulness of DBN in ECG signal detection with different thresholds (discerning noisy and clean signals) in Chapter 4 and Chapter 5. In this research, we extend this previous work by designing a DBN-based algorithm for ECG quality

quantification in a discrete scale manner. To create discrete scales of quality, we will generate signals in four different SNR levels from -20 to +10dB in 10dB steps and apply them to the DBN-based algorithm we have designed.

6.2 Methods

6.2.1 Dataset

In many heart disorders, such as AFib and atrial flutter, the ECG exhibits a sinus (normal) rhythm in some episodes and arrhythmic rhythm in others [130]. Thus, in a diagnostic algorithm for such disorders, there is a combination of normal and arrhythmic ECG segments to work with.

Since the ultimate outcome of this research can be used in wearable devices which are designed to detect a variety of heart arrhythmias (including those with a combination of normal and arrhythmic ECG segments), we need to confirm that our proposed algorithm is able to properly quantify the signal quality when the input contains both normal and abnormal ECG segments. To do so, we create a new data set which is a combination of various signals with different arrhythmias (MIT-BIH Arrhythmia Database [77]), normal signals (MIT-BIH Normal Sinus Rhythm Database [77]) and Atrial Fibrillation signals (MIT-BIH Atrial Fibrillation Database [77]).

The dataset includes 21 clean ECG recordings from MIT-BIH Arrhythmia Database which are approximately 30 minutes in length [77], 18 clean ECG recordings from MIT-BIH Normal Sinus Rhythm Database, approximately 30 minutes of each and 21 ECG recordings from MIT-BIH Atrial Fibrillation Database, approximately 30 minutes of each. Signals in MIT-BIH Arrhythmia, MIT-BIH Normal Sinus Rhythm and MIT-BIH Atrial Fibrillation Database [77]

have a sampling frequency of 360, 128 and 250 Hz respectively. Signals with higher sampling frequencies are down sampled to 128 Hz for further analysis.

6.2.2 Training and Testing Sets

We have used one tenth of each part of the dataset (including signals from MIT-BIH Arrhythmia Database, MIT-BIH Normal Sinus Rhythm Database and MIT-BIH Atrial Fibrillation Database [77]) for testing and the rest for training. There is no overlap between training and testing sets, with each recording from a subject being entirely in the training set or entirely in the test set. A 10-fold cross validation is performed.

We have contaminated ECG signals with auto regressive model of "em" signal available in MIT-BIH Noise Stress Test Database (NSTDB) [77], as we explained in 5.2.4. We have generated a unique version of AR model of "em" for each signal to contaminate. Four datasets are created, each one contains all signals contaminated to have one of the desired SNRs including -20, -10, 0 and 10 dB. Contamination technique is as we have previously described in 4.2.1. All the signals are divided into 5-second segments after contaminating.

6.2.3 Classifying

We have designed a four-layer DBN (including three generative and one discriminative layers) to classify ECG segments based on their SNR. Each generative RBM has 1000 hidden units and 1000 visible units whereas the discriminative RBM has 2000 hidden and 2000 visible units. Contrastive Divergence (CD) method [109] is applied to train the RBMs through 200 epochs. Fine tuning is performed by employing a Back-Propagation (BP) method [110].

Each group of signals with a specific SNR is given a unique label and the DBN is trained to estimate the SNR of each segment based on SNR, and since we have four classes, we need four labels. Each ECG segments is assigned one of the labels, representing its level of SNR.

Next, the test set is applied to the DBN and the output will be one of the labels we have defined for each SNR class. After executing a 10-fold cross validation the labels given to the ECG segments by the DBN are compared to their real labels corresponding to its SNR level, to evaluate the DBN performance. The average of each performance metric across all folds is reported.

Imagining we have four classes including A, B, C and D, true positive, true negative, false positive and false negative four each class (e.g., A), are defined as follows:

TP for class A: signals in A which are correctly classified as A

FN for class A: Signals in A which are incorrectly classified as B or C or D

TN for class A: signals in all other classes (B, C or D) which are correctly classified as anything other than A.

FP for class A: signals in other classes (B, C or D) which are incorrectly classified as A.

6.3 Results

There are four classes of ECG segments to be classified with the DBN. To evaluate the performance of DBN, we will measure its metrics including accuracy, specificity, precision and recall as they have been defined in section 4.2.3 for each class. TP, FN, TN and FP for this multi-class classification are also defined in 6.2.3.

Results attained based on these definitions are shown in Table 6.1and Table 6.2.

Table 6.1 Results for multi-class classification

SNR	-20dB	-10dB	0dB	10dB
Accuracy (%)	99.47	94.98	90.08	91.21
Precision (%)	98.01	83.87	77.73	95.49
Recall (%)	99.92	98.97	84.54	68.06
Specificity (%)	99.32	93.66	91.92	98.93

In order to create a clear idea of the multi-class classification of ECG signals with DBN, as we have done in this study, we provide a confusion table (Table 6.2) of the DBN performance.

Table 6.2, shows that the majority of errors are between adjacent SNRs (e.g., 10dB does not frequently get mixed with -20 dB or -10 dB). In addition, low SNR signals are classified with very high accuracy. It is important and desired that a low SNR signal is not misclassified as having a high SNR, which could lead to misdiagnosis/misinformation. A high SNR misclassified as low SNR would mean the signal is rejected, losing a potentially useful signal; however, as this is not too frequent, such errors are better than the low SNRs being misclassified as a high SNR.

Table 6.2 Confusion table for multi-class classification

		Truth (%)			
		-20dB	-10dB	0dB	10dB
Predicted (%)	-20dB	99.92	0.077	0	0
	-10dB	0.9	98.97	0.13	0
	0dB	0.54	11.70	84.54	3.22
	10dB	0.59	7.25	24.10	68.06

6.4 Discussions

We have utilized DBN to perform a multi-class classification and quantify ECG signals based on their SNRs in a discrete scale. In this approach, only limited number of SNRs of ECG signals (-20, -10, 0 and 10 dB) are considered. However, in reality there are infinite numbers of them in a continuous manner and not a discrete one. How DBN will behave when it receives signals with SNRs between the discrete numbers we have considered in this work, is almost unclear. Also, for signals out of the range of our four SNRs, the classification accuracy is not obtained.

Another possible approach for ECG quantification, is regression approach which is left for future works.

6.5 Conclusions

In this chapter, we artificially contaminated a combined set of ECG signals to create a noisy dataset which contains normal and arrhythmic ECG signals. Signals are contaminated with

motion artifact noise, in calibrated SNRs to resemble signals being recorded by a wearable device. Then, DBN is utilized to discern signals based on their level of quality (SNR). DBN performs this multi-class classification and the results as we have shown, suggest that DBN is an appropriate candidate for multi-classification applications where we need to classify ECG signals based on their quality. Such applications can be imagined to be used in wearable devices designed for several purposes (e.g. heart rate measurement, myocardial ischemia detection, tachycardia detection, etc.) with different acceptability thresholds of quality. A DBN can be trained to effectively decides which signal to be used for each purpose and consequently reduces the false alarms in each specific application.

Chapter 7 **Conclusion and Future Work**

We studied the ECG wearable devices and sources of noise that affect the quality of signals recorded by them. We also, designed algorithms based on deep learning techniques to distinguish the quality of ECG signals. In this concluding chapter, we summarize all the contributions and achievements and discuss potential directions for future work in this area.

7.1 Summary of Results

- We first, investigated impact of “pressure” as a source of noise which influences the quality of signals recorded by wearable devices, whereas it is not an issue in clinical devices. We modeled the interface between the device and the body, which is the “skin–electrode interface impedance” for three different types of electrodes. An equivalent electrical circuit represents this impedance which

includes a few components. We have extracted them when the interface is under pressure and when there is no pressure; which are the two possible states when they are being used in a wearable device. The results show in each type of electrode, how each component varies due to the applied pressure. The irreversibility (in limited time) of those changes are also investigated.

- Second, we focused on the quality of recorded signals by a wearable device and designed an algorithm based on DBN which is able to discern clean ECG signals from noisy ones. We have examined several quality levels of ECG, and our DBN-based algorithm was able to discriminate clean signals from noisy signals.

- We proposed an algorithm based on the results we achieved in the previous step, to reduce the rate of false alarms in an automatic AFib detection algorithm. False alarms are a frustrating issue in non-wearable and wearable devices. They can be very problematic when they occur in heart arrhythmia detection devices. Therefore; reducing them is essential and leads to more robust and accurate arrhythmia detections. Our proposed algorithm works based on DBN and its ability to discriminate between ECG signals with different qualities. We first determine an acceptability threshold of ECG quality for AFib detection algorithm and then train the DBN to differentiate between signals from lower and higher qualities of this threshold. Signals which are qualified and can pass the DBN, will be applied to the AFib detection algorithm. Results show that, using this method we can highly improve the rate of false alarm occurrence.

- We have proposed and implemented a DBN based algorithm which is able to classify ECG signals of various levels of quality (SNR) into separate classes. This is a multi-class classification application which is applicable in multi-purpose ECG wearable devices. Results show that DBN has a powerful performance and can distinguish several levels of ECG quality.

7.2 Suggestions for Future Work

In our research thus far; we have addressed a few challenges wearable devices are struggling with from the signal quality point of view. There are several possible extensions for this research. Our plan to expand our research in the future includes the followings:

- Recording ECG signals while calibrated amount of pressure is applied on the ECG electrodes and also when the pressure is released. This will help us to visually compare the quality of signals in both states. We will be able to formulate the impacts of pressure on the quality of recorded signals.

- Investigating the impacts of pressure for other types of electrodes including electrodes which are applied for EEG recording and acquiring EEG signals while the pressure is applied and released.

- Implementing our algorithms on a hardware platform and improving them in a practical scene.

Several scenarios can be imagined, for instance we can implement our algorithm on ARM microcontrollers and add them to an existing wearable ECG device.

- Investigating all signal quality guides and indices applicable to ECG signals and determining which one applies to wearable devices with certain applications such as arrhythmia detection.

Several signal quality indices (SQI) for ECG signals have been so far defined [131]. But they are not compared in terms of applicability in case of different heart arrhythmias. We have plans to compare the accuracy and applicability of different SQIs in arrhythmic ECG signals.

- Utilizing deep learning techniques for other biosignals such as EEG and EMG to identify their signal quality.

In this research, promising results have been achieved with DBN in ECG signal quality assessment. Hence, performing similar experiments for other biosignals is another path of expansion for this study.

References

[1] "https://www.marketsandmarkets.com/PressReleases/wearable-medical-device.asp," [Online]. Available: https://www.marketsandmarkets.com/PressReleases/wearable-medical-device.asp.

[2] "IDC," 21 June 2017. [Online]. Available: https://www.idc.com/getdoc.jsp?containerId=prUS42818517. [Accessed 2017].

[3] G. Clifford, F. Azuaje and P. McSharry, "ECG Statistics, Noise, Artifacts, and Missing Data," in *Advanced Methods and Tools For ECG Data Analysis*, Norwood, MA, Artech house, 2006, pp. 55-99.

[4] M. Ferdjallah and R. Barr, "Adaptive digital notch filter design on the unit circle for the removal of powerline noise from biomedical signals," *IEEE Transactions on Biomedical Engineering*, vol. 41, no. 6, pp. 529-536, 1994.

[5] M. Alfaouri and K. Daqrouq, "ECG signal denoising by wavelet transform thresholding," *American Journal of applied sciences*, vol. 5, no. 3, pp. 276-281, 2008.

[6] S. Redmond, N. Lovell, J. Basilakis and B. Celler, "ECG quality measures in telecare monitoring," in *Engineering in Medicine and Biology Society, EMBS*, 2008.

[7] G. D. Fraser, A. D. C. Chan, J. R. Green and D. T. MacIsaac, "Automated Biosignal Quality Analysis for Electromyography using a One-Class Support Vector Machine," *IEEE Transactions on Instrumentation and Measurement,* vol. 63, no. 12, pp. 2919-2930, 2014.

[8] A. Rehman, M. Mustafa, I. Israr and M. Yaqoob, "Survey of Wearable Sensors with Comparative Study of Noise," *Inernational Journal of Computing and Network Technology,* vol. 1, no. 1, pp. 61-81, 2013.

[9] B. Taji, S. Shirmohammadi, V. Groza and I. Batkin, "Impact of skin electrode interface on ECG measurements using conductive textile electrodes," *IEEE Transactions on Instrumentation and Measurement,* p. 11 pages, 2013.

[10] J. Wald and L. McCormack, "Patient empowerment and health information technology," Healthcare Information and Management Systems Society by RTI International, 2011.

[11] Y. L. Zheng, X. R. Ding, C. C. Y. Poon, B. P. L. Lo, H. Zhang, X. L. Zhou, G. Z. Yang, N. Zhao and Y. T. Zhang, "Unobtrusive sensing and wearable devices for health informatics," *IEEE Transactions on Biomedical Engineering*, vol. 61, no. 5, pp. 1538-1554, 2014.

[12] S. Patel, H. Park, P. Bonato, L. Chan and M. Rodgers, "A review of wearable sensors and systems with application in rehabilitation," *Journal of NeuroEngineering and Rehabilitation,* vol. 9, no. 12, pp. 1-17, 2012.

[13] D. C. Claudio, A. Meduri and M. and Rosario, "A smart ECG measurement system based on web-service-oriented architecture for telemedicine applications," *IEEE Transactions on Instrumentation and Measurement,* vol. 59, no. 10, p. 2530–2538, October 2010.

[14] L. Fanucci, S. Saponara, T. Bacchillone, M. Donati, P. Barba, I. Sánchez-Tato and C. Carmona, "Sensing devices and sensor signal processing for remote monitoring of vital signs in CHF patients," *IEEE Transactions on Instrumentation and Measurement*, vol. 62, no. 3, pp. 553-569, 2013.

[15] B. Gosselin, M. Sawan and C. Chapman, "A low-power integrated bioamplifier with active low-frequency suppression," *IEEE Transactions on Biomedical Circuits and Systems,* vol. 1, no. 3, pp. 184-192, 2007.

[16] D. H. Gordon, "Triboelectric interference in the ECG," *IEEE Transactions on Biomedical Engineering,* Vols. BME-22, pp. 252-255, 1975.

[17] J. G. Webster, "Reducing Motion Artifacts and Interference in Biopotential Recording," *IEEE Transactions on Biomedical Engineering,* Vols. BME-31, no. 12, p. 823–826, Dec. 1984.

[18] J. Webster, Medical instrumentation: application and design, 4 ed., John Wiley & Sons, 2009.

[19] S. Grimnes and O. Martinsen, Bioimpedance and bioelectricity basics, 2nd ed., Amsterdam: Academic Press, 2008.

[20] E. Warburg, "About the behaviour of so-called “impolarizable electrodes” in the present of alternating current," *Ann. Phys. Chem,* vol. 67, pp. 493-499, 1899.

[21] L. A. Geddes, "Historical evolution of circuit models for the electrode-electrolyte interface," *Annals of biomedical engineering,* vol. 1, no. 25, pp. 1-14, 1997.

[22] C. Assambo, A. Baba, R. Dozio and M. J. Burke, "Determination of the Parameters of the Skin-Electrode Impedance Model for ECG Measurement," in *Proceedings of the 6th WSEAS international conference on electronics, hardware, wireless and optical communications,*, 2007.

[23] L. A. Geddes and L. E. Baker, Principles of Applied Biomedical Instrumentation, New York: John Wiley and Sons, 1968.

[24] B. R. Eggins, "Skin contact electrodes for medical applications," *Analyst,* vol. 118, no. 4, pp. 439-442, 1993.

[25] D. Swanson and J. Webster, A model for skin-electrode impedance, Academic Press, 1974, pp. 117-128.

[26] L. A. Geddes and M. E. Valentinuzzi, "Temporal changes in electrode impedance while recording the electrocardiogram with “dry” electrodes," *Annals of Biomedical Engineering,* vol. 1, no. 3, pp. 536-367, 1973.

[27] M. Neuman, Biopotential Electrodes , In: Medical Instrumentation application and Design, 3rd ed., John Wiley & Sons, 1998, pp. 183-232.

[28] K. Kaczmarek and G. Webster, "Voltage-current characteristics of the electrotactile skin-electrode interface," in *Proceedings of Annual International Conference of the IEEE Engineering in Medicine and Biology Society*, 1989.

[29] K. S. Cole and R. H. Cole, "Dispersion an absorption in dielectrics," *The Journal of Chemical Physics,* vol. 9, no. 4, pp. 341-351, 1941.

[30] S. Grimnes and O. Martinsen, "Cole electrical impedance model-A critique and an alternative," *IEEE Transactions on Biomedical Engineering,* vol. 52, no. 1, pp. 132-135, 2005.

[31] O. Martinsen and S. Grimnes, Bioimpedance and bioelectricity, Academic press, 2011.

[32] R. Gudivaka, D. Schoeller and R. Kushner, "Effect of skin temperature on multifrequency bioelectrical impedance analysis," *Journal of Applied Physiology*, vol. 81, no. 2, pp. 838-845, 1996.

[33] A. Elwakil and B. Maundy, "Extracting the Cole-Cole impedance model parameters without direct impedance measurement," *Electronics letters,* vol. 46, no. 20, pp. 1367-1368, 2010.

[34] M. Tripathy and S. Behera, "Modelling and Analysis of Fractional Capacitors," *International Journal of Engineering and Applied Siences,* vol. 2, no. 10, pp. 29-32, 2015.

[35] M. S. Spach, R. C. Barr, J. W. Havstad and E. Long, "Skin-Electrode Impedance and Its Effect on Recording Cardiac Potentials," *Circulation,* vol. 34, no. 4, pp. 649-656, 1966.

[36] G. Medrano, A. Ubl, N. Zimmermann, T. Gries and S. Leonhardt, "Skin Electrode Impedance of Textile Electrodes for Bioimpedance Spectroscopy," in *13th International Conference on Electrical Bioimpedance and the 8th Conference on Electrical Impedance Tomography*, 2007.

[37] P. Deurenberg, A. Tagliabue and F. Schouten, "Multi-frequency impedance for the prediction of extracellular water and total body water," *British Journal of Nutrition,* vol. 73, no. 3, pp. 349-358, 1995.

[38] R. Rangayyan and N. Reddy, "Biomedical Signal Analysis: A Case-study," *Annals of Biomedical Engineering,* vol. 30, no. 7, pp. 983-983, 2002.

[39] A. Searle and L. Kirkup, "A direct comparison of wet, dry and insulating bioelectric recording electrodes," *Physiological Measurement,* vol. 21, no. 2, pp. 271-283, May 2000.

[40] S. Grimnes, "Impedance measurement of individual skin surface electrodes," *Medical and Biological Engineering and Computing,* vol. 21, no. 6, pp. 750-755, 1983.

[41] L. A. Geddes and L. E. Baker, "Relationship between input impedance and electrode area," *Med. Biol. Eng,* vol. 4, no. 5, pp. 439- 449, 1966.

[42] D. P. Burbank and J. G. Webster, "Reducing skin potential motion artefact by skin abrasion," *Medical and Biological Engineering and Computing,* vol. 16, pp. 31-38, 1978.

[43] H. W. Tam and J. G. Webster, "Minimizing electrode motion artifact by skin abrasion," *EEE Transactions on Biomedical Engineering,* vol. 24, no. 2, p. 134, 1977.

[44] T. Yamamoto and Y. Yamamoto, "Electrical properties of the epidermal stratum corneum," *Med. Biol. Eng.*, vol. 14, no. 2, p. 151–158, 1976.

[45] E. T. McAdams, J. Jossinet, A. Lackermeier and F. Risacher, "Factors affecting electrode-gel-skin interface impedance in electrical impedance tomography," *Med. Biol. Eng. Comput,* vol. 34, no. 6, pp. 397-408, 1996.

[46] K. W. Kim, H. Y. Choi, M. H. Sim, I. C. Jeong and H. Yoon, "Compensation on Impedance of the Stratum Corneum," *Journal of Electrical Engineering and Technology,* vol. 3, no. 3, pp. 444-449, 2008.

[47] R. Edelberg, "Relation of electrical properties of skin to structure and physiologic state," *Journal of Investigative Dermatology,* vol. 69, no. 3, pp. 324-327, 1977.

[48] M. A. Lorraine, "Electrical properties of human stratum corneum and transdermal drug transport," *Journal of the Chemical Society, Faraday Transactions,* vol. 89, no. 15, pp. 2839-2845, 1993.

[49] I. Nicander and S. Ollmar, "Electrical impedance measurements at different skin sites related to seasonal variations," *Skin Research and Technology,* vol. 6, no. 2, pp. 81-86,, 2000.

[50] R. V. Hill, J. C. Jansen and J. L. Fling, "Electrical impedance plethysomography: a critical analysis," *Journal of applied physiology,* vol. 22, no. 1, pp. 161-168, 1967.

[51] A. Karilainen, S. Hansen and J. Müller, "Dry and capacitive electrodes for long-term ECG-monitoring,," in *8th Annual Workshop on Semiconductor Advances*, 2005.

[52] B. Taji, S. Shirmohammadi and V. Groza, "Measuring Skin-electrode Impedance Variation of Textile Electrode under Pressure," in *IEEE International Instrumentation and Measurement Technology*, Montevideo, Uruguay, 2014.

[53] A. Albulbul and A. D. C. Chan, "Electrode-skin impedance changes due to an externally applied force," in *Medical Measurements and Applications Proceedings (MeMeA)*, Budapest, Hungary, May 2012.

[54] R. Dozio, A. Baba, C. Assambo and M. J. Burke, "Time based measurement of the impedance of the skin-electrode interface for dry electrode ECG recording," in *Engineering in Medicine and Biology Society*, 2007.

[55] A. Baba and M. J. Burke, "Measurement of the electrical properties of ungelled ECG electrodes," *International journal of biology and biomedical engineering*, vol. 2, no. 3, pp. 89 - 97, 2008.

[56] D. K. Swanson, Pressure-Induced Changes in Skin-Through-Electrode Impedance, M. Sc. Thesis, Univ. Wisconsin, 1972.

[57] J. Behar, J. Oster, Q. Li and G. D. Clifford, "ECG signal quality during arrhythmia and its application to false alarm reduction," *IEEE Transactions on Biomedical Engineering*, vol. 60, no. 6, pp. 1660-1666, 2013.

[58] S. Nizami, J. Green and C. McGregor, " Implementation of artifact detection in critical care: A methodological review," *IEEE reviews in biomedical engineering*, vol. 6, pp. 127-142, 2013.

[59] D. Hayn, B. Jammerbund and G. Schreier, "QRS detection based ECG quality assessmen," *Physiological measurement*, vol. 33, no. 9, p. 1449, 2012.

[60] Q. Li, R. Mark and G. Clifford, "Robust heart rate estimation from multiple asynchronous noisy sources using signal quality indices and a Kalman filter," *Physiological measurement*, vol. 29, no. 1, p. 15, 2007.

[61] M. Abdelazez, P. Quesnel, A. D. C. Chan and H. Yang, "Signal quality analysis of ambulatory electrocardiograms to gate false myocardial ischemia alarms," *IEEE Transactions on Biomedical Engineering*, vol. 64, no. 6, pp. 1318-1325, 2017.

[62] M. Abdelazez, M. Hozayn, G. S. Hanna and A. D. C. Chan, "Gating of False Identifications in Electrocardiogram based Biometric System," in *Medical Measurements and Applications Proceedings (MeMeA), 2017 IEEE International Symposium*, 2017.

[63] C. Daluwatte, L. Johannesen, L. Galeotti, J. Vicente, D. Strauss and C. Scully, "Assessing ECG signal quality indices to discriminate ECGs with artefacts from pathologically different arrhythmic ECGs," *Physiological Measurement*, vol. 37, no. 8, p. 1370, 2016.

[64] C. Yu, Z. Liu, T. McKenna, A. T. Reisner and J. Reifman, "A method for automatic identification of reliable heart rates calculated from ECG and PPG waveforms," *Journal of the American Medical Informatics Association*, vol. 13, no. 3, pp. 309-320, 2006.

[65] G. D. Clifford, J. Behar, Q. Li and I. Rezek, "Signal quality indices and data fusion for determining clinical acceptability of electrocardiograms," *Physiological measurement*, vol. 33, no. 9, p. 1419, 2012.

[66] J. Kužílek, M. Huptych, V. Chudáček, J. Spilka and L. Lhotská, "Data driven approach to ECG signal quality assessment using multistep SVM classification," *Computing in Cardiology*, pp. 453-455, 2011.

[67] H. Lee, P. Pham, Y. Largman and A. Y. Ng, "Unsupervised feature learning for audio classification using convolutional deep belief networks," *Advances in neural information processing systems*, pp. 1069-1104, 2009.

[68] Y. Su, M. H. Fisher, A. Wolczowski, G. Bell, D. J. Burn and R. X. Gao, "Towards an EMG-controlled prosthetic hand using a 3-D electromagnetic positioning system," *IEEE transactions on instrumentation and measurement*, vol. 56, no. 1, pp. 178-186, 2007.

[69] P. McCool, G. D. Fraser, A. D. C. Chan, L. Petropoulakis and J. J. Soraghan, "Identification of Contaminant Type in Surface Electromyography (EMG) Signals," *IEEE Transactions on Neural Systems and Rehabilitation Engineering*, vol. 22, no. 4, pp. 774-783, 2014.

[70] K. R. Foster, R. Koprowski and J. D. Skufca, "Machine learning, medical diagnosis, and biomedical engineering research-commentary.," *Biomedical engineering online*, vol. 13, no. 1, 2014.

[71] K. Polat and S. Güneş, "Detection of ECG Arrhythmia using a differential expert system approach based on principal component analysis and least square support vector machine," *Applied Mathematics and Computation*, vol. 18, no. 1, pp. 898-906, 2007.

[72] S. Mitra, M. Mitra and B. Chaudhuri, "A rough-set-based inference engine for ECG classification," *IEEE Transactions on instrumentation and measurement*, vol. 55, no. 6, pp. 2198-2206, 2006.

[73] K. Englehart, B. Hudgins and A. D. C. Chan, "Continuous multifunction myoelectric control using pattern recognition," *Technology and Disability*, vol. 15, no. 2, pp. 95-103, 2003.

[74] A. D. C. Chan, M. Hamdy, A. Badre and V. Badee, "Wavelet distance measure for person identification using electrocardiograms," *IEEE transactions on instrumentation and measurement*, vol. 57, no. 2, pp. 248-253., 2008.

[75] L. Biel, O. Pettersson, L. Philipson and P. Wide, "ECG analysis: a new approach in human identification," *IEEE Transactions on Instrumentation and Measurement*, vol. 50, no. 3, pp. 808-812, 2001.

[76] Q. Li, C. Rajagopalan and G. Clifford, "A machine learning approach to multi-level ECG signal quality classification," *Computer methods and programs in biomedicine*, vol. 117, no. 3, pp. 435-447, 2014.

[77] A. L. Goldberger, L. A. Amaral, L. Glass, J. M. Hausdorff, P. C. Ivanov, R. G. Mark, J. E. Mietus, G. B. Moody, C. K.Peng and H. E. Stanley, "PhysioBank, PhysioToolkit, and PhysioNet: components of a new research resource for complex physiologic signals," *Circulation*, vol. 101, no. 23, p. e215–e220, Jun 2000.

[78] Y. Lv, Y. Duan, W. Kang, Z. Li and F. Y. Wang, "Traffic Flow Prediction with Big Data: A Deep Learning Approach," *IEEE Transactions on Intelligent Transportation Systems*, vol. 16, no. 2, pp. 865-873, 2015.

[79] M. Huanhuan and Z. Yue, "Classification of Electrocardiogram Signals with Deep Belief Networks," in *IEEE 17th International Conference on Computational Science and Engineering (CSE)*, 2014.

[80] Y. Bengio, A. Courville and P. Vincent, "Representation Learning: A Review and New Perspectives," *IEEE transactions on pattern analysis and machine intelligence*, vol. 35, no. 8, pp. 1798-1828, 2013.

[81] H. Lee, R. Grosse, R. Ranganath and A. Y. Ng, "Convolutional deep belief networks for scalable unsupervised learning of hierarchical representations," in *Proceedings of the 26th annual international conference on machine learning*, 2009.

[82] D. Erhan, Y. Bengio, A. Courville, P. A. Manzagol, P. Vincent and S. Bengio, "Why Does Unsupervised Pre-training Help Deep Learning," *Journal of Machine Learning Research*, vol. 11, pp. 625-660, 2010.

[83] G. E. Hinton, S. Osindero and Y. W. Teh, "A fast learning algorithm for deep belief nets," *Neural computation*, vol. 18, no. 7, pp. 1527-1554, 2006.

[84] R. Salakhutdinov and H. Larochelle, "Efficient learning of deep Boltzmann machines," in *Proceedings of the thirteenth international conference on artificial intelligence and statistics*, 2010.

[85] Y. Liu, S. Zhou and Q. Chen, " Discriminative deep belief networks for visual data classification," *Pattern Recognition*, vol. 44, no. 10-11, pp. 2287-2296, 2011.

[86] A. J. Camm, P. Kirchhof, G. Y. Lip, U. Schotten, I. Savelieva, S. Ernst, I. C. Van Gelder and N. Al-Attar, "Guidelines for the management of atrial fibrillation: the Task Force for the Management of Atrial Fibrillation of the European Society of Cardiology (ESC)," *European heart journal*, vol. 31, no. 19, pp. 2369-2429, 2010.

[87] S. Heidt, A. Kratz, K. Najarian, A. Hassett, H. Oral, R. Gonzalez, B. Nallamothu, D. Clauw and H. Ghanbari, "Symptoms In atrial fibrillation: a contemporary review and future directions," *Journal of atrial fibrillation*, vol. 9, no. 1, 2016.

[88] D. Clark, V. Plumb, A. Epstein and G. Kay, "Hemodynamic effects of an irregular sequence of ventricular cycle lengths during atrial fibrillation," *Journal of the American College of Cardiology*, vol. 30, no. 4, pp. 1039-1045, 1997.

[89] P. Laferriere, E. D. Lemaire and A. D. C. Chan, "Surface electromyographic signals using dry electrodes," *IEEE Transactions on Instrumentation and Measurement*, vol. 60, no. 10, pp. 3259-3268, 2011.

[90] H. de Talhouet and J. G. Webster, "The origin of skin-stretch-caused motion artifacts under electrodes," *Physiological Measurement*, vol. 2, no. 17, pp. 81-93, 1996.

[91] E. Richard and A. D. C. Chan, "Non-obtrusive electrocardiogram system for the Smart Rollator," in *IEEE Intl. Symp. MeMeA*, Budapest, Hungary, 2012.

[92] P. H. Devlin, G. M. Roger and J. W. Ketchum, "Detection electrode motion noise in ecg signals by monitoring electrode impedance," in *Computers in Cardiology*, 1984.

[93] P. S. Hamilton, M. G. Curley, R. M. Aimi and C. Sae-Hau, "Comparison of methods for adaptive removal of motion artifact," in *Computers in Cardiology*, 2000.

[94] K. E. Sparks and A. T. Rood, "A comparison of ECG signal quality between a novel dry electrode and standard gel electrode," *Med. Sci. Sports Exercise*, vol. 38, no. 1, p. S5, 2006.

[95] K. P. Hoffmann and R. Ruff, "Flexible dry surface-electrodes for ECG long-term monitoring," in *Engineering in Medicine and Biology Society*, 2007.

[96] T. A. Kosierkiewicz, "Dry and flexible elastomer electrodes outperform similar hydrogel and Ag/AgCl electrodes," in *Medical Measurements and Applications Proceedings (MeMeA)*, 2013.

[97] J. Muhlsteff, O. Such, R. Schmidt, M. Perkuhn, H. Reiter, J. Lauter, J. Thijs, G. Musch and M. Harris, "Wearable approach for continuous ECG-and activity patient-monitoring," in *Engineering in Medicine and Biology Society*, 2004.

[98] "http://www.orbitalresearch.com/PDFs/ORI_ACSM_Abstract.pdf," [Online].

[99] R. Pethig, "Dielectric properties of body tissues," *Clinical Physics and Physiological Measurement,* vol. 8, no. 4A, pp. 5-12, 1987.

[100] J. Muhlsteff and O. Such, "Dry electrodes for monitoring of vital signs in functional textiles," in *Engineering in Medicine and Biology Society*, 2004.

[101] "www.heart.org," 2015. [Online]. Available: https://www.heart.org/idc/groups/ahamah-public/@wcm/@sop/@smd/documents/downloadable/ucm_470704.pdf.

[102] C. De Capua, A. Meduri and R. Morello, "A smart ECG measurement system based on web-service-oriented architecture for telemedicine applications," *IEEE Transactions on Instrumentation and Measurement,* vol. 59, no. 10, pp. 2530-2538, 2010.

[103] E. Institute, "Top 10 Health Technology Hazards for 2012," *Health Devices,* vol. 40, no. 11, Nov 2011.

[104] E. Institute, "Top 10 Health Technology Hazards for 2013," *Health Devices,* vol. 41, no. 11, Nov 2012.

[105] E. Institute, "Top 10 Health Technology Hazards for 2014," *Health devices,* vol. 42, no. 11, Nov 2013.

[106] E. Institute, "Top 10 Health Technology Hazards for 2015," Nov 2014.

[107] Q. Zhang, C. Zahed, V. Nathan, D. Hall and R. Jafari, "An ECG dataset representing real-world signal characteristics for wearable computers," in *Biomedical Circuits and Systems Conference (BioCAS)*, 2015.

[108] "physionet," [Online]. Available: https://www.physionet.org/physiotools/wag/nst-1.htm.

[109] M. A. Carreira-Perpinan and G. E. Hinton, "On contrastive divergence learning," *Artificial Intelligence and Statistics*, vol. 10, pp. 33-40, 2005.

[110] R. Hecht-Nielsen, "Theory of the backpropagation neural network," in *International Joint Conference* , 1989.

[111] S. Dash, K. Chon, S. Lu and E. Raeder, "Automatic real time detection of atrial fibrillation.," *Annals of biomedical engineering,* vol. 37, no. 9, pp. 1701-1709, 2009.

[112] K. Tateno and L. Glass, "Automatic detection of atrial fibrillation using the coefficient of variation and density histograms of RR and ΔRR intervals," *Medical and Biological Engineering and Computing,* vol. 36, no. 6, pp. 664-671, 2001.

[113] "http://www.healthline.com/health/atrial-fibrillation/effects-on-body," [Online].

[114] "http://www.heartandstroke.ca/heart/conditions?gclid=CN6j9cbQvdQCFQi2wAodHcgL7Q," [Online].

[115] https://www.cdc.gov/dhdsp/data_statistics/fact_sheets/docs/fs_atrial_fibrillation.pdf. [Online].

[116] "http://www.hrsonline.org/Patient-Resources/Heart-Diseases-Disorders/Atrial-Fibrillation-AFib," [Online].

[117] "http://www.who.int/mediacentre/factsheets/fs310/en/," [Online].

[118] S. Narayan, D. Krummen and W. Rappel, "Clinical mapping approach to diagnose electrical rotors and focal impulse sources," *Journal of cardiovascular electrophysiology,* vol. 23, no. 5, pp. 447-454, 2012.

[119] C. January, L. Wann, J. Alpert, H. Calkins, J. Cleveland, J. Cigarroa, J. Conti, P. Ellinor, M. Ezekowitz, M. Field and K. Murray, "2014. 2014 AHA/ACC/HRS guideline for the management of patients with atrial fibrillation," *Circulation,* vol. 130, no. 23, pp. 199-267, 2014.

[120] C. Lin, K. Chang, C. Lin, C. Chiang, S. Lu, S. Chang, B. Lin, H. Liang, R. Chen, Y. Lee and L. Ko, "An intelligent telecardiology system using a wearable and wireless ECG to detect atrial fibrillation," *IEEE Transactions on Information Technology in Biomedicine,* vol. 14, no. 3, pp. 726-733, 2010.

[121] X. Zhou, H. Ding, B. Ung, E. Pickwell-MacPherson and Y. Zhang, "Automatic online detection of atrial fibrillation based on symbolic dynamics and Shannon entropy," *Biomedical engineering online,* vol. 13, no. 1, p. 18, 2014.

[122] D. Duverney, J. Gaspoz, V. Pichot, F. Roche and R. Brion, "High accuracy of automatic detection of atrial fibrillation using wavelet transform of heart rate intervals," *Pacing and clinical electrophysiology* , vol. 25, no. 4, pp. 457-462, 2002.

[123] B. Taji, A. D. C. Chan and S. Shirmohammadi, "Classifying Measured Electrocardiogram Signal Quality Using Deep Belief Networks," in *2017 IEEE International Instrumentation and Measurement Technology Conference, I2MTC 2017-Proceedings*, 2017.

[124] D. Krummen, G. Feld and S. Narayan, "Diagnostic accuracy of irregularly irregular RR intervals in separating atrial fibrillation from atrial flutter," *The American journal of cardiology,* vol. 98, no. 2, pp. 209-214, 2006.

[125] A. Petrėnas, V. Marozas and L. Sörnmo, "Low-complexity detection of atrial fibrillation in continuous long-term monitoring," *Computers in biology and medicine,* vol. 65, pp. 184-191, 2015.

[126] J. Pan and W. J. Tompkins, "A real-time QRS detection algorithm," *IEEE Transaction on Biomedical Engineering,* Vols. BME-32, no. 3, pp. 230-236, 1985.

[127] H. Sedghamiz, "Complete Pan Tompkins Implementation ECG QRS Detector," Linkoping University, Linkoping, Sweden, 2014.

[128] H. Bozdogan, "Model selection and Akaike's information criterion (AIC): The general theory and its analytical extensions," *Psychometrika,* vol. 52, no. 3, pp. 345-370, 1987.

[129] G. Friesen, T. Jannett, M. Jadallah, S. Yates, S. Quint and H. Nagle, "A comparison of the noise sensitivity of nine QRS detection algorithms," *IEEE Transactions on biomedical engineering,* vol. 37, no. 1, pp. 85-98, 1990.

[130] M. Suttorp, J. Kingma, E. Koomen, A. van't Hof, J. Tijssen and K. Lie, " Recurrence of paroxysmal atrial fibrillation or flutter after successful cardioversion in patients with normal left ventricular function," *American Journal of Cardiology,* vol. 71, no. 8, pp. 710-713, 1993.

[131] U. Satija, B. Ramkumar and M. S. Manikandan, "A Review of Signal Processing Techniques for Electrocardiogram Signal Quality Assessment," *IEEE Reviews in Biomedical Engineering.,* 2018.

[132] A. Usakli and S. Gurkan, "Design of a novel efficient human–computer interface: an electrooculagram based virtual keyboard," *IEEE Transactions on Instrumentation and Measurement*, vol. 59, no. 8, pp. 2099-2108, 2010.